

# **Fluorogenic Labeling of Oligonucleotides by Means of Photoclick-Reaction and Strain-Promoted Sydnone Alkyne Cycloaddition**

Zur Erlangung des akademischen Grades einer  
**DOKTORIN DER NATURWISSENSCHAFTEN**

(Dr. rer. nat.)

von der KIT-Fakultät für Chemie und Biowissenschaften

des Karlsruher Instituts für Technologie (KIT)



genehmigte

**DISSERTATION**

von

M. Sc. Katja Krell

1. Referent: Prof. Dr. Hans-Achim Wagenknecht

2. Referentin: Prof. Dr. Ute Schepers

Tag der mündlichen Prüfung: 10.12.2020



*meiner Familie*



---

*“I would like to be remembered as someone  
who used whatever talent she had  
to do her work to the very best of her  
ability.”*

*-Ruth Bader Ginsburg*

---



## Danksagung

---

Die vorliegende Arbeit wurde im Zeitraum Dezember 2017 bis Dezember 2020 in der Arbeitsgruppe von Prof. Dr. Wagenknecht am Institut für Organische Chemie am KIT angefertigt.

Zunächst möchte ich mich bei Prof. Dr. Wagenknecht für die Betreuung dieser Arbeit und die interessante Themenstellung bedanken. Weiterhin möchte ich mich beim gesamten Arbeitskreis für die lustigen Mittagspausen, Einstände aber auch für gute wissenschaftliche Gespräche bedanken:

Dr. Christoph Bickmann, Anke Culetto, Dr. Larissa Doll, Dorothée Ganz, Dr. Yannic Fritz, Julian Gebhard, Philipp Geng, Dennis Harijan, Dr. Sergej Hermann, Lara Hirsch, Annette Hochgesand, Dr. Robert Hofsäß, Arthur Kuhlmann, Fabian Lang, Rita Michenfelder, Michaela Mijic, Karen Möbius, Sara Müller, Dr. Damian Ploschik, Dr. David Rombach, Dr. Franziska Rönicke, Dr. Ulrike Reisacher, Daniel Sack, Maximilian Seifermann, Nicola Seul, Fabienne Seyfert, Dr. Jeannine Steinmeyer, Desirée Steuernagel, Claudia Sommer, Hülya Ucar, Fabian Weick, Dr. Samantha Wörner.

Besonders bedanken möchte ich mich bei:

Claudia für das Erledigen aller möglichen organisatorischen Dinge und für das geduldige Beantworten, jeder noch so blöden Frage. Annette für die Messung unzähliger MALDI-Proben in gefühlt tausend unterschiedlichen Konzentrationen und für das Bestellen aller möglichen Chemikalien, Farbstoffen und Laborgeräten. Außerdem möchte ich mich bei dir für die zahlreichen netten Gespräche bedanken.

Dem „Mangolabor“ 203 für die lustige Zeit in Bologna, insbesondere Fabienne für die Bereitstellung ihrer Hausapotheke. Arthur möchte ich für die Hilfsbereitschaft danken, wenn mal wieder irgendeine Flasche, das Kieselgelfass oder der Stickstoffdewar nicht aufging. Premium, mit dem das Trinken von Chilischnaps immer besonders unterhaltsam war. Yannic für seine fröhliche Art und die interessanten Diskussionen, die wir immer geführt haben, auch wenn wir oft nicht einer Meinung waren.

Allen aus Labor 204 möchte ich für ihre große Hilfsbereitschaft bedanken. Samantha für die Unterstützung beim Wandern in Obergurgl, außerdem dafür,

dass du dich so oft gut um mich gekümmert hast, wenn es mir mal nicht so gut ging. „Okay Fabian“ für den technischen Support sowohl was Computer als auch den Synthesizer anging. Außerdem für die vielen Gespräche, die wir über unnütze Dinge, die wir wissen, geführt haben. Nicola für ihre liebe, ruhige Art. Julian für seine lebenswürdige, hilfsbereite und witzige Art und für die Hilfe an der HPLC. Außerdem möchte ich mich für das Korrekturlesen dieser Arbeit bedanken. Hülya für die vielen Gespräche, die wir übers Kochen, Backen oder Sonstiges geführt haben und für deine lebenswerte, direkte Art, die so oft für Lacher gesorgt hat. Rita für die Zeit, die wir im Zelllabor zusammen verbracht haben und für die vielen netten Gespräche, die wir geführt haben. Sara möchte ich für die seelische und moralische Unterstützung der letzten drei Jahre danken. Danke, dass du für mich in allen Lebenslagen da warst und es geschafft hast, mich immer wieder aufzumuntern. Außerdem will ich dir dafür danken, dass du mich im ersten Jahr der Promotion gefühlt wöchentlich mit Fisch durchgefüttert hast.

Meinen Kollegen aus Labor 205 möchte ich mich für die große Unterstützung in allen Lebenslagen danken. Larissa, ohne dich wäre diese Arbeit so nicht möglich gewesen. Ohne dich wäre ich am RNase freien Arbeiten und am Synthetisieren der Phosphoramidite sicher (noch mehr) verzweifelt. Danke, dass du es immer wieder geschafft hast, mich mit deiner ruhigen, fröhlichen Art auf den Boden der Tatsachen zurück zu bringen, wenn ich mich mal wieder furchtbar über irgendwas aufgeregt habe. Max für seine witzige, trockene Art und seine Hilfsbereitschaft. Danke für die ganzen Gespräche, die wir auf dem Balkon geführt haben und für die guten Ratschläge und die Unterhaltung bei diversen Einständen durch Singstar oder Tanzeinlagen.

Franzi möchte ich dafür danken, dass sie insbesondere in den letzten Wochen so viel Zeit mit mir im Zelllabor und vor dem Mikroskop verbracht hat. Vielen Dank für das geduldige Erklären aller Zellkulturtechniken und dafür, dass du mir immer zugehört und weitergeholfen hast, wenn ich Fragen oder Ideen hatte.

Damian für die große Hilfe während des Studiums und in sonstigen Lebenslagen. Vielen Dank, dass du mir immer mit Rat und Tat zur Seite gestanden hast und für die vielen lustigen Spieleabende und Feiern während der letzten Jahre. Danke dafür, dass ich mich immer auf dich verlassen kann.

Sophie und Luca für die vielen Kaffeedates und die Unterstützung in allen Lebenslagen. Vielen Dank, dass ihr mir so oft ein Dach über dem Kopf gegeben habt und einfach immer für mich da seid, sei es in schwierigen Lebenslagen oder wenn hier mal wieder irgendwas betoniert werden muss.

Marvin und Jonathan für die vielen lustigen Abende in diversen Restaurants. Danke, dass ihr euch immer meine Laborprobleme angehört habt, obwohl ihr damit nicht immer etwas anfangen konntet.

Als letztes möchte ich mich bei meiner Familie bedanken:

Bei meinen Eltern, ohne die all das nicht möglich gewesen wäre. Vielen Dank für die Unterstützung in allen Lebenslagen.

Johannes, Jessica und Sophia möchte ich dafür danken, dass ihr mir ein Dach über dem Kopf gegeben habt und euer Kühlschrank immer für mich offensteht. Johannes und Sophia für all die Umarmungen und das Trösten, wenn wieder mal etwas vollkommen schiefgelaufen ist. Jessica dafür, dass sie in allen Lebenslagen mein Rettungsanker ist und einfach immer für mich da ist.

Eren, thank you for being always by my side, in good times as well as bad times. Thank you for always being patient with me and always making me laugh.



## Zusammenfassung

---

Im Rahmen dieser Arbeit wurden bioorthogonale Markierungen von Nukleosiden und Oligonukleotiden durch Photoclickreaktion und ringspannungsgetriebener Sydnon-Alkin-Cycloaddition durchgeführt.

Im ersten Teil wurde ein tetrazolmodifiziertes Ribonukleosid synthetisiert und anschließend über Festphasensynthese in zwei RNA-Stränge unterschiedlicher Sequenzen (intern, 5'-terminal) eingebaut. Die Untersuchung der Photoclickreaktion wurde mit Fokus auf Optimierung des Systems für fluoreszente Bildgebung in Zellen ausgelegt. Die Photoclickreaktion wurde mit drei verschiedenen Farbstoffmaleinimidkonjugaten (AF555, sulfo-Cy3 und AF647) durch Belichtung mit einer 300 nm LED durchgeführt deren Ausbeute und fluorogenes Verhalten untersucht. Dabei konnte durch einen *Förster-Resonanzenergietransfer* zwischen dem in der Photoclickreaktion entstehenden Pyrazolin als Donor und dem jeweiligen Farbstoff als Akzeptor ein bis zu 9,4-facher Anstieg der Fluoreszenz beobachtet werden. Weiterhin konnten Markierungsausbeuten bis zu 84% erreicht werden.

Im zweiten Teil dieser Arbeit wurden drei verschiedene sydnonmodifizierte Nukleoside synthetisiert. Zunächst wurden die Nukleoside entweder in der ringspannungsgetriebenen Sydnon-Alkin-Cycloaddition oder in der Photoclickreaktion untersucht. Die Photoclickreaktion konnte dabei effizient durch Belichtung mit einer 405 nm LED durchgeführt werden. Dabei konnte ebenfalls ein *Förster-Resonanzenergietransfer* zwischen dem Pyrazolin und verschiedenen Farbstoffen beobachtet werden. Weiterhin wurden zwei sydnonmodifizierte DNA-Stränge durch postsynthetische Modifikation synthetisiert und ebenfalls in der ringspannungsgetriebenen Sydnon Alkin Cycloaddition untersucht. Die Markierung erfolgte dabei in hoher Ausbeute und Geschwindigkeit. Im Anschluss wurden die Ergebnisse der ringspannungsgetriebenen Sydnon-Alkin-Cycloaddition auf fixierte *HeLa* Zellen übertragen.



# Table of Contents

---

1	Aim and Motivation .....	1
2	Theoretical Background .....	3
2.1	Bioorthogonal Labeling.....	3
2.2	Copper-Free Labeling techniques .....	6
2.2.1	Strain-Promoted Azide-Alkyne Cycloaddition (SPAAC) .....	6
2.2.2	Strain-Promoted Sydnone-Alkyne Cycloaddition (SPSAC) .....	9
2.2.3	Light-Induced Bioorthogonal Reactions.....	12
3	Tetrazole-Modified Oligonucleotides for Bioorthogonal Labeling .....	19
3.1	Synthesis of Tetrazole-Modified Nucleoside 9 .....	20
3.2	Synthesis and Characterization of Tetrazole-Modified Oligonucleotides .....	24
3.3	Photoclick Experiments .....	26
3.4	Cell Experiments .....	36
3.5	Conclusion and Outlook.....	38
4	Sydnone-Modified Oligonucleotides for Bioorthogonal Labeling .....	40
4.1	Synthesis of Sydnone-Modified Nucleosides 31, 32 and 33 .....	40
4.2	Synthesis and Characterization of Sydnone-Modified DNA strands .....	43
4.3	Bioorthogonal Labeling Experiments .....	45
4.3.1	SPSAC Experiments .....	45
4.3.2	Photoclick Experiments .....	55
4.4	Cell Experiments .....	62
4.5	Conclusion and Outlook.....	65
5	Experimental Section .....	67
5.1	Materials and Methods .....	67
5.2	Synthetic Procedures .....	71
5.2.1	Ribonucleosides.....	71

5.2.2	2'-Deoxyribonucleosides.....	83
5.3	Oligonucleotides .....	96
5.3.1	RNA.....	96
5.3.2	DNA.....	102
5.3.3	Sequences and Characterization.....	107
5.3.4	Bioorthogonal Labeling Experiments.....	107
5.3.5	HPLC-Methods .....	109
5.4	Determination of the Reaction Rate Constant .....	109
5.5	Cell Experiments.....	111
6	Additional Data and Spectra.....	112
6.1	Reaction Conditions Peroxodisulfate Oxidation.....	112
6.2	Spectra of Reaction between RNA1 and dye maleimides .....	112
6.3	Spectra of Reaction between DNA4 and Cy3 DIBAC.....	114
6.4	Spectra of Reaction of nucleoside 33 .....	115
7	References.....	117
8	Appendix .....	122
8.1	Publikationen.....	122
8.2	Konferenzen und Poster .....	122
8.3	Ehrenwörtliche Erklärung.....	123

## Abbreviations

---

ACN	acetonitrile
BARAC	biarylazacyclooctyne
BCN	bicyclononyne
BPS	bathophenanthroline disulfonate disodium salt
BSA	bovine serum albumin
Bz	benzoyl
COMBO	carboxymethylmonobenzocyclooctyne
CuAAC	copper-catalyzed azide-alkyne cycloaddition
d	doublet
dd	doublet of doublet
dt	doublet of triplet
DCM	dichloromethane
DIBAC	dibenzoazacyclooctyne
DIBO	dibenzocyclooctyne
DIFBO	difluorobenzocyclooctyne
DIFO	difluorocyclooctyne
DIPEA	<i>N,N</i> -diisopropylethylamine
DMF	<i>N,N</i> -dimethylformamide
DMSO	dimethylsulfoxide
DNA	deoxyribonucleic acid
DMTr	4,4'-dimethoxytrityl
Em.	emission
ESI	electron-spray ionization
Exc.	excitation
FAB	fast-atom bombardment
FE	fluorescence enhancement
FRET	Förster resonance energy transfer
GFP	green fluorescent protein

HeLa	human cervical cancer cells
HOMO	highest occupied molecular orbital
HPLC	high performance liquid chromatography
HRMS	high resolution mass spectrometry
HyD	hybrid detector
I	intensity
iEDDA	inverse electron-demand Diels-Alder cycloaddition
LUMO	lowest unoccupied molecular orbital
m	multiplet
MALDI	matrix-assisted laser desorption ionization
MeOH	methanol
mRNA	messenger ribonucleic acid
MS	mass spectrometry
Na-P <sub>i</sub>	sodium phosphate
NHS	N-hydrocysuccinimide
NMM	N-methylmaleimide
OCT	cyclooctyne
PBS	phosphate buffered saline
PTC	phase-transfer catalyst
q	quartet
Quant.	quantitative
R <sub>f</sub>	retention factor
r.t.	room temperature
RNA	ribonucleic acid
ROS	reactive oxygen species
s	singlet
sfGFP	super-folder green fluorescent protein
SPAAC	strain-promoted azide-alkyne cycloaddition
SPSAC	strain-promoted sydnone-alkyne cycloaddition

t	triplet
T	temperature
TBDMS	<i>tert</i> -butyldimethylsilyl
TBTA	tris((1-benzyl-1H-1,2,3-triazol-4-yl)methyl)amine
TCO	trans cyclooctene
THF	tetrahydrofuran
THPTA	tris(hydroxypropyltriazolyl)-methylamine
TLC	thin-layer chromatography
TMS	tetramethylsilane
TOF	time of flight
UV	ultraviolet (light)
Vis	visible (light)



# 1 Aim and Motivation

---

Throughout the past few decades, nucleic acid research has emerged as a strongly growing field in science. In recent times, it has gained even more importance and recognition not only in the scientific world, but also in everyday life. For example, the Nobel prize in 2020 was awarded to *Jennifer Doudna* and *Emmanuelle Charpentier* for employing the “genetic scissors” CRISPR-Cas9 as a versatile tool for genome editing.<sup>[1-2]</sup> Further examples include the development of mRNA based vaccines and nucleoside based therapeutics, such as *Remdesivir* against the current outbreak of SARS-CoV-2.<sup>[3-5]</sup> To achieve applications like the previously mentioned examples, the investigation and visualization of cellular processes controlled by biomolecules, such as proteins, glycans, lipids and nucleic acids, is an extremely important task to understand biological processes in living systems. A widely used tool for this is the fusion of fluorescent proteins to a target protein to understand and visualize cellular pathways.<sup>[6-7]</sup> One of the most prominent fluorescent protein is the *green fluorescent protein* (GFP) that was first discovered and extracted from *Aequorea* jellyfish by *Shimomura et al.* in 1962.<sup>[8]</sup> In further work by *Tsien* and *Chalfie*, GFP was used to monitor, among other things, gene expression, which was rewarded with a noble prize in 2008.<sup>[6, 9]</sup> Considering biomolecules other than proteins, e.g. glycans, lipids and nucleic acids, this strategy is not applicable because the relatively large size of GFP might affect the target molecule’s function, which led to the development of bioorthogonal chemistry.<sup>[10]</sup>

This work focuses on bioorthogonal modification of nucleosides and oligonucleotides by means of photoclick reaction and strain-promoted sydnone alkyne cycloaddition.

The first part comprises the synthesis and incorporation of a tetrazole-modified ribonucleoside into two different oligonucleotides *via* solid-phase synthesis, followed by investigation of the photoclick reaction between the tetrazole and dye maleimide conjugates by UV/vis absorbance and fluorescence spectroscopy. The optical properties of the reaction should be adjusted by employing a *FRET* between the formed pyrazoline as a donor and the different dye maleimide conjugates as

## 1 Aim and Motivation

---

acceptors. This work focuses on investigating and identifying the most suitable conditions for future cellular applications of the system.

The second part investigates the applicability of bioorthogonal labeling techniques with sydnones on nucleic acids and describes the synthesis of three different sydnone-modified nucleosides, followed by employing them in either a strain-promoted sydnone alkyne cycloaddition or the photoclick reaction. The reactions were monitored by spectroscopic methods and analytical HPLC. Additionally, the results of the strain-promoted sydnone alkyne cycloaddition should be transferred to sydnone-modified oligonucleotides and the applicability of the reaction investigated in fixed *HeLa* cells.

## 2 Theoretical Background

---

### 2.1 Bioorthogonal Labeling

In the early 2000s, the term “Bioorthogonal Chemistry” was first introduced by the group of *Bertozzi*.<sup>[11]</sup> Ever since, bioorthogonal reactions have emerged as a versatile tool to label biomolecules such as proteins, glycans, lipids and nucleic acids. A bioorthogonal reaction follows the general process of modifying one building block of a biomolecule of interest with a bioorthogonal reporter - a chemical functionality which should ideally not be present in the biological system -, incorporation into the biomolecule by chemical or natural pathways, followed by reaction with a probe molecule offering the complementary chemical functionality and a label, e.g. a chromophore (Figure 1).<sup>[12-13]</sup>

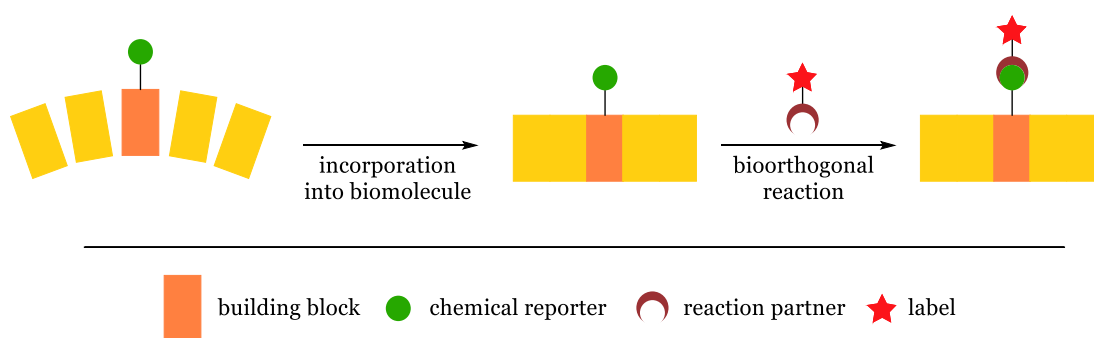


**Figure 1.** Schematic representation of bioorthogonal labeling. After incorporation of a building block (orange) modified with a chemical reporter (green) into a biomolecule of interest (yellow), the chemical reporter reacts with its reaction partner (brown), which is modified with e.g. a chromophore (red).

In addition, there are a few prerequisites<sup>[12-14]</sup> a reaction needs to fulfill to be classified as bioorthogonal reaction: (i) starting materials, products and potential side-products should be non-toxic and stable in a cellular environment, (ii) the chemical reporter and the reaction partner should react highly selective and in high yield with each other under physiological conditions (neutral pH, physiological temperature, aqueous medium) to avoid side-reactions with naturally occurring cell components, (iii) as the reagents are naturally occurring in rather low concentrations in biological environment, and bioorthogonal labeling reactions typically follow second-order kinetics, they should offer high rate constants to ensure efficient labeling. Furthermore, a high rate constant prevents problems regarding the solubility and toxicity of the used reagents.<sup>[12-13]</sup> Most of these criteria

## 2 Theoretical Background

match with the “Click Chemistry” approach that *Sharpless et al.*<sup>[15]</sup> established, and during the past two decades, a couple of reactions that meet these criteria have been developed and applied to biomolecules. The most noteworthy are strain-promoted azide-alkyne cycloadditions (SPAAC), photoclick-type reactions, copper-catalyzed azide-alkyne cycloadditions (CuAAC), and inverse electron-demand *Diels-Alder* cycloadditions (iEDDA). Figure 2 displays the general course of each mentioned reaction and their corresponding range of reaction rates.<sup>[14]</sup>

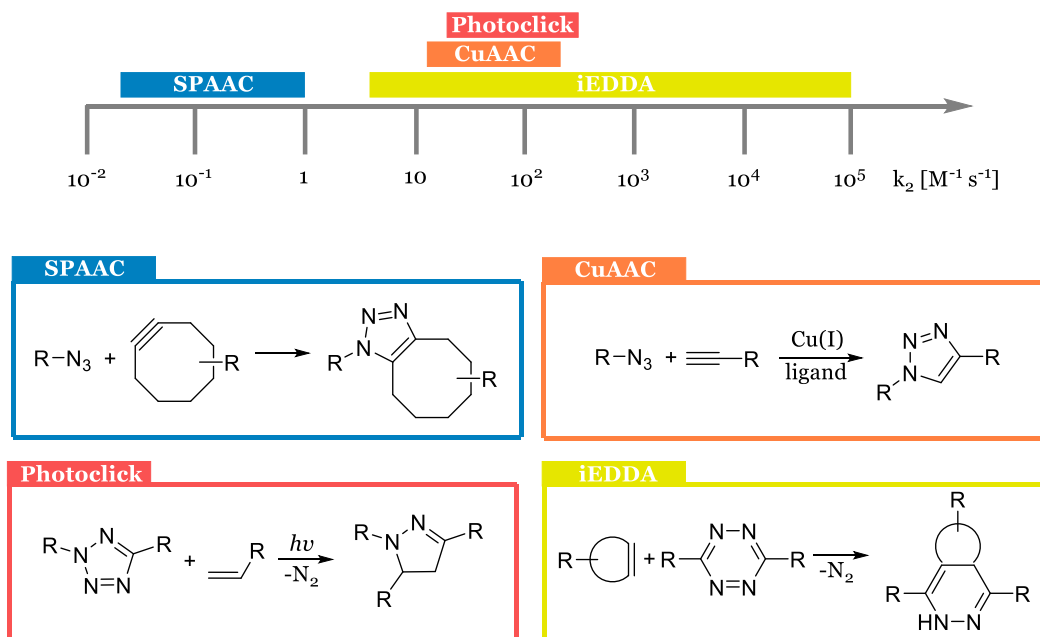


**Figure 2.** Overview of commonly used bioorthogonal labeling methods and their respective margin of rate constants.<sup>[14]</sup>

One of the first and fastest (up to  $k_2 = 200 \text{ M}^{-1} \text{ s}^{-1}$ )<sup>[14]</sup> methods that was employed for labeling of biomolecules is the CuAAC. The underlying reaction dates back to the 1960s, when *Huisgen* first discovered a set of 1,3-dipolar cycloadditions, azide-alkyne cycloadditions being one of them.<sup>[16-18]</sup> Azides are practically absent in living systems and stable under physiological conditions, additionally organic azides have not been reported to be cell-toxic which makes them a suitable reagent for bioorthogonal labeling strategies.<sup>[19]</sup> However, the reaction needed elevated temperatures to proceed which made it unsuitable for bioorthogonal labeling until its improvement by the groups of *Sharpless* and *Meldal* in 2002.<sup>[20-21]</sup> Both groups reported independently of each other that the use of copper(I) salts as catalyst lead to high conversion of various azides and alkynes to the resulting triazoles even at room temperature.<sup>[20-21]</sup> Furthermore, the reaction was reported to exhibit a high

## 2 Theoretical Background

---

regioselectivity to produce 1,4-disubstituted 1,2,3-triazoles almost exclusively.<sup>[20-21]</sup> Ever since, this technique has been used to modify numerous molecule classes including nucleic acids, glycans, proteins, and lipids.<sup>[22-26]</sup> Considering nucleic acids, the building blocks can bear both the alkyne and the azide functionality. The modifications can be attached to e.g. either the base (5-position in pyrimidines,<sup>[27-29]</sup> 7-position in 7-deazapurines as purine analogues)<sup>[30-31]</sup> or the 2'-position of the sugar moiety.<sup>[32-35]</sup> The incorporation of the azide-modified building block into oligonucleotide strands, however, is limited, as the azide moiety can react with phosphorus(III) compounds that are commonly used in standard solid phase phosphoramidite synthesis.<sup>[33, 36-37]</sup> This limitation can be overcome by using phosphodiester building blocks instead of phosphoramidites,<sup>[33, 37]</sup> postsynthetic *in situ* formation of the azide<sup>[27]</sup> or enzymatic<sup>[30]</sup> and even metabolic<sup>[38]</sup> incorporation of the azide-modified building block. Although a few examples of CuAAC labeling in living cells<sup>[39-40]</sup> have been reported during the past few years, the use of this reaction type in living systems is generally limited. Commonly used reagents for CuAAC include Cu(II) salts (e.g. CuSO<sub>4</sub>) and a reducing agent (e.g. sodium ascorbate) for *in situ* formation of the required Cu(I) ion. Both reagents can lead to the formation of *reactive oxygen species* (ROS) which cannot only lead to damage of proteins, nucleic acids and lipids, but furthermore might also contribute to diseases such as diabetes, *Parkinson's* disease, and cervical cancer.<sup>[41-44]</sup> The damaging effects could be notably reduced by employing copper-chelating ligands such as tris((1-benzyl-1H-1,2,3-triazol-4-yl)methyl)amine (TBTA),<sup>[45-46]</sup> tris(hydroxypropyltriazolyl)-methylamine (THPTA),<sup>[47]</sup> and bathophenanthroline disulfonate disodium salt (BPS),<sup>[48]</sup> but nevertheless these copper-ligand complexes display a considerably high toxicity towards cells, in case of the TBTA and the BPS complexes even higher than unligated copper.<sup>[49]</sup> On this premise, research was considerably shifted towards development of copper-free labeling techniques such as the previously mentioned iEDDA, SPAAC, and photoclick-type cycloadditions. Regarding the relevance to this work, only the latter two types will be discussed in detail.

## 2.2 Copper-Free Labeling techniques

### 2.2.1 Strain-Promoted Azide-Alkyne Cycloaddition (SPAAC)

The reaction between strained alkynes and azides (Figure 3) was first described by *Blomquist* and *Liu* in 1952 as they described that cyclooctyne and phenyl azide reacted explosively.<sup>[50]</sup>

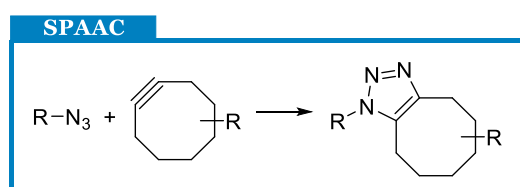


**Figure 3.** General reaction scheme of the strain-promoted azide-alkyne cycloaddition (SPAAC): an azide reacts with a strained alkyne, e.g. a cyclooctyne, to form a triazole.

After further investigation of the reaction, *Wittig* and *Krebs* identified the product as a triazole.<sup>[51]</sup> Nearly half a century later, the group of *Bertozzi* was the first to employ the reaction between azides and strained alkynes in a bioorthogonal manner by synthesis of a biotinylated cyclooctyne derivative followed by reaction with an azido-modified sugar for glycan labeling.<sup>[52]</sup> However, with rate constants of  $k_2 = 1.1 \times 10^{-3} \text{ M}^{-1}\text{s}^{-1}$  -  $2.4 \times 10^{-3} \text{ M}^{-1}\text{s}^{-1}$ , depending on the used azide, the reaction is considerably slow compared to the CuAAC.<sup>[52-53]</sup> Additional to the structure of the used azide, the solvent used for carrying out the reaction plays an important role, as water was reported to accelerate 1,3-dipolar cycloadditions when compared to e.g. methanol or acetonitrile.<sup>[54]</sup> This makes reported reaction rates in varying solvents only comparable to limited extent. As described before (Chapter 2.1), a higher rate constant is favorable for bioorthogonal labeling, as the reagent concentrations should be maintained low to prevent toxicity and solubility issues.<sup>[12-13]</sup> This led to the development of new strained alkynes (Figure 4) that offer faster reaction rates while still maintaining a reasonable stability.<sup>[55]</sup> The reported compounds feature a cyclooctyne core, as that is the smallest stable, but still reactive cyclic alkyne that can be modified in different ways to increase the reactivity.<sup>[55-56]</sup>

## 2 Theoretical Background

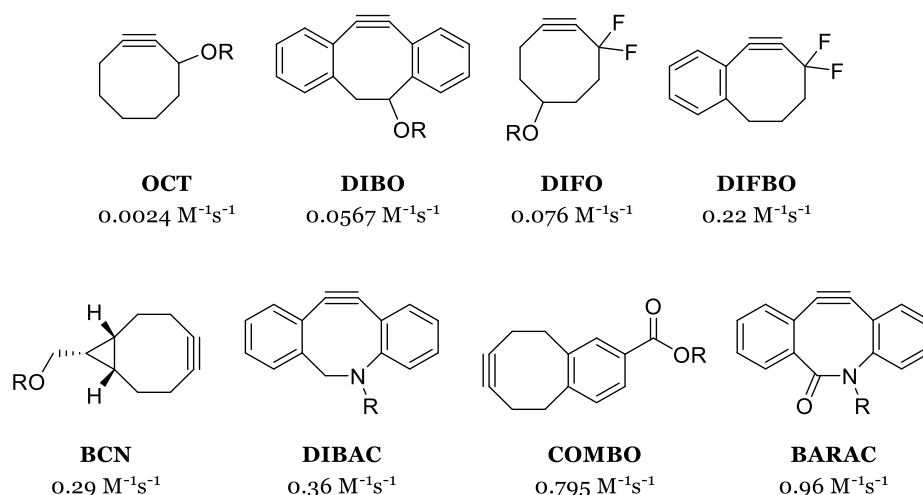


**Figure 4.** Strained cyclooctyne derivatives for SPAAC and their respective rate constants for reaction with benzyl azide in acetonitrile/water (ratios given in parentheses). Cyclooctyne (**OCT**, 1/0),<sup>[52-53]</sup> dibenzocyclooctyne (**DIBO**, MeOH),<sup>[57]</sup> difluorocyclooctyne (**DIFO**, 1/0),<sup>[58]</sup> difluorobenzocyclooctyne (**DIFBO**, 1/0),<sup>[59]</sup> bicyclononyne (**BCN**, 1/2),<sup>[60]</sup> dibenzoazacyclooctyne (**DIBAC**, 0/1),<sup>[61]</sup> carboxymethylmonobenzocyclooctyne (**COMBO**, 4/3),<sup>[62]</sup> and biarylazacyclooctyne (**BARAC**, 1/0).<sup>[63]</sup>

To achieve this, either electron-withdrawing substituents such as a geminal difluoro group (**DIFO**, **DIFBO**) or cyclopropyl (**BCN**) or phenyl rings (**DIFBO**, **DIBO**, **DIBAC**, **BARAC**, **COMBO**) can be added to the **OCT** core. In the latter case, the reactivity is enhanced by the increased number of  $\text{sp}^2$ -hybridised carbons leading to higher ring strain, which correlates to the bond angle of the alkyne.<sup>[55]</sup> This can also be achieved by incorporating heteroatoms into the system, as in **DIBAC** or **BARAC**.<sup>[55]</sup> The downside to this concept is both the increasing lipophilicity and steric hindrance which can make the SPAAC in aqueous, living systems difficult.<sup>[55]</sup> A solution to this was the development of **BCN** by the group of *van Delft* in 2010.<sup>[60]</sup> The two-step synthetic procedure yielded endo- and exo-**BCN**, whereas endo-**BCN** resulted in higher rate constants up to  $k_2 = 0.29 \text{ M}^{-1}\text{s}^{-1}$  which is 120-fold higher than the rate constant of **OCT**.

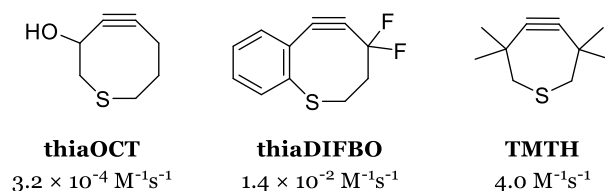


**Figure 5.** Thiacycloalkynes reported by *Bertozzi et al.* for SPAAC labeling. The rate constants were determined by reaction with benzyl azide in acetonitrile.

Another approach by *Bertozzi et al.* was the incorporation of sulfur into different cycloalkyne rings.<sup>[56]</sup> They synthesized three new thiacycloalkynes **thiaOCT**,

## 2 Theoretical Background

**thiaDIFBO**, and **TMTH** and investigated their respective reactivity towards azides (Figure 5). Compared to the parent compounds **OCT** and **DIFBO**, the reaction proceeded considerably slower. However, in case of **thiaDIFBO** no polymerization occurred as reported with the parent compound **DIFBO**.<sup>[56, 59]</sup> The resulting lower reaction rate constant is related to the bond length of a sulfur-carbon bond ( $sp^3$ , 1.81 Å) which is slightly longer than a carbon-carbon bond ( $sp^3$ , 1.54 Å) and therefore reduces the ring strain.<sup>[56]</sup> By including the sulfur atom into a cycloheptyne ring, stabilization of the usually instable cycloheptynes was achieved and lead to a comparably high reaction rate of  $k_2 = 4.0 \text{ M}^{-1}\text{s}^{-1}$  which is presumably the highest achieved rate constant up to this point.

In terms of nucleic acids, several modifications with cyclooctyne derivatives were reported, including **OCT** and **DIBO** as base surrogates,<sup>[64-65]</sup> and **DIFO**, **DIBO**, and **BCN** at the 5-position of pyrimidine bases and 2'-position of the sugar moiety.<sup>[66-68]</sup> As for the azides, the previously described building blocks (chapter 2.1) can also be used for SPAAC labeling. *Luedtke et al.* synthesized a 5-azidomethyl-2'-deoxyuridine that was incorporated metabolically into *HeLa* cells and after fixation, the cells were modified by either CuAAC or SPAAC reaction. Even *in vivo* labeling was achieved by *Wagenknecht et al.* with a **COMBO**-modified building block and an azido-modified fluorescent dye in *HeLa* cells and by the group of *Bertozzi* even in zebrafish and mice.<sup>[69-71]</sup>

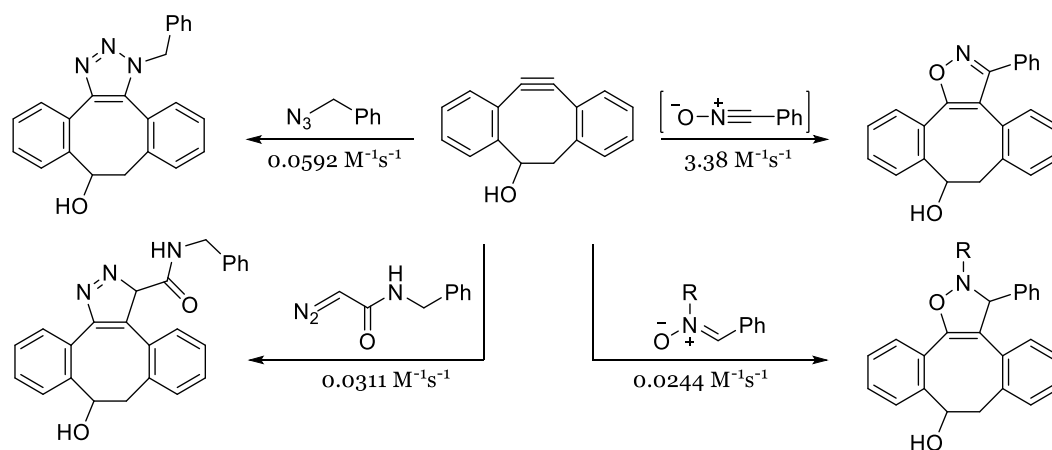


**Figure 6.** Reaction products and rate constants of the reaction of **DIBO** with different dipoles in methanol.<sup>[72]</sup>

Additionally, strained cycloalkynes were also found to be reactive towards other dipoles, such as *in situ* generated nitrile-oxides,<sup>[64, 72-73]</sup> nitrones<sup>[60, 72-75]</sup> and diazo compounds.<sup>[72-73, 76]</sup> *Boons et al.* compared the different dipoles and measured their

## 2 Theoretical Background

respective rate constants for reaction with **DIBO** (Figure 6).<sup>[72]</sup> The reaction with the *in situ* generated nitrile-oxide lead to a second-order rate constant of  $3.38 \text{ M}^{-1}\text{s}^{-1}$  which is almost 60 times higher than the rate constant of the addition with benzyl azide ( $k_2 = 0.0592 \text{ M}^{-1}\text{s}^{-1}$ ). The reaction with diazo compounds and nitrones was of comparable reaction rate to the azide, albeit slightly lower. However, the rate constant is highly dependent of both the alkyne and the dipole. The group of *Pezacki* synthesized a set of nitrones with different electronic properties and determined the rate constants in a model reaction with benzannulated cyclooctyne in benzene, reaching rate constants up to  $1.5 \text{ M}^{-1}\text{s}^{-1}$ .<sup>[74]</sup> *Van Delft et al.* showed that similar results can be reached in a reaction between **BCN** and a nitron, leading to rate constants up to  $1.66 \text{ M}^{-1}\text{s}^{-1}$ , which is significantly higher than the reaction with benzyl azide.<sup>[60]</sup>

### 2.2.2 Strain-Promoted Sydnone-Alkyne Cycloaddition (SPSAC)

Another class of molecules that emerged during the past few years for bioorthogonal labeling are sydnones (Figure 7). Sydnones are mesoionic compounds that were found to be stable under physiological conditions, which enables them for use in a bioorthogonal manner.

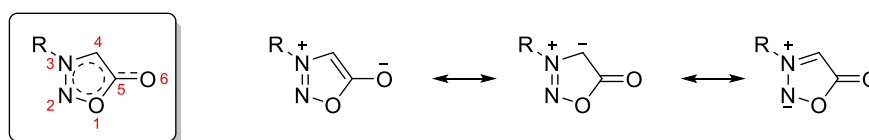


**Figure 7.** Different resonance structures of sydnones.<sup>[77]</sup>

The first example was reported by the group of *Taran* in 2013 and demonstrated the labeling of *BSA* by reaction of a sydnone with a terminal alkyne in a CuAAC-type reaction.<sup>[78]</sup> As this offered very little improvement in terms of bioorthogonal labeling, the reactivity of sydnones towards strained alkynes was investigated and found to be suitable for bioorthogonal labeling (Figure 8).

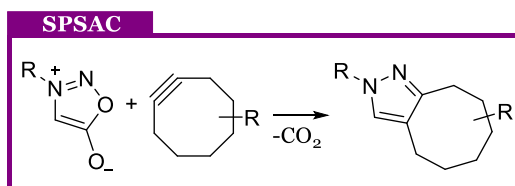
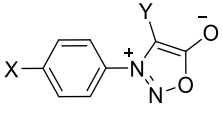


**Figure 8.** General reaction scheme of the strain-promoted sydnone-alkyne cycloaddition (SPSAC): a sydnone reacts with a strained cycloalkyne under carbon dioxide extrusion to form a pyrazoline.<sup>[79]</sup>

## 2 Theoretical Background

Both the groups of *Chin* and *Taran* reported the reactivity of phenyl sydnone towards **BCN**.<sup>[79-80]</sup> The modification of proteins was demonstrated by both groups by incorporating either the sydnone-moiety into *BSA*<sup>[79]</sup> or **BCN** into *sfGFP*,<sup>[80]</sup> followed by reaction with **BCN-TAMRA** or a **BODIPY**-sydnone, respectively. Furthermore, the group of *Taran* investigated the dependence of the rate constant of the substitution pattern of the sydnone core (Table 1).<sup>[79]</sup> Electron-donating substituents at the 3-N position decreased the rate constant compared to the unmodified phenyl sydnone (entry 1 vs. 2), whereas electron-withdrawing substituents such as carboxy, trifluoromethyl and nitro groups accelerated the reaction 2 to 10-fold (entries 3-5). As for the modifications on the 4-position, halogen substituents increased the reaction rate, whereas other electron-withdrawing substituents such as a nitrile group drastically decreased the rate constant (entries 8-10 vs. 7). The combination of electron-withdrawing substituents at the 3-position and a halogen at the 4-position lead to rate constants up to 1.593 M<sup>-1</sup>s<sup>-1</sup>. Compared to the reaction of **BCN** with azides, the sydnone-alkyne cycloaddition proceeds significantly faster, and the same trend could be observed with various other strained alkynes.

Table 1. Influence of different substituents on the rate constant of SPSAC.<sup>[79]</sup>



entry	X	Y	k <sub>2</sub> [M <sup>-1</sup> s <sup>-1</sup> ]	entry	X	Y	k <sub>2</sub> [M <sup>-1</sup> s <sup>-1</sup> ]
1	OMe	H	0.006	7	H	CN	0.003
2	H	H	0.027	8	H	I	0.306
3	COOH	H	0.059	9	H	Br	0.592
4	CF <sub>3</sub>	H	0.199	10	H	Cl	0.872
5	NO <sub>2</sub>	H	0.289	11	COOH	Br	0.798
6	H	C <sub>6</sub> H <sub>5</sub>	0.018	12	COOH	Cl	1.593

The groups of *Houk* and *Murphy* calculated activation free energies for different sydnone-alkyne cycloadditions and validated the results experimentally.<sup>[81]</sup> The most promising results were achieved by reaction of phenyl sydnone with **DIBAC** and **BARAC** with reaction rate constants of 0.902 M<sup>-1</sup>s<sup>-1</sup> and 1.46 M<sup>-1</sup>s<sup>-1</sup> respectively. Furthermore, they showed that sydnone-alkyne cycloadditions could be employed orthogonally to tetrazine-norbornene *Diels-Alder* cycloadditions. The reaction rate was even further enhanced by fluorinating the sydnone instead of

## 2 Theoretical Background

---

chlorinating it, leading to rate constants of  $42 \text{ M}^{-1}\text{s}^{-1}$  (**BCN**),  $900 \text{ M}^{-1}\text{s}^{-1}$  (**DIBAC**) and  $1500 \text{ M}^{-1}\text{s}^{-1}$  (**TMTH**).<sup>[82]</sup>

Great progress has also been achieved during the past few years in terms of fluorogenic labeling with sydnone. The group of *Friscourt* investigated the reaction of differently substituted sydnone with the previously reported fluorogenic strained cycloalkyne **Fl-DIBO**.<sup>[83-84]</sup> Upon reaction with an azide, a remarkable 1000-fold fluorescence enhancement (FE) could be achieved.<sup>[83]</sup> Reaction with a chlorinated sydnone lead to a 235-fold FE (Figure 9), and was used for visualization of bioorthogonally labeled *BSA*.<sup>[84]</sup>

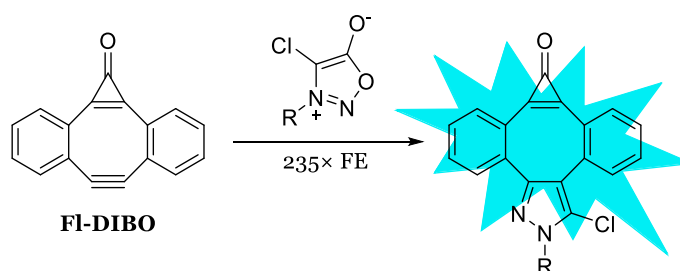


**Figure 9.** Reaction between Fl-DIBO and a chlorinated sydnone lead to 235-fold fluorescence enhancement (FE).

Another approach investigated the fluorescence quenching ability of sydnone in combination with coumarin.<sup>[85]</sup> The quenching of the fluorescence of coumarin by several functionalities, including azides<sup>[86]</sup> and alkynes<sup>[87-88]</sup> has been demonstrated in literature before. Upon reaction with the opposite functionality, the quenching was reversed, leading to a significant *turn-on* effect. The group of *Friscourt* investigated the quenching behavior of sydnone and observed a significant quenching effect on the coumarin moiety ( $\Phi_{\text{FCoumarin}} = 0.03$ ,  $\Phi_{\text{FCoumarinsydnone}} = 0.005$ ), which lead to a 132-fold FE upon reaction with **BCN** ( $\Phi_{\text{FPyrazole}} = 0.66$ ). Another remarkable property of sydnone that has been investigated recently is photoactivation, which will be discussed in chapter 2.2.3. Up to this point, SPSAC has not been demonstrated on nucleic acids.

### 2.2.3 Light-Induced Bioorthogonal Reactions

The great disadvantage of the previously mentioned methods to modify biomolecules is the lack of spatiotemporal control, as the reagents react spontaneously without a specifically chosen starting point. Considering the visualization of highly dynamic biological processes, this might lead to reaction before the modified compounds even reach their cellular destination. A solution to overcome this problem is the use of light to induce the desired reaction. Albeit organic photochemistry has been of great interest for more than one century, it has only been employed for bioorthogonal labeling for the past decade. Photocontrollable reactions in biomolecules can be generally classified into three subtypes: (i) photo-isomerization for reversible regulation of biomolecules, (ii) photo-induced formation of bonds, (iii) photo-activated *in situ* generated reactive species that can undergo further reaction.<sup>[89]</sup> The latter type is the most commonly used in terms of bioorthogonal labeling where photoclick-type reactions and photo-SPAAC reactions are the most established examples and will be discussed below.

#### 2.2.3.1 Photoclick-type Cycloadditions

One of the first light-induced bioorthogonal labeling methods is the photoclick reaction between an upon irradiation of a tetrazole generated nitrile-imine and an electron-deficient alkene (Figure 10).

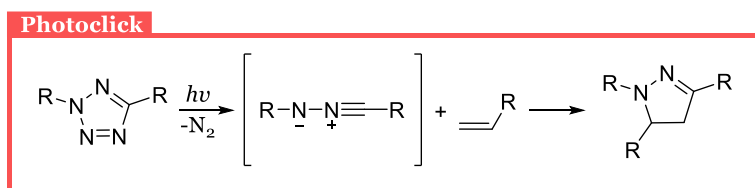


**Figure 10.** General reaction scheme of the nitrile-imine/alkene photoclick reaction: upon irradiation, a diaryltetrazole releases nitrogen to form a nitrile-imine that reacts with an electron-deficient alkene to a fluorescent pyrazoline.<sup>[90]</sup>

The underlying reaction mechanism again dates back to the studies of *Huisgen*, who reported the release of nitrogen upon heating (150 °C) as well as UV-irradiation (high pressure mercury lamp) of a diaryltetrazole <sup>[91]</sup> However, this reaction was not applied for bioorthogonal chemistry until about four decades later the group of *Lin* reported the modification of proteins by means of photoclick reaction.<sup>[90, 92]</sup> They first synthesized a diaryltetrazole that was afterwards fused to lysozyme. The photoclick reaction was induced by irradiation with light of a simple

## 2 Theoretical Background

---

hand-held UV lamp ( $\lambda = 302$  nm), followed by reaction with acrylamide as an electron-deficient reaction partner.<sup>[90]</sup> Even live cell imaging was achieved by incorporating an allyl phenyl ether as alkene functionality into *E. coli*, followed by photoclick reaction with different diaryltetrazoles.<sup>[92]</sup> Due to the natural fluorogenicity of the reaction by formation of an intrinsically fluorescent pyrazoline, imaging of the labelled cells could be achieved without employing further fluorescent markers.<sup>[92]</sup> In both cases, the photolysis was described to be very rapid with a first order rate constant of  $k_1 = 0.14$  s<sup>-1</sup>, whereas the second order rate constant is highly dependent of the employed alkene.<sup>[90, 92]</sup> In case of acrylamide as a reaction partner, rate constants up to  $k_2 = 11.0$  M<sup>-1</sup>s<sup>-1</sup> could be observed, making it at least two magnitudes faster than SPAAC with commonly used strained alkynes.<sup>[90]</sup> The photoclick reaction, as 1,3-dipolar cycloadditions in general, was found to be inversely dependent of the HOMO/LUMO gap energy between the dipole and the dipolarophile.<sup>[93-94]</sup> As a result of this, the reaction can be accelerated by lifting the HOMO of the dipole or lowering the LUMO of the dipolarophile. The latter case can be achieved by adding either ring strain or electron-withdrawing substituents to the alkene. In terms of the photoclick reaction, the second strategy is commonly used to keep the alkene comparably small, leading to electron-deficient alkenes such as methyl methacrylate, dimethyl fumarate, acrylamide, and N-methyl maleimide as the reaction partner of choice. Apart from alkenes, electron-deficient alkynes were also found to be reactive towards nitrile-imines, but received only little attention in literature.<sup>[95]</sup>

The group of *Lin* further investigated how lifting of the HOMO of the dipole could be achieved and how the rate constant was influenced by this.<sup>[94]</sup> They synthesized different tetrazoles bearing electron-pushing or -pulling substituents at either the N- or C-phenyl ring, calculated the corresponding HOMO energies and compared it with the rate constants that were measured for the reaction of the different tetrazoles with 4-penten-1-ol as dipolarophile. Generally, electron-withdrawing substituents such as ester and nitrile groups at both the N- and the C-phenyl ring decreased the HOMO energy as well as the corresponding rate constant significantly (one to two magnitudes, depending on substituent and position) compared to unsubstituted diaryltetrazole. Electron-donating groups showed the opposite behavior, as they were observed to increase both the HOMO energy and the rate constant. In case of modification of the C-phenyl ring with methyl or

## 2 Theoretical Background

---

methoxy groups, the rate constant was only increased very slightly compared to the unmodified tetrazole. The modification of the N-phenyl ring with the same groups however led to a 2 to 4-fold acceleration, respectively. Furthermore, these results were confirmed by *in vivo* experiments with methoxy-modified diaryltetrazole and *E. coli* cells expressing alkene-Z proteins, leading to a fluorescent signal within 30 s irradiation time, which could not be achieved with unmodified diaryltetrazole.<sup>[94]</sup> Additionally, substitution also affects the activation wavelength of the photoclick reaction. The previously mentioned examples typically use light of  $\lambda = 302$  nm to induce the photoclick reaction. Considering the typical absorbance window of biomolecules, especially nucleic acids, this can lead to severe damages such as e.g. T-T-dimers and oxidative damage, resulting in alteration of cellular mechanisms including protein synthesis. Thus several groups developed tetrazoles that could be activated with light of longer wavelengths.<sup>[96-98]</sup> The group of *Lin* modified the para position of the N-phenyl ring of the diaryltetrazole core with either auxochromic groups such as amino or dimethylamino groups or conjugative groups such as a styryl group which lead to significant bathochromic shifts up to 60 nm.<sup>[99]</sup> Furthermore, this complied with the activation wavelength needed to initiate the reaction, as the photoclick reaction using these modified tetrazoles was successfully carried out by irradiation with light of  $\lambda = 365$  nm, whereas the parent compound did not undergo any reaction under this condition. However, in most cases the yields of the reaction upon 302 nm irradiation were higher than upon 365 nm irradiation, which could be attributed to the fact that the formed pyrazolines absorb light around 365 nm, thus creating a filtering effect leading to decreased conversion rates.<sup>[99]</sup> Even visible light activation could be achieved by changing the phenyl rings to either larger aromatic systems such as pyrene (410-420 nm excitation)<sup>[100-101]</sup> or naphthalene (700 nm two-photon excitation).<sup>[102]</sup> Another approach was to interchange the phenyl rings with an oligothiophene moiety which led to an excitation wavelength of  $\lambda = 405$  nm.<sup>[103-104]</sup>

Aside from protein modification, the photoclick reaction has also been used several times to label oligonucleotides. The first example was the postsynthetic modification of a DNA strand bearing a diaryltetrazole with a sulfo-Cy3 maleimide dye that was reported by our group in 2014.<sup>[105]</sup> The *N,N*-dimethylamino modified tetrazole was attached to a 2'-deoxyuridine building block at the 5-position *via* a C3-linker (Figure 11, left). The photoclick reaction could be initiated by irradiation

## 2 Theoretical Background

with  $\lambda = 365$  nm light and led to 34% labeling yield, the rate constant was determined to be  $k = 23 \pm 7 \text{ M}^{-1}\text{s}^{-1}$ . Both the yield and the rate constant of the reaction could be considerably improved by omitting the linker and attaching the tetrazole moiety directly to the 5-position of 2'-deoxyuridine (Figure 11, right) as demonstrated by our group in 2018, leading to 62% yield and a rate constant of  $k = 67 \pm 6 \text{ M}^{-1}\text{s}^{-1}$ .<sup>[106]</sup>

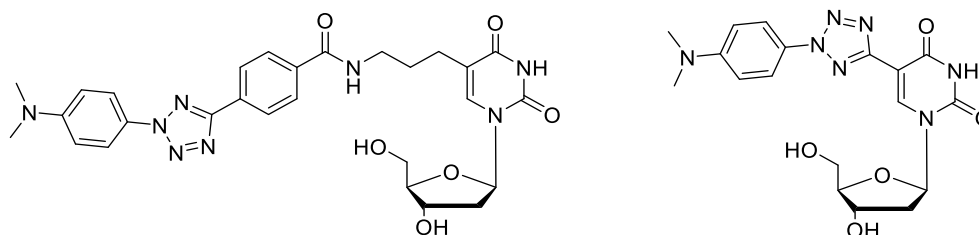


**Figure 11.** Structures of nucleosidic building blocks bearing *N,N*-dimethylamino-modified tetrazoles for photoclick reaction.<sup>[105-106]</sup>

The same work showed that yield and rate constant could be increased even further by substituting the *N,N*-dimethylamino moiety with a bromine group, leading to 74% yield and a rate constant of  $k = 89 \pm 13 \text{ M}^{-1}\text{s}^{-1}$  at an initiation wavelength of  $\lambda = 300$  nm. Both building blocks were incorporated into DNA strands either *via* solid-phase synthesis or enzymatically by primer extension.<sup>[105-108]</sup> Another example by the group of *Zhou* incorporated both the tetrazole and the alkene moiety into the same molecule, leading to a highly fluorescent pyrazoline upon reaction without the need of any additional fluorescent markers.<sup>[109]</sup> Apart from incorporating the tetrazole moiety into the oligonucleotide, the incorporation of the alkene moiety has also been demonstrated several times. The group of *Rentmeister* modified a guanosine with a vinyl group and, after incorporation into an oligonucleotide as a 5'-mRNA cap, performed a photoclick reaction with a diaryltetrazole, presenting the first example of RNA labeling by photoclick reaction.<sup>[110]</sup> The groups of *Zhang* and *Xing* incorporated 5-vinyl-2'-deoxyuridine into cellular DNA in A549 cells by a metabolic pathway, followed by photoclick reaction ( $\lambda = 350$  nm) with a water-soluble coumarin-fused tetrazole, leading to a high fluorescence both in living cells and zebrafish.<sup>[111]</sup>

Apart from tetrazoles, azirines and sydnone were reported to undergo photoclick-type reactions upon irradiation. In relevance to this work, only the latter will be discussed. The photolysis of sydnone has already been investigated in the late

## 2 Theoretical Background

---

1960s and early 1970s: upon irradiation, the sydnone moiety rearranges to a diazirine under extrusion of carbon dioxide, followed by further reaction to the highly reactive nitrile-imine intermediate (Figure 12).<sup>[112-114]</sup> The following cycloaddition step is identical to the previously described tetrazole-alkene photoclick reaction, leading to fluorescent pyrazoline or pyrazole moieties.<sup>[113]</sup>

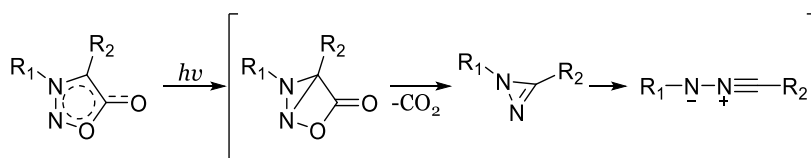


**Figure 12.** Reaction mechanism of sydnone photolysis: a diazirine is formed under extrusion of carbon dioxide, which reacts further to a nitrile-imine.<sup>[112-114]</sup>

The sydnone-alkene photoclick reaction received little attention in bioorthogonal chemistry until 2018, when the group of Yu reported the labeling of proteins by photoclick-type reaction between diarylsydnes and alkenes.<sup>[115]</sup> Similar to the tetrazoles, the optical properties of the sydnes can be changed by electron-donating and -withdrawing substituents at the N3 and C4 phenyl rings respectively, leading to a bathochromic shift. Furthermore, this substitution pattern is beneficial to the reactivity, as the diarylsydnone bearing a methoxy group at the N3 phenyl ring and a trifluoro methyl group at the C4 phenyl ring led to the highest yield (83%, 60 s irradiation at  $\lambda = 311$  nm) compared to differently substituted diarylsydnes.<sup>[115]</sup> As an example for a bioconjugation reaction using the diarylsydnone photoclick reaction, a TCO-modified lysozyme was incorporated into sfGFP and upon treatment with the previously mentioned sydnone irradiated at  $\lambda = 311$  nm, leading to 14% yield.<sup>[115]</sup> Further work by the group of Yu investigated the orthogonality of the diarylsydnone photoclick reaction and the previously described SPSAC reaction towards strained alkynes.<sup>[116]</sup> The reactivity was tuned in favor of the diarylsydnone photoclick reaction by employing a methoxy group at the N3 phenyl ring and a naphthalene ring bearing a methyl carboxylate group instead of a phenyl ring at the C4 position. Another benefit of this substitution pattern was the bathochromic shift, enabling irradiation at  $\lambda = 405$  nm. The viability of the system was even demonstrated on living A549 cells, where the photoirradiated cells showed significant fluorescence, while the samples that were left in the dark did not show any signal.<sup>[116]</sup> While most of the criteria for bioorthogonal reactions, such as fast reaction kinetics and non-toxic reagents and

## 2 Theoretical Background

byproducts are met excellently by the photoclick-reaction, the selectivity of nitrile-imines towards alkenes while other nucleophiles are present was in some cases reported as rather low.

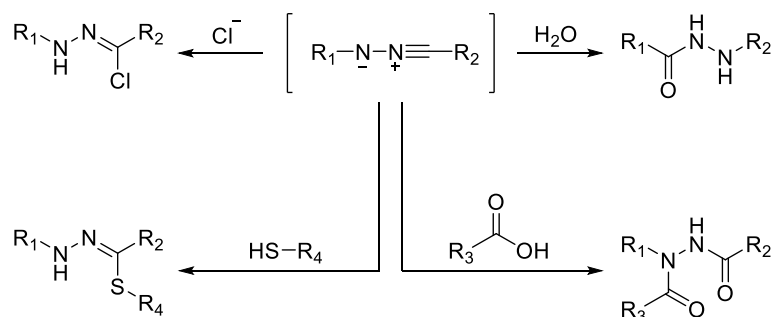


**Figure 13.** The highly reactive nitrile-imine species shows reactivity towards chloride, thiols, carboxylic acids, and water.<sup>[117-120]</sup>

There were a few examples reported in literature that showed cross-reactivity with moieties that are present in cellular environment (Figure 13), such as chloride,<sup>[117]</sup> thiols,<sup>[118]</sup> carboxylic acids,<sup>[119-120]</sup> and water,<sup>[117]</sup> which might decrease the labeling efficiency when alkenes are the favored reaction partner. Nevertheless, as mentioned before, nitrile-imine based photoclick reactions were already applied successfully in living cells, proving the suitability of the reaction for bioorthogonal labeling, even though side-reaction may occur.<sup>[111, 116]</sup>

### 2.2.3.2 Photo-SPAAC

Another example of a photoactivated bioorthogonal reaction is the photo-activated strain-promoted azide alkyne cycloaddition. The reaction is a more spatiotemporally controllable advancement to the classical SPAAC, as the reactive alkyne moiety is masked by a cyclopropanone group.

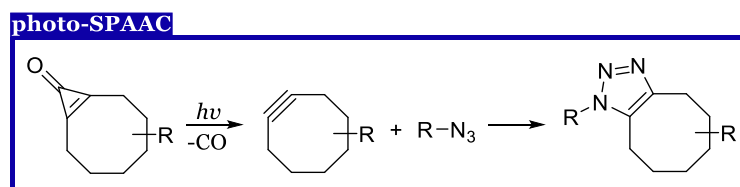


**Figure 14.** General reaction scheme of the photo-activated strain-promoted azide alkyne cycloaddition: the reactive alkyne species is masked by a cyclopropanone moiety which can be removed by irradiation with light of  $\lambda = 350$  nm, followed by cycloaddition with an azide to form a triazole.<sup>[121]</sup>

Upon irradiation with light ( $\lambda = 350$  nm), decarbonylation to the alkyne occurs which can afterwards react with an azide to a triazole (Figure 14). The presumably

## 2 Theoretical Background

first example by the groups of *Popik* and *Boons* in 2009 showed that a cyclopropenone-masked dibenzocyclooctyne derivative did not display any reactivity towards azides, whereas upon irradiation a cycloaddition to an triazole took place, making it possible to control the start point of the reaction.<sup>[121]</sup> Furthermore, they demonstrated that the reaction was also suitable for cellular environments by introducing an azide group into the cell surface of Chinese hamster ovary cells and afterwards performing reaction with biotinylated dibenzocyclooctyne. The results showed that upon irradiation of the samples by light, followed by incubation with avidin-AlexaFluor488, produced a fluorescent signal at the cell surface. However, the samples that were left in the dark only showed negligible fluorescence.<sup>[121]</sup> The concept was further improved by incorporating two cyclopropenone-masked alkyne moieties into one molecule by the group of *Popik*.<sup>[122]</sup> Depending on the irradiation time and wavelength, the cyclopropenone moieties could be cleaved independently of each other, leading to one masked alkyne and one reactive alkyne moiety. The latter was reacted with an azide to form the triazole moiety, followed by a second decarbonylation upon irradiation. Because of the additional ring strain caused by the triazole, the second cycloaddition proceeds with a substantially faster reaction rate of  $k = 34 \text{ M}^{-1}\text{s}^{-1}$  compared to the reaction rate of the first cycloaddition ( $k = 1.66 \times 10^{-2} \text{ M}^{-1}\text{s}^{-1}$ ).

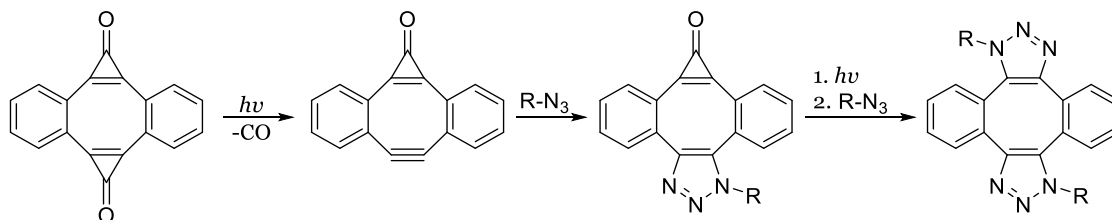


**Figure 15.** Upon irradiation, carbonylation of one of the cyclopropenone groups occurs, setting one of the reactive alkyne moieties free, followed by cycloaddition with an azide. Second decarbonylation occurs upon repeated irradiation, leading to an increase in reaction rate for the second cycloaddition.

In terms of nucleic acid modifications, presumably the only example of this type of reaction was reported by the groups of *Popik* and *Spitale*.<sup>[123]</sup> A biotinylated, photoactivatable dibenzocyclooctyne derivative was reacted with 2'-azidoadenosine either upon irradiation at  $\lambda = 350 \text{ nm}$  or in the dark. The irradiated samples showed efficient labeling, whereas the non-irradiated samples did not show any labeling.

### 3 Tetrazole-Modified Oligonucleotides for Bioorthogonal Labeling

---

In terms of cellular functions, such as gene expression and protein synthesis, especially messenger RNA is of great importance to transport and regulate genetic information, thus this work is focusing on investigating the applicability of the photoclick reaction on RNA. To achieve this, a uridine building block bearing a bromoaryl tetrazole at the 5-position was synthesized and incorporated into oligonucleotides, followed by photoclick reaction with dye maleimide conjugates.

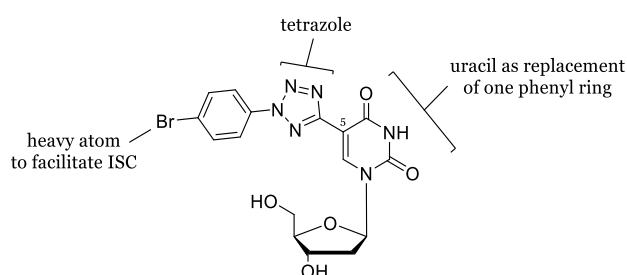


**Figure 16.** Structure of the previously reported tetrazole-modified 2'-deoxyuridine building block.<sup>[106]</sup>

In previous experiments of our group with a structurally alike 2'-deoxyuridine building block (Figure 16), the bromo substituent at the aryl moiety was reported to be necessary for an efficient photoclick reaction, presumably by facilitating the population of the triplet state due to the heavy-atom effect.<sup>[106, 124]</sup> Furthermore, the structural motif of the uracil ring replacing one of the aryl moiety of the usually employed diaryltetrazoles was preserved to keep the modification comparably small and therefore minimize the structural perturbation of the RNA strand. Additionally, uridine can be easily modified at the 5-position which is favorable, as the modification points into the major groove which makes it more accessible for bioorthogonal reactions.<sup>[44]</sup> Another advantage is that no additional protecting groups are needed for standard phosphoramidite solid-phase synthesis.

### 3.1 Synthesis of Tetrazole-Modified Nucleoside **9**

The synthesis of uridine building block **9** (Figure 17) was adapted from the previously mentioned 2'-deoxyuridine building block published by our group in 2018, and the general route for tetrazole synthesis reported by *Kakehi*.<sup>[106, 125]</sup> The most crucial step towards building block **9** is the synthesis of the protected 5-formyluridine derivatives **1ab**. There are two possible ways to achieve this, one of them was reported in literature before on 2'-deoxynucleosides (Figure 17, steps c and d).<sup>[126-127]</sup>

Starting from 5-methyluridine (**2**), the first step was the protection of the 2'-, 3'- and 5'-hydroxy groups with *tert*-butyldimethylsilyl (TBDMS) chloride and imidazole to give the TBDMS-protected nucleoside **3** in quantitative yield, followed by oxidation of the methyl group to the aldehyde by peroxodisulfate. The literature procedure on TBDMS-protected thymidine describes the use of potassium peroxodisulfate along with 2,6-lutidine as a phase-transfer catalyst (PTC) and copper(II) sulfate as an activator in water/acetonitrile (1/1, v/v).<sup>[126-128]</sup> However, in case of the ribonucleoside **3** used in this work, those conditions did not show any conversion of the starting material. As a first step, potassium peroxodisulfate was exchanged with sodium peroxodisulfate as described in previous works by our group, as the solubility of sodium peroxodisulfate is about 10-fold higher than the solubility of potassium peroxodisulfate (55.6 g/100 mL vs. 5.20 g/100 mL).<sup>[108, 129-130]</sup> Nevertheless, no conversion could be observed under these reaction conditions. 2,6-lutidine was substituted by pyridine, as during the course of the reaction a color change from bright blue to brown occurred, indicating degradation of either copper(II) or 2,6-lutidine. After this change, formation of product could be observed. However, only very inconsistent yields of 9-26% could be achieved. Further optimization steps (employing different phase-transfer catalysts, activators and changing the temperature, see chapter 6.1 for details) did not lead to any success, as either no conversion or only side-product was observed.

The alternative route (Figure 17, steps a and b) starts with an *Vorbrüggen* reaction to build the glycosidic bond between the sugar moiety and the base.<sup>[131]</sup> The reaction conditions were adapted from a literature procedure for a spin-labeled uridine building block.<sup>[132]</sup>

### 3 Tetrazole-Modified Oligonucleotides for Bioorthogonal Labeling

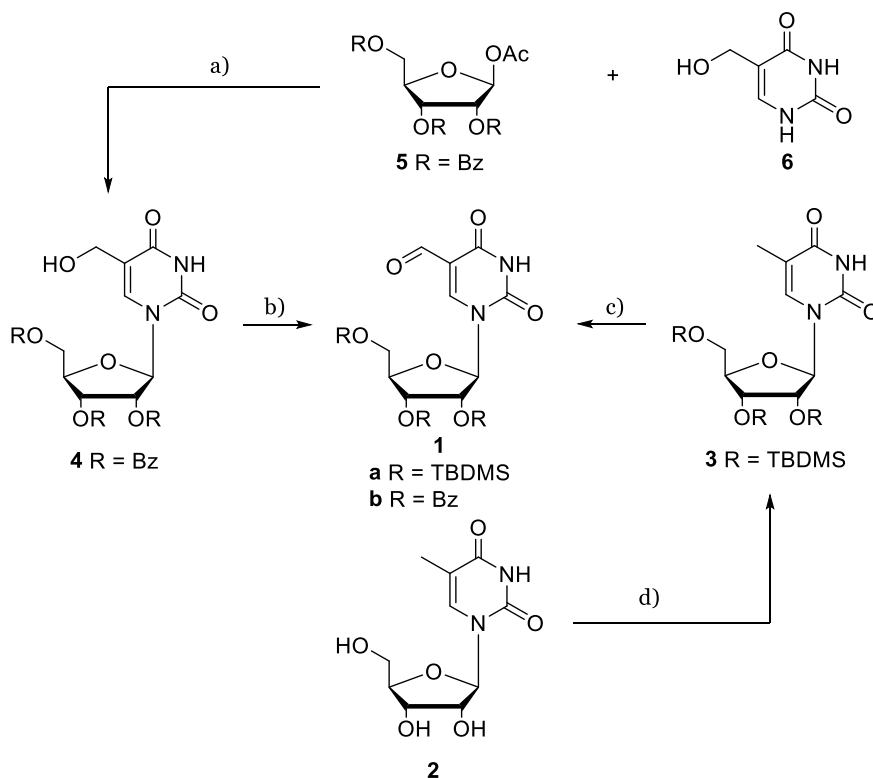


**Figure 17.** Synthetic routes to synthesize protected 5-formyluridine derivatives **1ab**: a) N,O-Bis(trimethylsilyl) acetamide, trimethylsilyl trifluoromethanesulfonate, acetonitrile, 60 °C, 2 h, 70% b) Dess-Martin-Periodinane, dichloromethane, r.t., 2 h, 72% c) Na<sub>2</sub>S<sub>2</sub>O<sub>8</sub>, CuSO<sub>4</sub> × 5H<sub>2</sub>O, pyridine, acetonitrile, water, 60 °C, 2 h, 9-26% d) imidazole, TBDMS-Cl, DMF, r.t., 12 h, quant.

First, the base **6** was *in situ* protected with trimethylsilyl protecting groups by addition of N,O-bis(trimethylsilyl) acetamide, then the sugar moiety **5** was activated with trimethylsilyl trifluoromethanesulfonate to selectively form the desired  $\beta$ -anomer **4** in 70% yield. Initially, the oxidation step was carried out following a literature procedure with activated manganese dioxide.<sup>[133]</sup> However, there were some disadvantages with this route. For successful oxidation, 20.0 equivalents of manganese dioxide had to be used, which were hard to remove from the reaction mixture by filtration because of the small particle size of the powder. Additionally, a large amount of solvent had to be used to completely recover the product from the filter cake. Furthermore, a strong inconsistency of the yields (37-60%) was observed when activated manganese dioxide from different manufacturers was used, therefore the reagent was exchanged with *Dess-Martin-Periodinane*, giving the desired product **1b** in reproducible 70% yield.<sup>[134]</sup> Subsequently, protected 5-formyluridine derivatives **1ab** were reacted with benzenesulfonyl hydrazide to hydrazones **7a** (90% yield) and **7b** (82% yield), respectively, followed by reaction with commercially available

### 3 Tetrazole-Modified Oligonucleotides for Bioorthogonal Labeling

4-bromobenzenediazonium tetrafluoroborate to give tetrazoles **8a** (55% yield) and **8b** (48% yield) (Figure 18). This reaction step led to an orange side product that was hard to remove by column chromatography but could be separated from the benzoyl protected nucleoside **8b** by precipitation with hexane out of dichloromethane. However, this strategy could not be applied to the TBDMS protected nucleoside **8a** because of the increased solubility in hexane compared to nucleoside **8b**. Afterwards, deprotection of the nucleosides by either triethylamine trihydrofluoride (nucleoside **8a**, 49% yield) or 7M ammonia in methanol (nucleoside **8b**, 65%) followed.

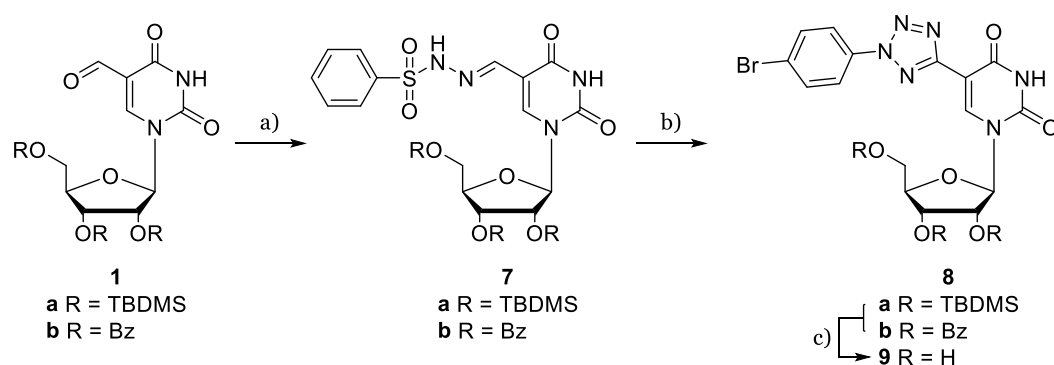


**Figure 18.** Synthetic route for building block **9**. a) benzenesulfonyl hydrazide, methanol, 60 °C, 2 h, **7a** 90%, **7b** 82% b) 4-bromobenzenediazonium tetrafluoroborate, pyridine, -15 °C, 0.5 h, **8a** 55%, **8b** 48% c) for **8a**: Et<sub>3</sub>N × 3HF, DMF, r. t., 24 h, 49%, for **8b**: 7M ammonia in methanol, 80 °C, 24 h, 65%.

For the next step – the incorporation of the phosphoramidite building block **12** into an RNA strand *via* solid-phase synthesis – the protection of the 5' position with and the 2' hydroxyl groups was necessary (Figure 19). The 5' position was protected with 4,4'-dimethoxytrityl chloride in 55% yield, the 2' position with TBDMS-Cl, silver(II) nitrate as a catalyst and pyridine as a base in 36% yield. As last step, the 3' hydroxy group was converted into the reactive phosphoramidite group by reaction with 2-cyanoethyl *N,N*-diisopropyl-chlorophosphoramidite and DIPEA as a base (87% yield).

### 3 Tetrazole-Modified Oligonucleotides for Bioorthogonal Labeling

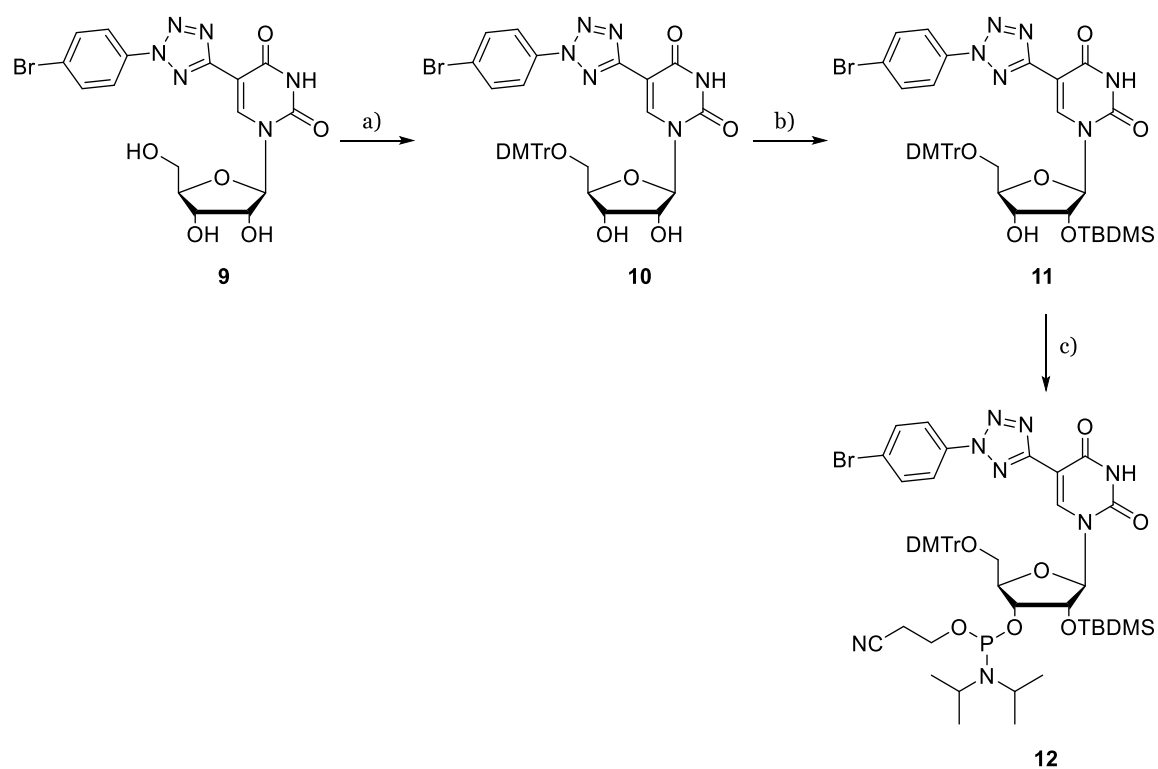


**Figure 19.** Protection of the 5'- and 2'-hydroxy groups. a) 4,4'-Dimethoxytrityl chloride, pyridine, r. t., 16 h, 55% b) TBDMS-Cl, silver(II) nitrate, pyridine, THF, r. t., 6 h, 36% c) 2-Cyanoethyl *N,N*-diisopropyl-chlorophosphoramidite, DIPEA, dichloromethane, r. t., 6 h, 87%.

### 3.2 Synthesis and Characterization of Tetrazole-Modified Oligonucleotides

The tetrazole-modified phosphoramidite **12** was incorporated into two different RNA sequences either internally (**RNA1**) or 5'-terminally (**RNA2**) *via* solid-phase synthesis (Figure 20). The sequences were adapted from previous experiments by our group.<sup>[105-106]</sup>

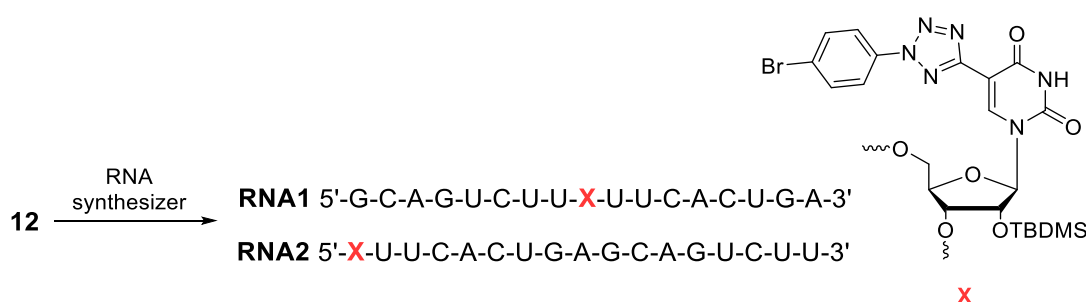


**Figure 20.** The phosphoramidite building block **12** was incorporated into two different oligonucleotides (**RNA1** and **RNA2**) *via* solid-phase synthesis.

After cleavage from the solid support, the oligonucleotide was purified *via* reversed-phase HPLC chromatography and identified by MALDI-TOF mass spectrometry (Table 2).

**Table 2.** Calculated and found masses of oligonucleotides RNA1 and RNA2.

sequence	calculated mass [Da]	measured mass [Da]
<b>RNA1</b>	5544.6	5547.0
<b>RNA2</b>	5544.6	5546.5

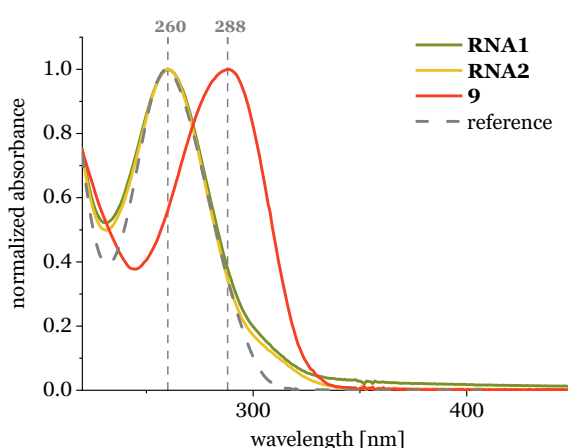


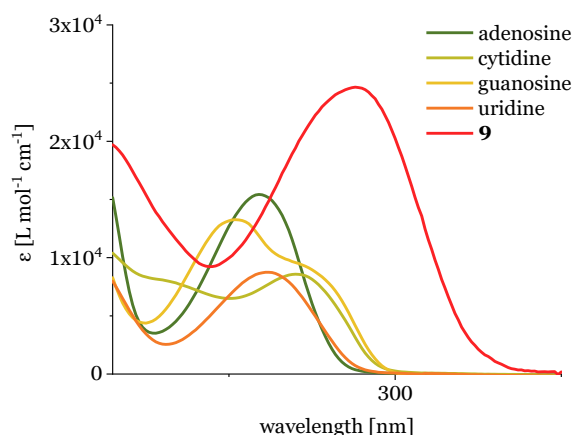
**Figure 21.** Normalized UV/vis spectra of the oligonucleotides **RNA1** and **RNA2** and nucleoside **9**, along with a random RNA sequence as a reference. Oligonucleotides **RNA1** and **RNA2** were measured as 2.5  $\mu\text{M}$  solution in 10 mM Na-P<sub>i</sub> buffer with 250 mM NaCl at pH 7 at 20 °C. Nucleoside **9** was measured as 25  $\mu\text{M}$  solution in water + 0.1% DMSO at 20 °C.

### 3 Tetrazole-Modified Oligonucleotides for Bioorthogonal Labeling

The oligonucleotides were quantified photometrically, characterized by UV/vis spectroscopy and the spectral properties compared to nucleoside **9** (Figure 21). The spectrum of the nucleoside **9** displays a distinct maximum at 288 nm, that can be assigned to the tetrazole moiety. **RNA1** and **RNA2** display the characteristic maximum of oligonucleotides at 260 nm. Furthermore, a tailing side band around 300 nm, that is absent in the reference, can be observed, which conforms with the absorbance of nucleoside **9**. Based on these results,  $\lambda = 300$  nm light was chosen to initiate the photoclick reaction.

As described in chapter 2.2.3.1, irradiation of oligonucleotides at  $\lambda = 300$  nm might lead to damaging of the oligonucleotide. To determine the viability of the photoclick reaction on the synthesized oligonucleotides **RNA1** and **RNA2**, the molar extinction coefficients of the natural nucleosides and the artificial building block **9** at 300 nm were calculated and compared (Table 3).

**Table 3.** Comparison of the molar extinction coefficients of A, C, G, U and **9**.



nucleoside	$\epsilon_{260}$ [L mol <sup>-1</sup> cm <sup>-1</sup> ]	$\epsilon_{300}$ [L mol <sup>-1</sup> cm <sup>-1</sup> ]
<b>adenosine</b>	15 400	60
<b>cytidine</b>	7 400	260
<b>guanosine</b>	11 500	110
<b>uridine</b>	8 700	90
<b>9</b>	13 800	20 300

The molar extinction coefficient at 300 nm of nucleoside **9** is significantly higher than those of the natural nucleosides, indicating that upon irradiation at  $\lambda = 300$  nm, the photoclick reaction is favored compared to oligonucleotide damaging reactions.

### 3.3 Photoclick Experiments

Subsequently, the synthesized oligonucleotides were labeled in a bioorthogonal manner by means of photoclick reaction (Figure 22). As described in chapter 2.2.3.1, electron-deficient alkenes present an ideal reaction partner for the *in situ* generated nitrile-imine because of the decreasing effect on the HOMO/LUMO gap.<sup>[93-94]</sup>

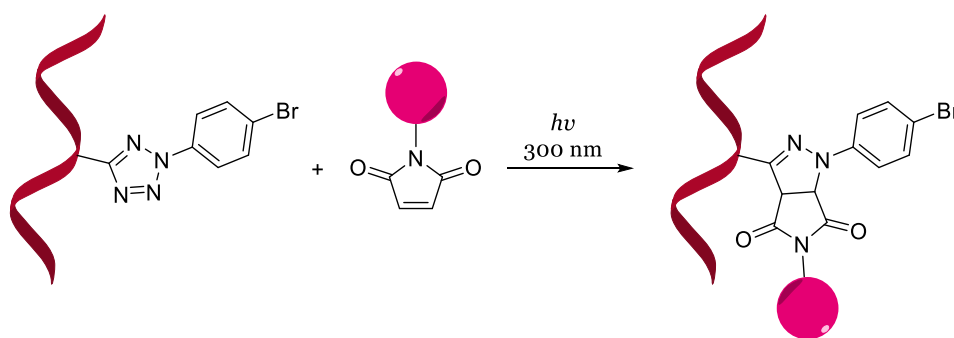


**Figure 22.** Schematic presentation of the photoclick reaction between a tetrazole-modified oligonucleotide and a maleimide dye conjugate upon irradiation at  $\lambda = 300$  nm.

Maleimide dye conjugates were chosen as a reaction partner in this work, as the double bond of maleimides is highly polarized by the two neighboring carbonyl groups. Furthermore, the optical properties of the labeled oligonucleotides can be easily adjusted because of the broad scope of commercially available maleimide dye conjugates. In previous experiments with the 2'-deoxyuridine analog of building block **9**, it was demonstrated that the fluorescent pyrazoline that is formed during the reaction is a suitable *Förster resonance energy transfer (FRET)* donor.<sup>[106, 135]</sup> A *FRET* is a radiationless energy transfer that occurs between a donor in the excited state and an acceptor in the ground state, resulting in the excitation of the acceptor, whereas the donor returns to the ground state.<sup>[136]</sup> This work focuses on investigating and enhancing the fluorescence properties of the photoclick reaction with different dye maleimide conjugates for future application in live cell experiments by application of *FRET*.

Exemplarily, **RNA2** was reacted with N-methylmaleimide (NMM) to both determine the fluorescence properties of the donor and verify the suitability of maleimides as a reaction partner. UV/Vis absorbance and fluorescence was recorded before irradiation (0 s) and after 300 s of irradiation. The resulting absorbance spectrum shows a decrease of the tetrazole band around 300 nm, whereas a new band around 320-420 nm is formed that can be assigned to the

### 3 Tetrazole-Modified Oligonucleotides for Bioorthogonal Labeling

pyrazoline (Figure 23, left). For the emission spectra, the excitation wavelength was set to 358 nm, which is close to the local maximum of the pyrazoline absorbance. In agreement with previous experiments by our group, a broad emission band between 400 and 700 nm was formed during the reaction.<sup>[106]</sup> Compared to other fluorophores, such as commercially available dyes, the pyrazoline moiety displays a low fluorescence intensity and quantum yield ( $\Phi_F = 0.028$ ,  $\lambda_{exc} = 400$  nm),<sup>[108]</sup> which makes it less suitable for fluorescence imaging. In contrast, when labeling with fluorescent dyes, a high background fluorescence of the free dye might be detected upon direct excitation of the dye. However, by combining both techniques by employing a *FRET*, the direct excitation of the dye can be mostly suppressed. Furthermore, a light-up effect can be observed upon increasing pyrazoline concentration during the reaction. Another benefit is the large Stokes' shift of the resulting *FRET* pair.

As a first simple assessment to determine the probability of a *FRET*, the emission band of the pyrazoline was compared with the absorbance spectra of the three commercially available, water-soluble maleimide dye conjugates (Figure 23, right) sulfo-Cy3 (Lumiprobe), AF555 (JenaBioscience) and AF647 (JenaBioscience).

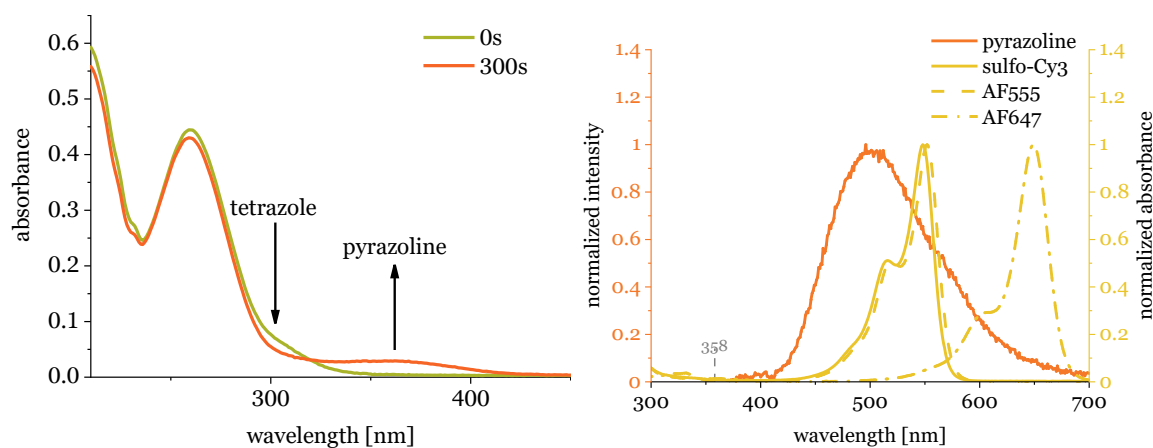


**Figure 23.** UV/vis absorbance (left) and overlap of the normalized emission spectrum (exc. = 358 nm) of the reaction between **RNA2** and N-methylmaleimide and the normalized absorbance of three different maleimide dye conjugates (sulfo-Cy3, AF555, AF647, right). 2.5  $\mu$ M **RNA2**, 3.75  $\mu$ M N-methylmaleimide in 10 mM Na-P<sub>i</sub> buffer, 250 mM NaCl, pH 7, 20 °C. Irradiation with  $\lambda = 300$  nm for 300 s.

A first indication for the possibility of a *FRET* is the spectral overlap between the emission of the pyrazoline (donor) and the absorbance of the respective dye (acceptor). In case of the structurally similar dyes sulfo-Cy3 and AF555, a high overlap can be observed, whereas AF647 displays a moderate overlap between the

### 3 Tetrazole-Modified Oligonucleotides for Bioorthogonal Labeling

pyrazoline emission and the dye absorbance. Additionally, the dyes show negligible absorbance at the excitation wavelength ( $\lambda = 358$  nm), indicating a low direct excitation of the dyes. Furthermore, the energy transfer efficiency depends on the distance and orientation of the donor and acceptor as well as the quantum yield of the donor, which will not be further investigated in this work.<sup>[136]</sup>

For each selected dye and oligonucleotide, UV/vis absorbance and fluorescence emission spectra were recorded at defined times over the course of 30 minutes (irradiation time). Subsequently, the fluorogenicity and yields of the reactions were determined and compared. Exemplarily, the spectra of the reactions between **RNA2** and the dye maleimide conjugates are displayed and discussed below. For spectra of **RNA1** see chapter 6.2.

The absorbance spectra (Figure 24, left) of the reaction of **RNA2** and sulfo-Cy3 maleimide show similar behavior to the reaction with NMM: a new broad band that can be assigned to the formation of the pyrazoline is formed between 320 and 420 nm, while the tetrazole absorbance around 300 nm is concomitantly decreased. Furthermore, the spectrum shows a distinct isosbestic point at 320 nm indicating clear conversion to the desired product without any long-living intermediate or side product.

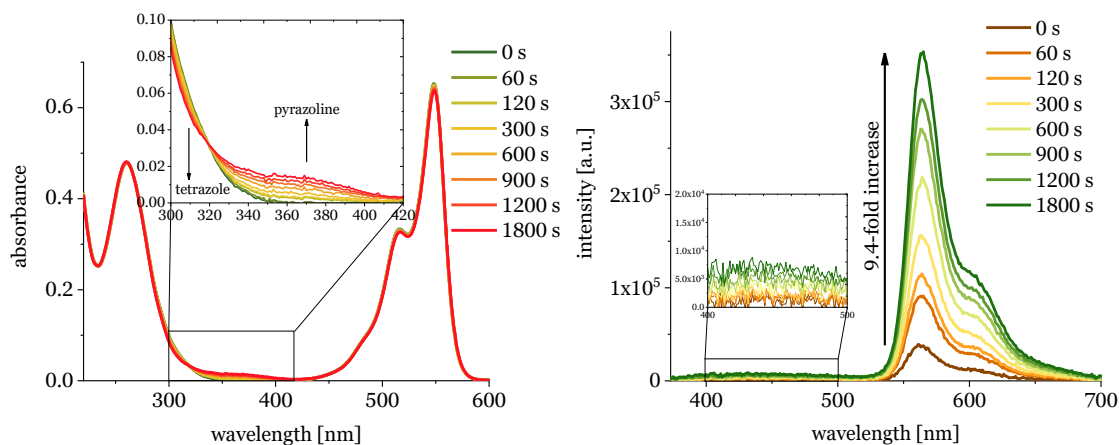


**Figure 24.** UV/Vis absorbance (left) and emission (exc. = 358 nm, right) spectra of the reaction between **RNA2** and sulfo-Cy3 maleimide over 30 minutes (irradiation time,  $\lambda = 300$  nm). 2.5  $\mu$ M **RNA2**, 3.75  $\mu$ M sulfo-Cy3 maleimide (1.50 equiv.) in 10 mM Na-P<sub>i</sub> buffer, 250 mM NaCl, pH 7 at 20 °C. Figures were published before.<sup>[137]</sup>

Upon excitation of the pyrazoline at  $\lambda = 358$  nm, the emission spectra show a strong 9.4-fold increase of the dye signal (em. = ~535-670 nm) within 30 minutes, but only negligible increase of fluorescence between 400 and 500 nm, indicating an

### 3 Tetrazole-Modified Oligonucleotides for Bioorthogonal Labeling

efficient energy transfer from the pyrazoline to the attached dye. Considering the absorbance and fluorescence spectra, the reaction does not reach the end point within 30 minutes, however this time span was chosen for better comparability with the other dyes.

The reaction of **RNA2** with AF555 maleimide shows similar behavior in the absorbance spectra (Figure 25, left) whereas the emission spectra (Figure 25, right) show only a 3.2-fold increase of fluorescence ( $\text{em} = \sim 535\text{-}670\text{ nm}$ ) upon excitation of the pyrazoline at  $\lambda = 358\text{ nm}$ , albeit the structural similarity of the two dyes. Contrary to the reaction with sulfo-Cy3 maleimide, both absorbance and emission spectra indicate the end of the reaction around 30 minutes irradiation time. Opposed to sulfo-Cy3, a minor increase of fluorescence around 400 to 500 nm can be observed, indicating a less efficient energy transfer.

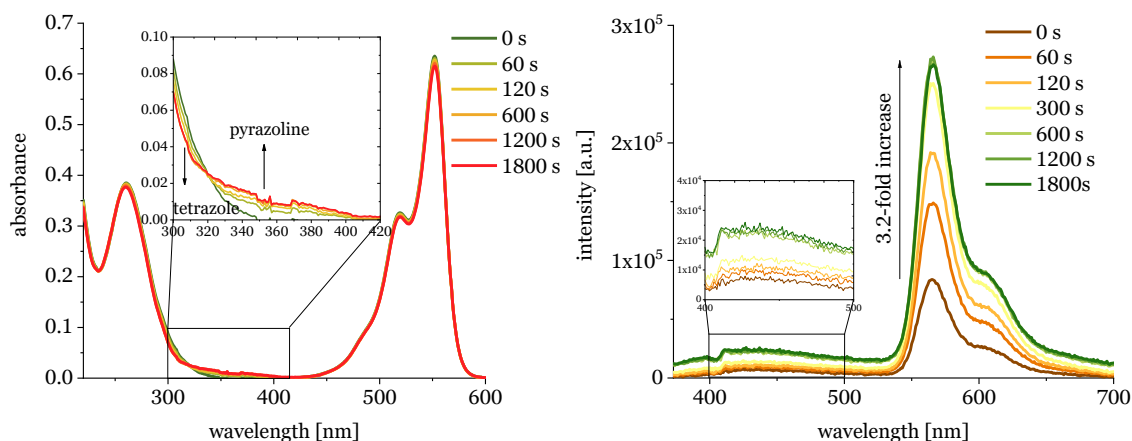


**Figure 25.** UV/Vis absorbance (left) and emission (exc. = 358 nm, right) spectra of the reaction between **RNA2** and AF555 maleimide over 30 minutes (irradiation time,  $\lambda = 300\text{ nm}$ ).  $2.5\ \mu\text{M}$  **RNA2**,  $3.75\ \mu\text{M}$  AF555 maleimide (1.50 equiv.) in 10 mM Na-P<sub>i</sub> buffer, 250 mM NaCl, pH 7 at 20 °C. Figures were published before.<sup>[137]</sup>

This observation can possibly be explained by the minor structural differences of the two dyes. AF555 features two additional sulfonated alkyl chains (Figure 26), which might lead to a slightly distorted orientation towards the pyrazoline compared to sulfo-Cy3. Furthermore, in case of AF555 the length of the linker between the maleimide and the dye was not provided by the manufacturer (JenaBioscience), therefore the distance between AF555 and the pyrazoline might be greater than the distance between sulfo-Cy3 and the pyrazoline. Both factors can affect the efficiency of the *FRET*.<sup>[136]</sup>

### 3 Tetrazole-Modified Oligonucleotides for Bioorthogonal Labeling

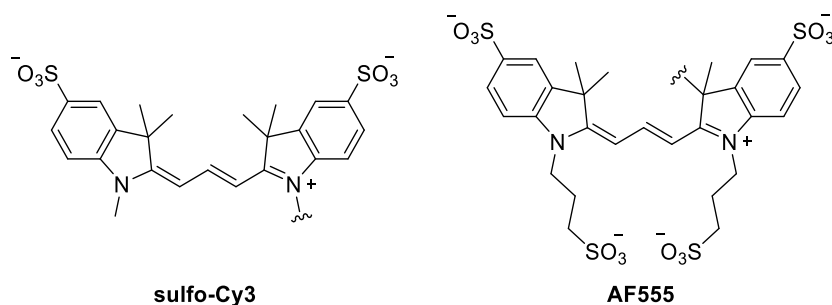


**Figure 26.** Structures of sulfo-Cy3 and AF555 as supplied by the manufacturer<sup>[138]</sup> or reported in literature.<sup>[139]</sup>

The absorbance spectra of the reaction of **RNA2** with AF647 maleimide (Figure 27, left) also indicate clear formation of the pyrazoline by formation of a new band between 320 and 420 nm with a distinct isosbestic point at 320 nm. The fluorescence spectra (Figure 27, right) display the least increase of fluorescence ( $\text{em} = \sim 620\text{-}700$  nm, 1.5-fold) compared to sulfo-Cy3 and AF555, which can be explained with the least overlap between the pyrazoline emission and dye absorbance out of the three dyes. Additionally, a minor increase of pyrazoline fluorescence between 400 and 500 nm can be observed, which is again indicating a less efficient energy transfer compared to sulfo-Cy3 maleimide.

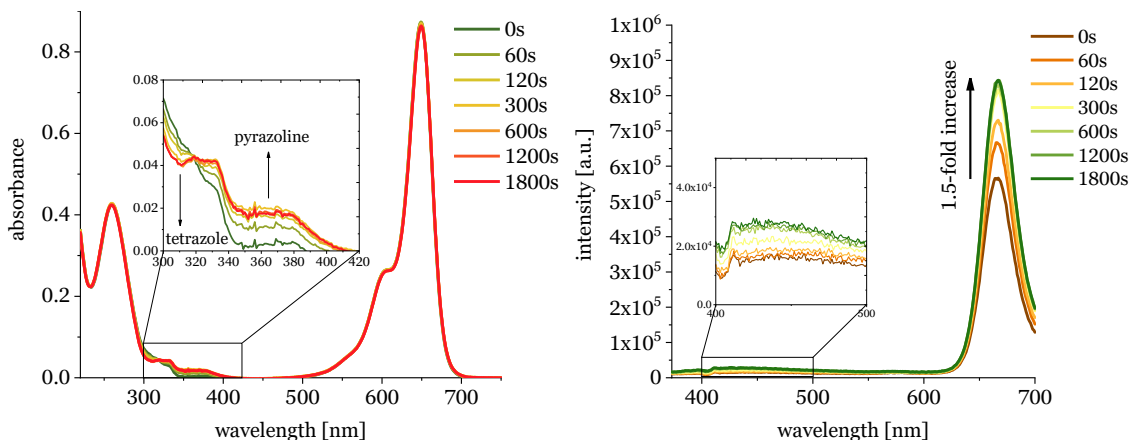


**Figure 27.** UV/Vis absorbance (left) and emission (exc. = 358 nm, right) spectra of the reaction between **RNA2** and AF647 maleimide over 30 minutes (irradiation time,  $\lambda = 300$  nm). 2.5  $\mu\text{M}$  **RNA2**, 3.75  $\mu\text{M}$  AF647 maleimide (1.50 equiv.) in 10 mM Na-P<sub>i</sub> buffer, 250 mM NaCl, pH 7 at 20 °C. Figures were published before.<sup>[137]</sup>

The experiments between **RNA1** and each of the dyes (chapter 6.2, Figure A1-Figure A3) were conducted under the same conditions and showed similar behavior. To compare and summarize the results of the reaction of each oligonucleotide with each dye, the fluorogenicity  $I/I_0$  of each reaction was plotted against the time (Figure 28).

### 3 Tetrazole-Modified Oligonucleotides for Bioorthogonal Labeling

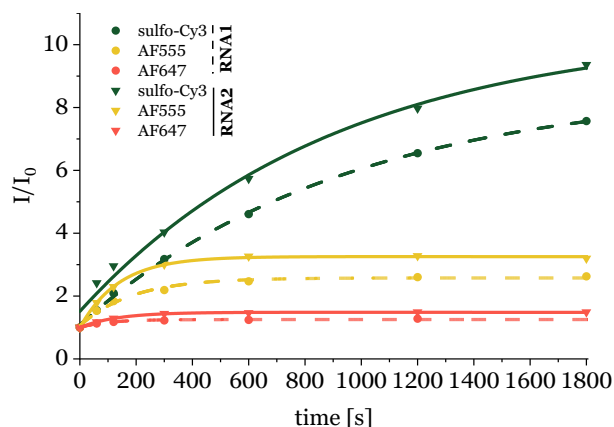


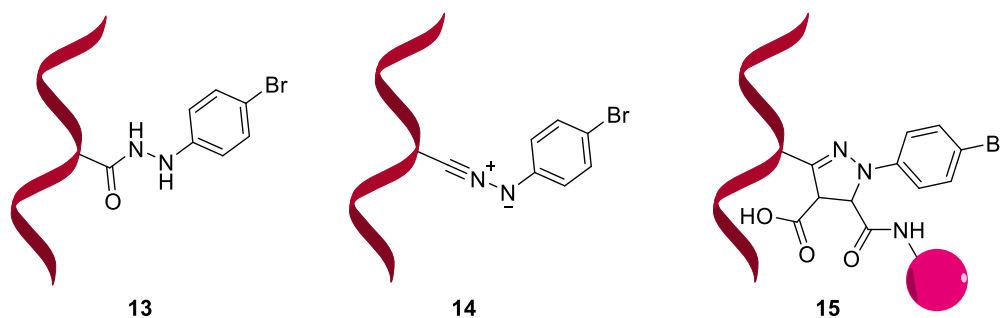
**Figure 28.** Changes of the fluorescence intensity during the reaction of **RNA1** (dashed lines) and **RNA2** (solid lines) with sulfo-Cy3, AF555 and AF647 maleimide in dependence of irradiation time (irradiation at  $\lambda = 300$  nm).  $I_0$  is the fluorescence intensity before irradiation. Figure was published before.<sup>[137]</sup>

In general, the increase of fluorescence during the reactions follows an exponential trend, indicating second-order reaction kinetics. The reactions with both AF555 and AF647 maleimide reach their respective end point around 600 s irradiation time, which is more rapid than sulfo-Cy3 maleimide. However, the highest increase of fluorogenicity can be observed for sulfo-Cy3 maleimide (7.5-fold for **RNA1**, 9.4-fold for **RNA2**). Both AF555 (2.6-fold for **RNA1**, 3.2-fold for **RNA2**) and AF647 (1.3-fold for **RNA1**, 1.5-fold for **RNA2**) display a significantly less fluorogenicity. In case of the oligonucleotides, the 5'-terminally modified oligonucleotide **RNA2** shows generally higher fluorogenicity than **RNA1**. There are two possible explanations for this observation: either the energy transfer is more efficient due to better orientation of the donor and acceptor or the yield of the reaction with **RNA2** is higher compared to **RNA1** because of the better accessibility because of the terminal position of the tetrazole.

The irradiated solutions ( $\lambda = 300$  nm, 30 minutes irradiation time, 2.5  $\mu$ M RNA, 3.75  $\mu$ M dye in 10 mM Na-P<sub>i</sub> buffer, 250 mM NaCl, pH 7 at 20 C, for experimental details see chapter 5.3) were purified *via* illustra™ NAP-5 columns to remove excess dye. Each **RNA** dye adduct was identified by MALDI-TOF mass spectrometry (Table 4). Apart from the masses of the oligonucleotide dye adducts, masses of the hydrazide **13** and nitrile-imine **14** could also be observed. Opposed to previous reports,<sup>[106]</sup> the mass of the hydrolyzed pyrazoline **15** could not be detected.

### 3 Tetrazole-Modified Oligonucleotides for Bioorthogonal Labeling

**Table 4.** Calculated and measured masses and structures of oligonucleotide dye adducts.



sequence	adduct	calculated mass [Da]	measured mass [Da]
<b>RNA1</b>	sulfo-Cy3	6253.9	6261.4
	AF555	6485.9	6486.2
	AF647	6497.9	6499.90
	H <sub>2</sub> O	5534.6	5536.2
<b>RNA2</b>	sulfo-Cy3	6253.9	6254.7
	AF555	6485.9	6485.1
	AF647	6497.9	6499.7
	H <sub>2</sub> O	5534.6	5534.7

To further investigate the reaction, the yields of the reactions were determined. The concentrations were determined spectroscopically by extinction of the dyes in their respective maximum (Figure 29).

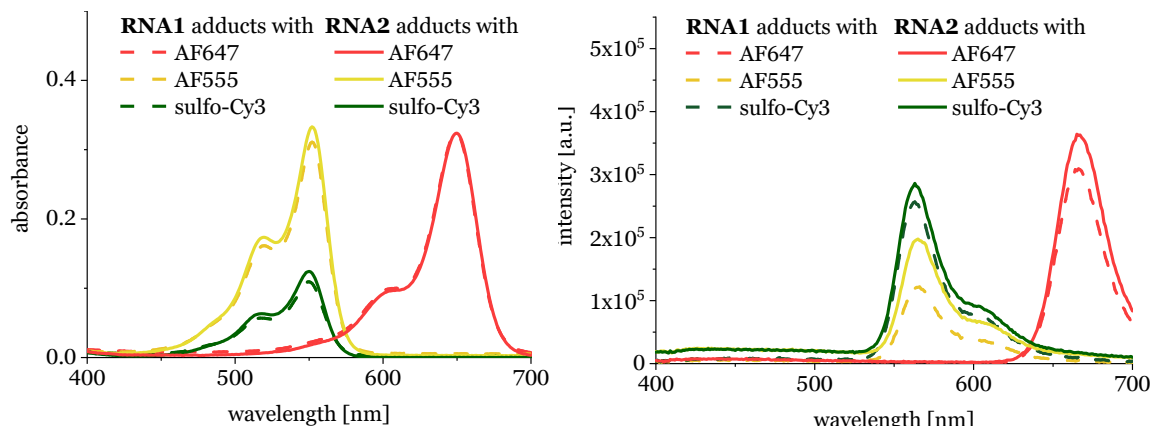


**Figure 29.** UV/Vis absorbance spectra (left) and emission spectra (exc. = 358 nm, right) of purified **RNA1** and **RNA2** dye adducts. Figures were published before.<sup>[137]</sup>

In agreement with the recorded UV/vis and fluorescence spectra, the yields of the **RNA2** dye adducts are slightly higher than the yields of the **RNA1** dye adducts (Table 5). The yields of the sulfo-Cy3 adducts are the lowest (**RNA1** 27%, **RNA2** 31%), whereas the AF555 achieved the highest yields (**RNA1** 78%, **RNA2** 84%). In case of AF647, identical labeling yields of 48% could be achieved, whereas the **RNA2** adduct displayed a higher fluorogenicity compared to the **RNA1** adduct.

### 3 Tetrazole-Modified Oligonucleotides for Bioorthogonal Labeling

This indicates a slightly better *FRET* efficiency of **RNA2** compared to **RNA1**. The increased yields of the AF dyes can be possibly explained by the higher solubility of both dyes compared to sulfo-Cy3 because of the additional sulfonate groups (Figure 26).

**Table 5.** Yields of the photoclick reaction of RNA1 and RNA2 with sulfo-Cy3, AF555 and AF647 maleimide in 10 mM Na-P<sub>i</sub> buffer, 250 mM NaCl, pH 7. Table was published before.<sup>[137]</sup>

dye adduct of	RNA1	RNA2
sulfo-Cy3	27%	31% (70%) <sup>a</sup>
AF555	78%	84%
AF647	48%	48%

<sup>a</sup>after reaction in presence of 10.0 equiv. sulfo-cy3 maleimide

Surprisingly, the fluorescence intensity of the sulfo-Cy3 conjugates is about 1.5 (**RNA2**) to 2-fold (**RNA1**) higher than the AF555 conjugates, respectively, even though the yields of sulfo-Cy3 are significantly lower. Considering the structural similarity and identical fluorescence quantum yields ( $\Phi_F = 0.1$ )<sup>[138, 140]</sup> of both dyes, along with the fluorescence spectra recorded during the reaction, this is another indication for a more efficient energy transfer between the pyrazoline and sulfo-Cy3. The experiments were repeated exemplarily with **RNA2** and 10.0 equivalents sulfoCy3 maleimide to assess if the fluorescence and yield can be further increased. Within the same reaction time (30 minutes irradiation,  $\lambda = 300$  nm), the yield could be more than doubled. The fluorescence intensity displayed almost linear behavior and was increased by a factor of 2 (Figure 30).

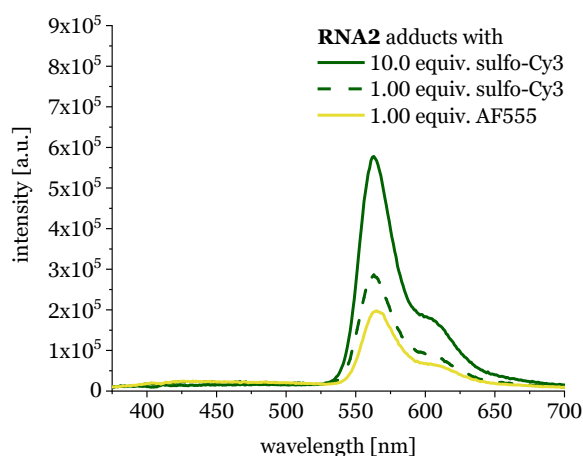


**Figure 30.** Fluorescence spectra (exc. = 358 nm) of the purified **RNA2** dye adducts after reaction with 10.0 equiv. sulfo-Cy3 maleimide and 1.00 equiv. sulfo-Cy3 and AF555 maleimide, respectively.

### 3 Tetrazole-Modified Oligonucleotides for Bioorthogonal Labeling

Regarding experiments in a cellular environment, however, an excitation wavelength of  $\lambda = 358$  nm is not suitable, as shorter wavelengths cause a significant amount of auto-fluorescence of the cells. To determine the viability of *FRET* in living cells, fluorescence spectra of the reaction between **RNA1** and the AF dyes were also recorded with the excitation wavelength set to 405 nm, as the lowest possible excitation wavelength a standard confocal microscope offers (Figure 31).

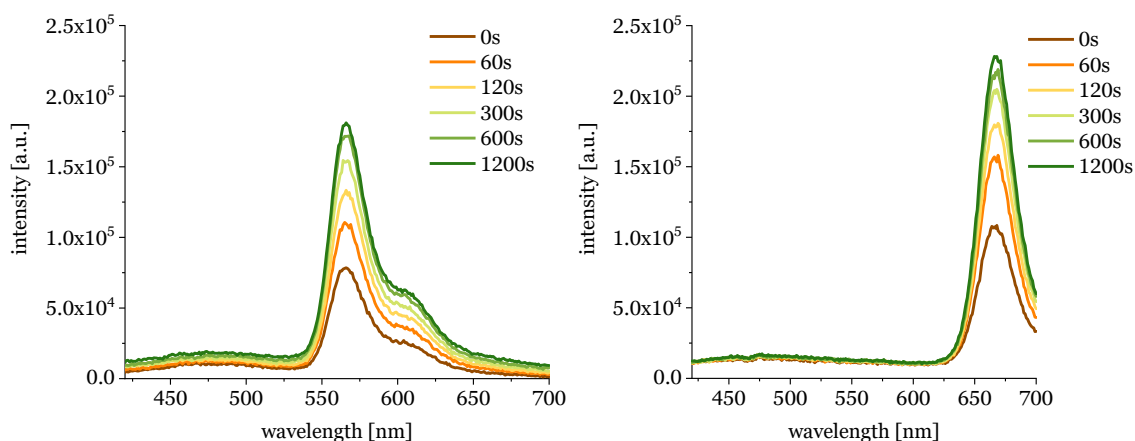


**Figure 31.** Emission (exc. = 405 nm) spectra of the reaction between **RNA1** and AF555 maleimide (left) and AF647 maleimide (right) over 20 minutes (irradiation time,  $\lambda = 300$  nm). 2.5  $\mu$ M **RNA1**, 3.75  $\mu$ M dye maleimide (1.50 equiv.) in 10 mM Na-P<sub>i</sub> buffer, 250 mM NaCl, pH 7 at 20 °C.

While the general fluorescence intensity is lower compared to excitation at  $\lambda = 358$  nm, a 2.3-fold (AF555) and 2.1-fold (AF647) fluorescence enhancement could be achieved, respectively. In case of AF647, this even represents a better result compared to the 1.3-fold increase of fluorescence upon excitation at  $\lambda = 358$  nm. This can possibly be explained by fewer direct excitation of the dye moiety by excitation at  $\lambda = 405$  nm compared to excitation at  $\lambda = 358$  nm.

Additionally, similar experiments were carried out with **RNA1** and AF555 or AF647 maleimide in *HeLa* cell lysate to determine the viability of the reaction in presence of cellular components (Figure 32). In both cases, an increase of dye fluorescence indicating successful reaction was observed. The reaction of **RNA1** with AF555 maleimide reached a 1.2-fold increase of fluorescence, whereas in case of AF647 maleimide a 1.4-fold increase was achieved. In comparison, under the same conditions in Na-P<sub>i</sub> buffer (Figure 31) a 2.0-fold (AF555) and 1.9-fold (AF647) increase of fluorescence was observed. This can possibly be explained by a filter effect of the cellular components, leading to less efficient generation of the nitrile-imine, and therefore decreased yields compared to the reaction in Na-P<sub>i</sub> buffer. However, a strong autofluorescence of the cell lysate over

### 3 Tetrazole-Modified Oligonucleotides for Bioorthogonal Labeling

almost the whole spectrum can be observed. In case of AF555 this results in a rather strong overlap of the lysate autofluorescence with the dye signal, which might interfere with the detection in living cells. AF647 might be a more suitable candidate for live cell imaging, as there is only very little overlap of the lysate and the dye fluorescence.

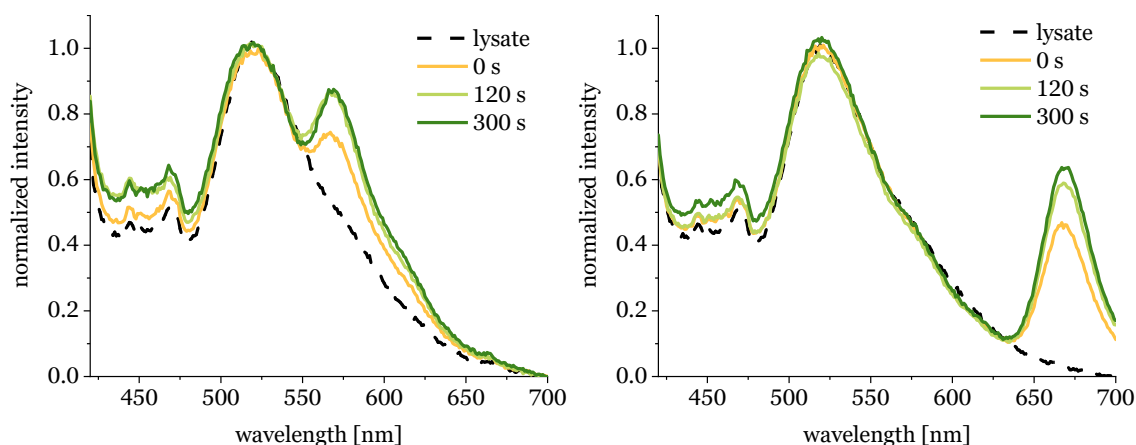


**Figure 32.** Normalized emission spectra (exc. = 405 nm) of the reaction between **RNA1** and AF555 (left) or AF647 (right) maleimide. 2.5  $\mu\text{M}$  **RNA1**, 3.75  $\mu\text{M}$  dye maleimide (1.50 equiv.) in *HeLa* cell lysate at 20 °C, 300 s irradiation time at  $\lambda = 300$  nm.

As a conclusion regarding photoclick experiments in living cells, each of the three dyes displays beneficial factors: sulfo-Cy3 maleimide achieved the highest fluorogenic increase, AF555 the highest yield and AF647 shows the best fluorescence properties compared to the cell lysate autofluorescence.

### 3.4 Cell Experiments

All cell experiments were performed under supervision and with the help of Dr. Franziska Röncke. As the final step, we attempted to transfer the results to *HeLa* cells. In principle, the fluorogenic behavior of the reaction originating from the energy transfer between the pyrazoline as a donor and the respective dye as an acceptor should facilitate detection of the labeled oligonucleotides. Upon excitation at  $\lambda = 405$  nm, ideally no fluorescence of the excess dye should be observable, as the excitation at this wavelength is rather low. To verify this assumption as well as to test the cell penetration of the dyes,  $4 \times 10^4$  *HeLa* cells (humane cervix carcinoma cells) were treated with 100 (AF555, sulfo-Cy3) or 50 pmol (AF647) of each *in vitro* used dye maleimides (AF555, AF647, sulfo-Cy3) and incubated overnight, followed by imaging by confocal laser microscopy. The emission of the dyes (AF555/sulfo-Cy3: 550-650 nm, AF647 650-750 nm) was investigated upon excitation at the donor excitation ( $\lambda = 405$  nm), as well as upon direct excitation (AF555/sulfo-Cy3:  $\lambda = 488$  nm, AF647  $\lambda = 638$  nm). The excess dye was not removed prior to examination of the cells under the microscope. All pictures were taken under the same conditions (23.6 % laser power, 600 V smart gain). Upon excitation at  $\lambda = 405$  nm, none of the dyes produced a detectable fluorescent signal (first row) which is beneficial regarding the visualization of the photoclick experiments. However, upon control by direct excitation (Figure 33, second row) of each dye at  $\lambda = 488$  nm (AF555, sulfo-Cy3) or  $\lambda = 638$  nm (AF647), it is clearly visible that the cell penetration of all the dyes within 24 h incubation time is rather low. Only very little fluorescence inside adherent cells can be observed, the strongest signal is produced from detached cells. In case of AF647 a diffuse, non-specific fluorescence in the culture medium can be observed. The low cell penetration can possibly be explained by the negatively charged sulfonate groups of the dyes. As this does not provide suitable conditions for live cell photoclick experiments, the results could not be transferred to cells in the limited time frame of this work. As possible alternatives, non-sulfonated dyes with similar optical properties such as Cy3 or Cy5 could be employed, however spectroscopical experiments would have to be performed beforehand to validate the fluorogenic behavior and the probability of a *FRET* of each dye.

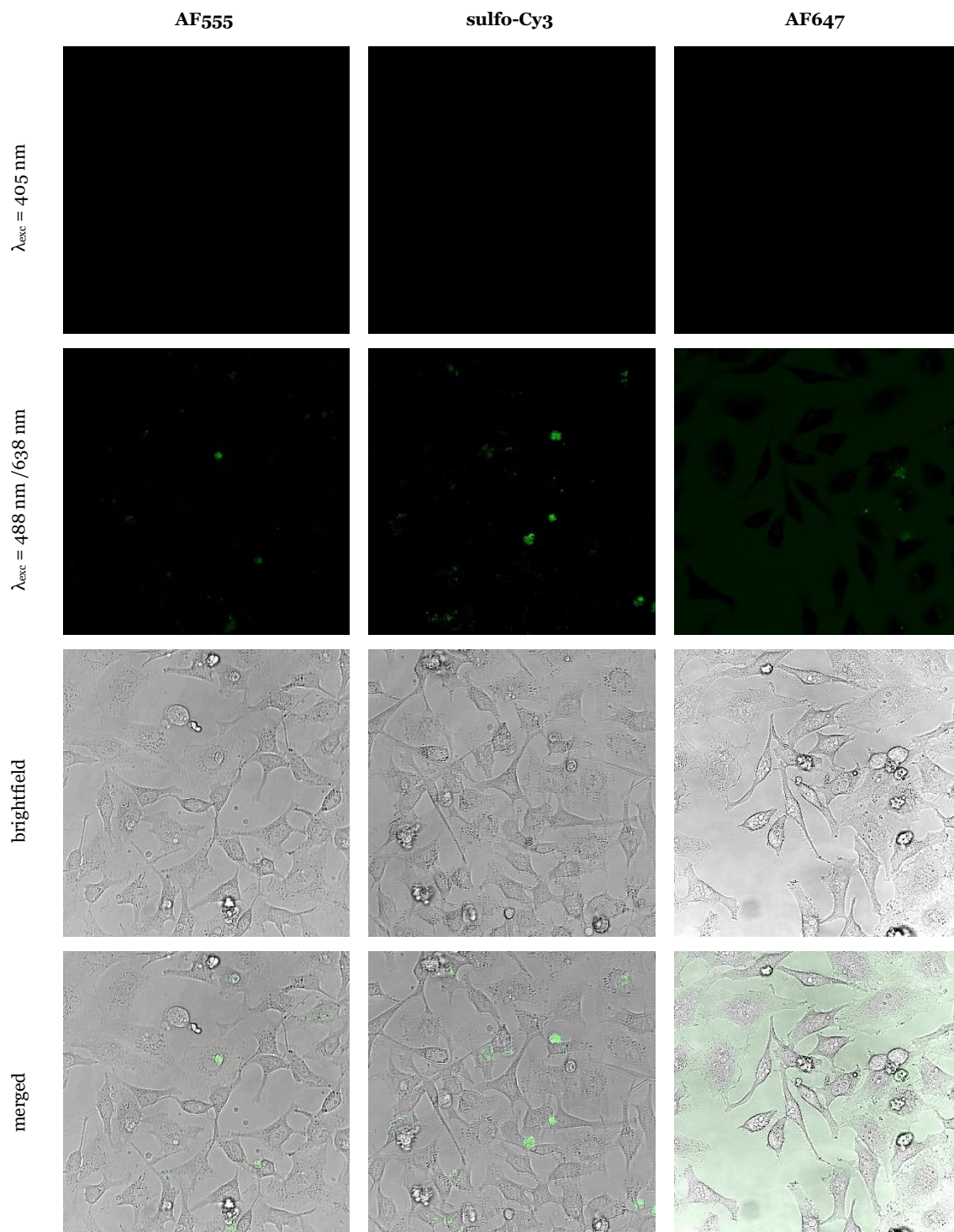


**Figure 33.** Confocal laser microscopy pictures of *HeLa* cells after treatment with 100 pmol of each dye maleimide. The excitation was set to either  $\lambda = 405 \text{ nm}$  to verify the absence of direct excitation of the dye at the donor wavelength or to the direct excitation wavelengths of either  $\lambda = 488 \text{ nm}$  (AF555, sulfo-Cy3) or  $\lambda = 638 \text{ nm}$  (AF647). The emission was set to  $\lambda_{em.} = 550\text{-}650 \text{ nm}$  (AF555, sulfo-Cy3) or  $\lambda_{em.} = 650\text{-}750 \text{ nm}$  (AF647). The merge shows the combination of the picture taken of direct excitation and the brightfield. The fluorescent spots observed in pictures of AF555 and sulfo-Cy3 is the accumulation of dye in detached cells.

### 3.5 Conclusion and Outlook

In this work, the previously reported system of a diaryltetrazole directly incorporated into a 2'-deoxyuridine building block was transferred to ribonucleoside uridine.<sup>[106, 108]</sup>

Building block **9** was successfully synthesized and the previously published synthetic procedure modified to increase the overall yield from 2.2-6.3% (TBDMS protected nucleosides) to 12.9% (Bz protected nucleosides) in five reaction steps. The building block was incorporated into two different oligonucleotide sequences: internally modified **RNA1** and 5'-terminally modified **RNA2**.

Both RNA sequences were modified in a bioorthogonal manner by photoclick reaction with either NMM or dye maleimide conjugates (AF555, sulfoCy3 and AF647). The reaction was carried out in aqueous Na-P<sub>i</sub> buffer system upon irradiation for up to 30 minutes at  $\lambda = 300$  nm. The *FRET* behavior between the pyrazoline as a donor and the respective dye as an acceptor was investigated (Figure 34).

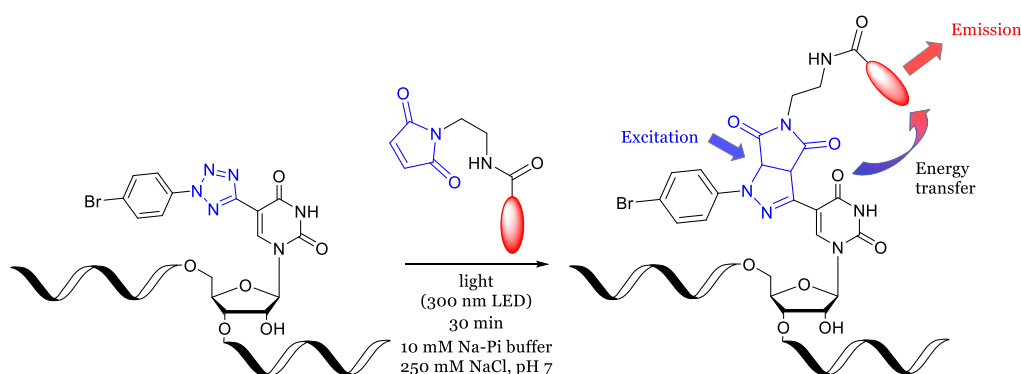


**Figure 34.** Schematic presentation of the photoclick reaction on **RNA1** and a dye maleimide conjugate. The pyrazoline formed during the reaction acts as a *FRET* donor, whereas the attached dye acts as an acceptor. Figure was published before.<sup>[137]</sup>

The reaction of each sequence with each dye was investigated in terms of yield, fluorogenicity and the ability to transfer to cells. In general, the yields and fluorogenic behavior of the reaction with the terminal sequence **RNA2** was greater than the respective reactions with **RNA1**. The highest yields (up to 84% upon reaction with **RNA2**) were achieved with AF555 maleimide as a reaction partner, whereas with sulfo-Cy3 maleimide the highest increase in fluorescence was achieved (up to 9.4-fold upon reaction with **RNA2**). Regarding cell experiments, the least autofluorescence of the cells was detected in the range of the emission of

### 3 Tetrazole-Modified Oligonucleotides for Bioorthogonal Labeling

AF647 or spectroscopical analogs of this dye, as demonstrated in spectroscopic experiments with *HeLa* cell lysate as solvent.

The three dyes AF555, sulfoCy3 and AF647 maleimide were further tested in experiments to determine the cell penetration of each of the dyes, however the dyes were proven to be unsuitable for live cell imaging because of poor cell penetration.

With respect to future cell experiments, the spectroscopic experiments should be repeated with uncharged or positively charged dye maleimides in the spectral range of the dyes used in this work, such as Cy3, Cy5 or BDP TMR maleimide to determine the *FRET* behavior of the system.

## 4 Sydnone-Modified Oligonucleotides for Bioorthogonal Labeling

During the past few years, sydnone have been employed in bioorthogonal labeling of proteins by SPSAC and photoclick-type reactions.<sup>[77, 79-81, 84-85, 115]</sup> As described in chapter 2.2.2, higher rate constants could be achieved by employing sydnone instead of azides in reaction with strained alkynes, such as **BCN**, which has - to the best of our knowledge - not been demonstrated on nucleic acids up to this point.

### 4.1 Synthesis of Sydnone-Modified Nucleosides **31**, **32** and **33**

As a first step towards the nucleosides, aminopropyl-modified nucleoside **22** was synthesized (Figure 35). 5-Iodo-2'-deoxyuridine (**16**) was reacted according to literature by *Sonogashira* reaction with trifluoroacetyl protected propargylamine (**17**) to nucleoside **18** in 76% yield, followed by hydrogenation of the triple bond by hydrogen with palladium on charcoal as a catalyst to give **19** in 86% yield.<sup>[141-143]</sup> As a last step, the trifluoroacetyl protecting group was removed by concentrated aqueous ammonia in quantitative yield.<sup>[107]</sup>

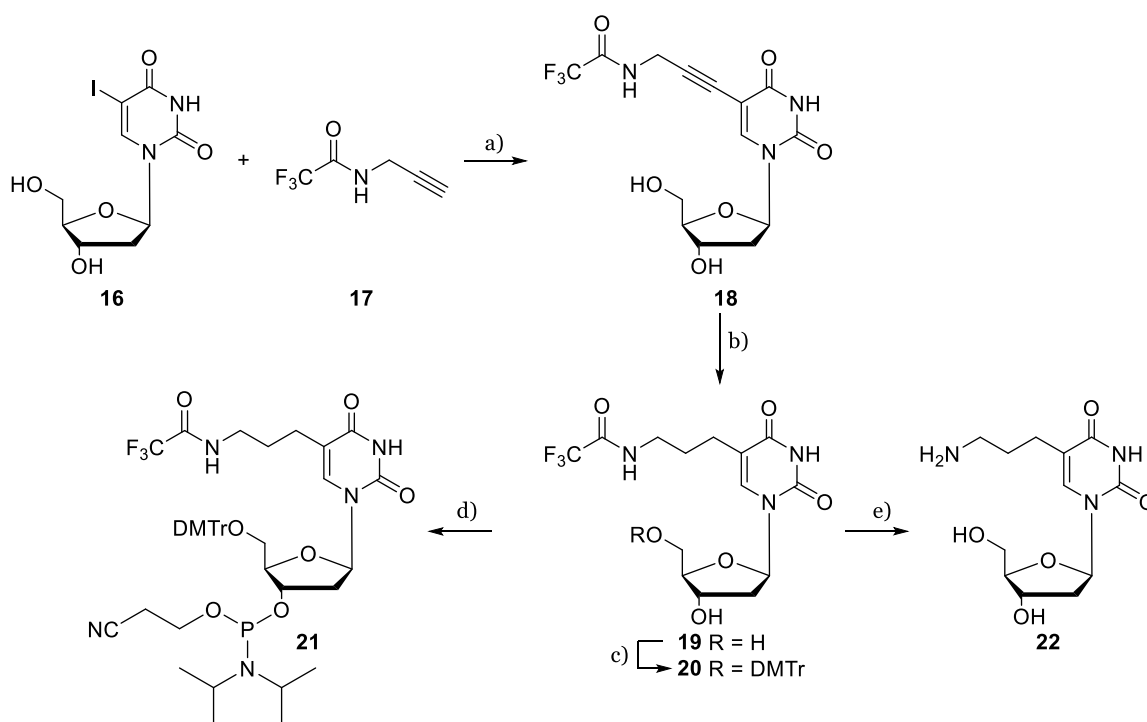


**Figure 35.** Synthesis of aminopropyl-modified building block **22** and phosphoramidite building block **21**: a) copper(I) iodide, tetrakis(triphenylphosphine)palladium(0), triethylamine, DMF, 50 °C, 5 h, 76% b) hydrogen, Pd/C, MeOH, r.t., 6 h, 86% c) 4,4'-dimethoxytrityl chloride, silver(II) nitrate, pyridine, r.t., 16 h, 46% d) 2-Cyanoethyl *N,N*-diisopropyl-chlorophosphoramidite, DIPEA, dichloromethane, r. t., 2 h, 62,% e) conc. NH<sub>4</sub>OH, r.t., 16 h, quant.

## 4 Sydnone-Modified Oligonucleotides for Bioorthogonal Labeling

Additionally, nucleoside **20** was synthesized in 46% yield by protection of the 5'-position of nucleoside **19** with 4,4'-dimethoxytrityl chloride and silver(II) nitrate as a catalyst, followed by reaction with 2-cyanoethyl *N,N*-diisopropylchlorophosphoramidite and DIPEA to give building block **21** in 62% yield.

Simultaneously, sydnone NHS-esters **28** and **29** were synthesized (Figure 36). Compound **29** was partially provided by the lab of *F. Friscourt* (University of Bordeaux, France). As a first step, compound **25** was synthesized following a literature procedure by reaction of 4-aminobenzoic acid (**23**) with sodium chloroacetate (**24**) to give compound **25** in 46% yield.<sup>[144]</sup>

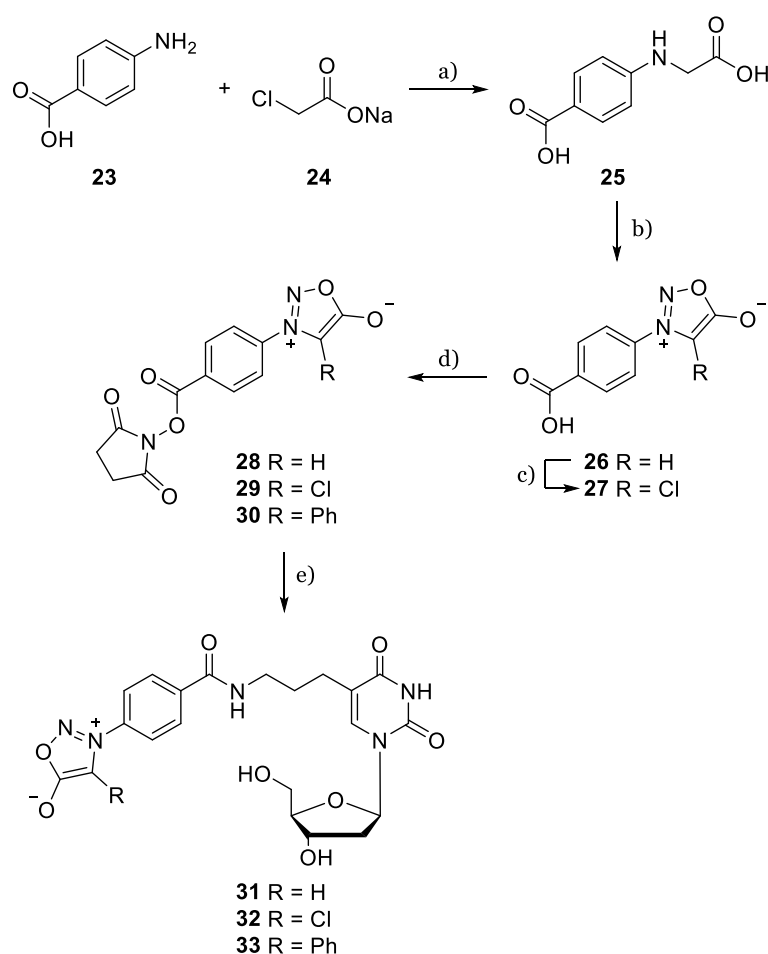


**Figure 36.** Synthesis of sydnone NHS-esters **28** and **29**: a) water, 100 °C, 4 h, 46%<sup>[107]</sup> b) *tert*-butyl nitrite, trifluoroacetic anhydride, THF, r.t., 2 h, 82%<sup>[84]</sup> c) sodium hypochlorite, dioxane/1M HCl, r.t., 20 h, 43%<sup>[79]</sup> d) *N*-hydroxysuccinimide, *N*-(3-dimethylaminopropyl)-*N'*-ethylcarbodiimide hydrochloride, DMF, r.t., 16 h, **28** 78%, **29** 89%<sup>[84]</sup> e) **22**, triethylamine, DMF, r.t., 16 h, **31** 29%, **32** 54%, **33** 23%.

Subsequently, compound **25** was reacted with *tert*-butyl nitrite to form a nitrosylated intermediate, followed by cyclization with trifluoroacetic anhydride to give sydnone **26** in 82% yield.<sup>[84]</sup> Sydnone **27** was synthesized by chlorination of

## 4 Sydnone-Modified Oligonucleotides for Bioorthogonal Labeling

---

sydnone **26** by sodium hypochlorite solution in 43% yield. For coupling to the nucleoside **22**, activation of the carboxylic acid was necessary, which was achieved by reaction of sydnones **26** and **27** with N-hydroxysuccinimide and N-(3-dimethylaminopropyl)-N'-ethylcarbodiimide hydrochloride to give NHS-esters **28** (78% yield) and **29** (89% yield).<sup>[84]</sup> As a last step, the NHS-esters were coupled to nucleoside **22** via standard amide-coupling using triethylamine as a base to give sydnone-modified nucleosides **31** (29% yield) and **32** (54% yield). Additionally, NHS-ester **30** (provided by the lab of *F. Friscourt*, University of Bordeaux, France) was coupled to nucleoside **22** under the same conditions to give compound **33** in 23% yield.

## 4.2 Synthesis and Characterization of Sydnone-Modified DNA strands

As a first step, phosphoramidite building block **21** was incorporated internally into DNA sequence **DNA3** using standard solid-phase synthesis protocol (Figure 37).

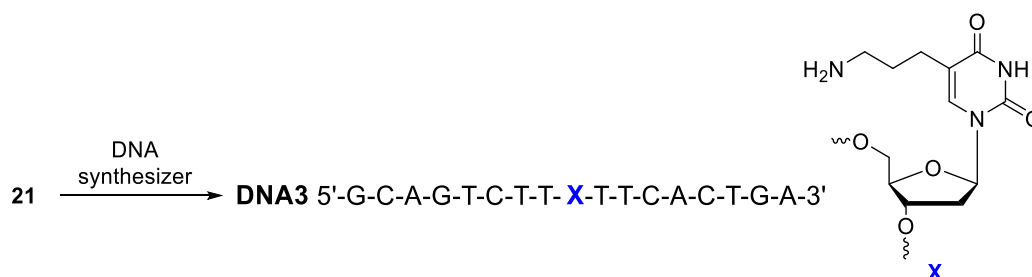


**Figure 37.** Phosphoramidite building block **21** was incorporated into oligonucleotide **DNA3** via standard solid-phase synthesis protocol.

The oligonucleotide was cleaved from solid support and the success of the synthesis verified *via* MALDI-TOF mass spectrometry (Table 6).

**Table 6.** Calculated and measured masses of oligonucleotide **DNA3**.

sequence	calculated mass [Da]	measured mass [Da]
<b>DNA3</b>	5191.9	5193.8

As a next step, the sydnone-modified oligonucleotides were synthesized. **DNA3** was reacted with either NHS-ester **28** or **29** with DIPEA as a base in DMSO to yield **DNA4** and **DNA5** (Figure 38).

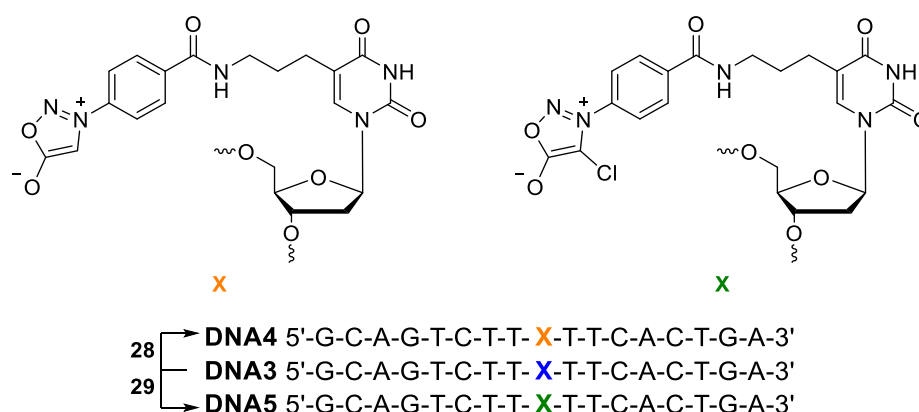


**Figure 38.** Sequences of **DNA4** and **DNA5**.

After purification of the modified strands *via* HPLC-chromatography, the success of the reaction was evidenced by MALDI-TOF analysis (Table 7). Upon measurement, additionally to the mass of the intact oligonucleotide, the mass of a

## 4 Sydnone-Modified Oligonucleotides for Bioorthogonal Labeling

decarboxylated and in case of **DNA5** also dechlorinated fragment was observed due to irradiation of the sample due to the laser.

**Table 7.** Calculated masses and structures of oligonucleotides **DNA4** and **DNA5** and their decarboxylated analogs **DNA4-CO<sub>2</sub>** and **DNA5-CO<sub>2</sub>-Cl**.

sequence	calculated mass [Da]	measured mass [Da]
<b>DNA4</b>	5379.9	5374.4
<b>DNA4-CO<sub>2</sub></b>	5336.0	5335.9
<b>DNA5</b>	5413.9	5414.9
<b>DNA5-CO<sub>2</sub>-Cl</b>	5336.0	5336.6

The oligonucleotides were quantified photometrically, characterized by UV/Vis spectroscopy and compared to nucleosides **31** and **32** (Figure 39). The nucleosides show a distinct band with a local maximum around 319 nm that can be assigned to the sydnone moiety. Apart from the maximum at 260 nm, **DNA4** and **DNA5** also display the sydnone band around 320 nm.

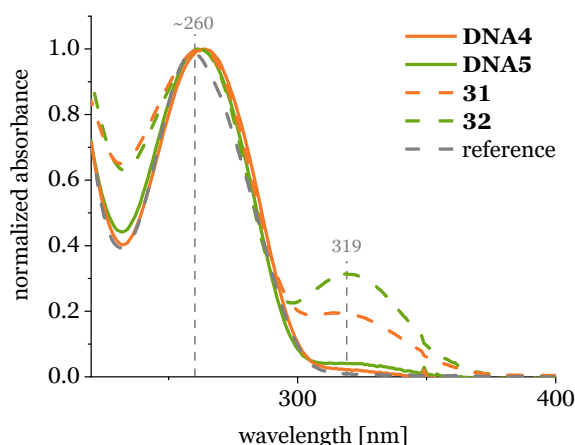


**Figure 39.** Normalized UV/vis spectra of the oligonucleotides **DNA4** and **DNA5** and nucleosides **30** and **31**, along with a random DNA sequence as a reference. Oligonucleotides **DNA4** and **DNA5** were measured as 2.5  $\mu\text{M}$  solution in 10 mM Na-P<sub>i</sub> buffer with 250 mM NaCl at pH 7 at 20 °C. Nucleosides **31** and **32** were measured as 25  $\mu\text{M}$  solution in methanol at 20 °C.

### 4.3 Bioorthogonal Labeling Experiments

#### 4.3.1 SPSAC Experiments

As a first step, SPSAC labeling experiments were performed on the nucleosides **30** and **31** to get an insight about the change of the absorbance and fluorescence properties for future cellular application, followed by transfer of the results to oligonucleotides **DNA4** and **DNA5**. As described in chapter 2.2.2, strained alkynes present suitable reaction partners for sydrones. In this work, BCN (**34**) was initially chosen as a reaction partner because of the commercial availability and the comparably small size (Figure 40).

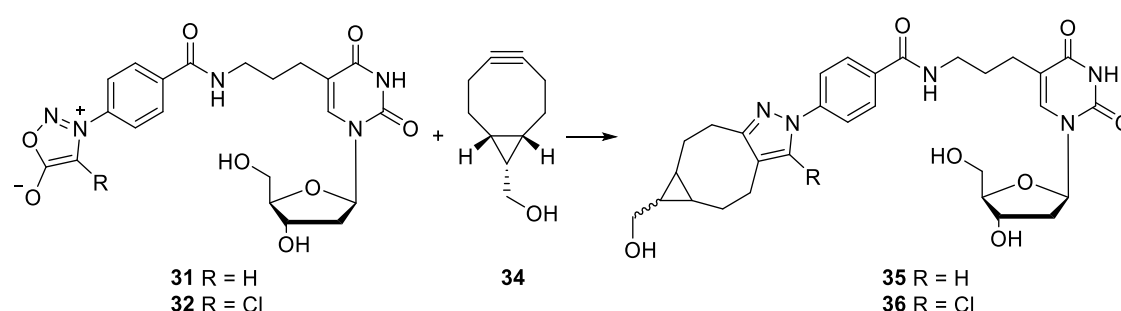


**Figure 40.** Reaction between sydnone-modified nucleosides **30** or **31** and BCN (**32**) results in pyrazoles **33** and **34**.

##### 4.3.1.1 Labeling Experiments with Nucleoside **31**

The pyrazole moiety formed during the reaction was presumed to be fluorescent, resulting in a fluorogenic behavior of the reaction. To verify this assumption, nucleoside **31** was reacted with BCN (**34**) and the UV/Vis absorbance and fluorescence recorded at defined times.

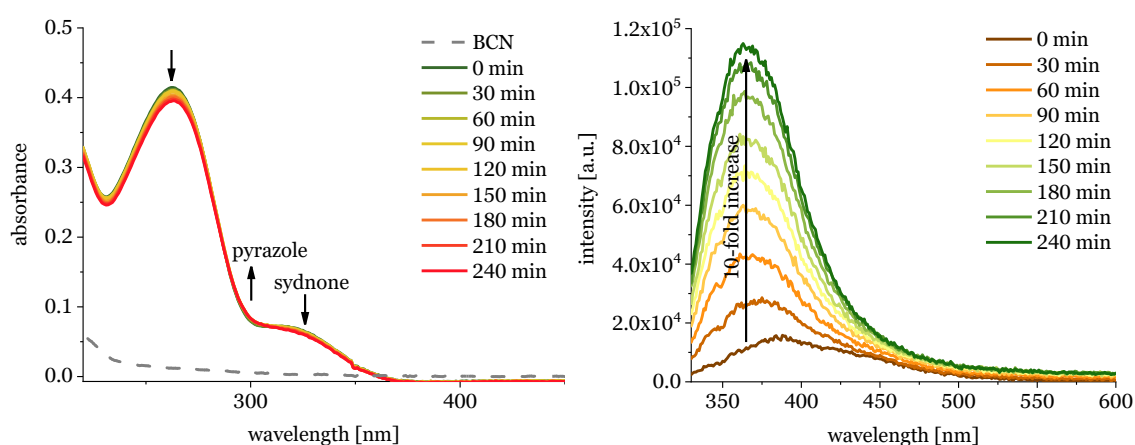


**Figure 41.** UV/Vis absorbance (left) and emission (exc. = 315 nm, right) spectra of the reaction between **31** and 1.00 equiv. BCN over 4 hours. 25  $\mu$ M **31**, 25  $\mu$ M BCN (1.00 equiv.) in methanol at 20 °C.

## 4 Sydnone-Modified Oligonucleotides for Bioorthogonal Labeling

At first, nucleoside **31** was reacted with 1.00 equivalent of BCN (Figure 41). Two samples were prepared, and the absorbance and emission spectra were collected every 30 minutes for 240 minutes in total. The absorbance spectra only show very little change in absorbance (Figure 41, left). A slight decrease of the sydnone absorbance around 325 nm can be observed, whereas the absorbance around 300 nm is increasing, which can be assigned to the formation of a pyrazole. Additionally, an isosbestic point is formed at 309 nm. Surprisingly, the emission spectra (Figure 41, right) show a significant 10-fold increase of fluorescence during the same reaction time which does not fully comply with the little change that is observed in the absorbance spectra. This might indicate different reactivity in the sample that was subjected to irradiation upon measurement of the emission, as the excitation wavelength of  $\lambda = 315$  nm is close to the local maximum of the sydnone absorbance. To verify this assumption, the experiments were repeated, but the same sample was used for measurement of both the absorbance and emission (Figure 42).

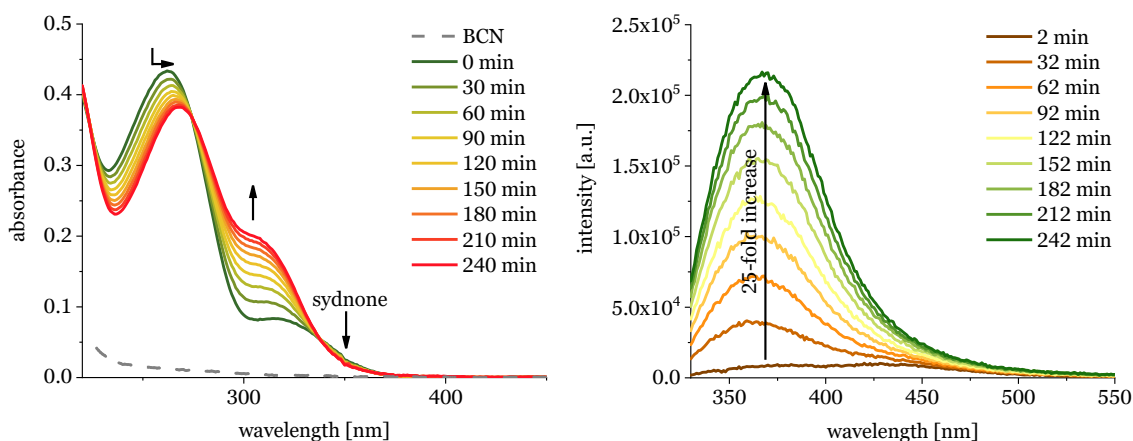


**Figure 42.** UV/Vis absorbance (left) and emission (exc. = 315 nm, right) spectra of the same sample of the reaction between **31** and 1.00 equiv. BCN over 4 hours. 25  $\mu$ M **31**, 25  $\mu$ M BCN (1.00 equiv.) in methanol at 20  $^{\circ}$ C.

Absorbance and emission spectra were recorded every 10 minutes to increase the total excitation time of the sample. For better clarity, only spectra taken every 30 minutes are presented. The absorbance spectra (Figure 42, left) show significantly increased change compared to the non-irradiated sample (Figure 41, left). The sydnone absorbance is increased, whereas a new band around 300 nm is formed. Furthermore, the maximum at 262 nm is shifted bathochromically to 269 nm while concomitantly being decreased. The spectra display two isosbestic points at  $\lambda = 337$  nm and  $\lambda = 274$  nm, compared to one isosbestic point at

## 4 Sydnone-Modified Oligonucleotides for Bioorthogonal Labeling

$\lambda = 309$  nm in the non-irradiated sample. This indicates that different reactions are taking place in the irradiated vs. non-irradiated sample. The emission spectra (Figure 42, right) even display a 25-fold increase of fluorescence, which is another indication for a photoactivated pathway, as this sample was in total irradiated longer compared to the first sample (Figure 41) because of the increased number of measurements. Additionally, a shift of the maximum from 354 nm (Figure 41, right) to 367 nm (Figure 42, right) was observed. At first, a photoclick-type pathway (Figure 43) was assumed as a concurring side reaction towards the SPSAC, as described in chapter 2.2.3.1.

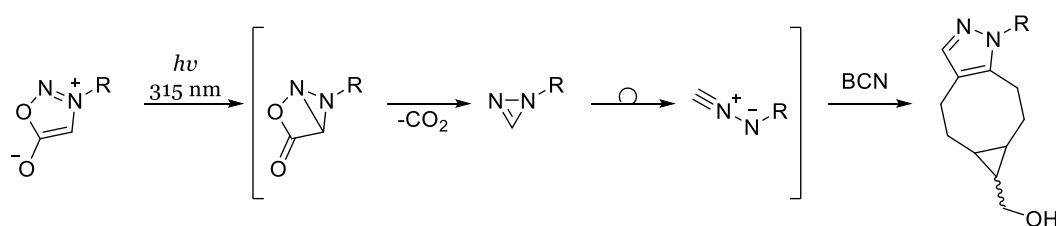


**Figure 43.** The photoclick-type pathway as a competing reaction to the SPSAC.

To further investigate this assumption, nucleoside **31** was irradiated at  $\lambda = 365$  nm in presence of 10.0 equivalents NMM as a reaction partner. NMM was chosen instead of BCN to prevent spontaneous reaction between the sydnone and the reaction partner. However, upon measurement of MALDI-TOF MS, only the mass of the starting material minus CO<sub>2</sub> was observed. Because of ionization by a laser during MALDI measurement, it was unclear if the decarboxylated molecule is a result of the reaction or of the ionization. To further verify this, an additional sample containing only nucleoside **31** in methanol and 10% water was prepared and irradiated at  $\lambda = 365$  nm for 120 s. ESI-MS measurement of that sample showed also the decarboxylated mass (Figure 44), whereas nucleoside **31** did not show no such fragment, indicating that the decarboxylated molecule is the product of irradiation. A possible structure of the formed reaction product can be the diazirine **37**, as this was described in literature as an intermediate upon photolysis of sydrones, however proof of that structure by NMR could not be achieved. [112-114]

## 4 Sydnone-Modified Oligonucleotides for Bioorthogonal Labeling

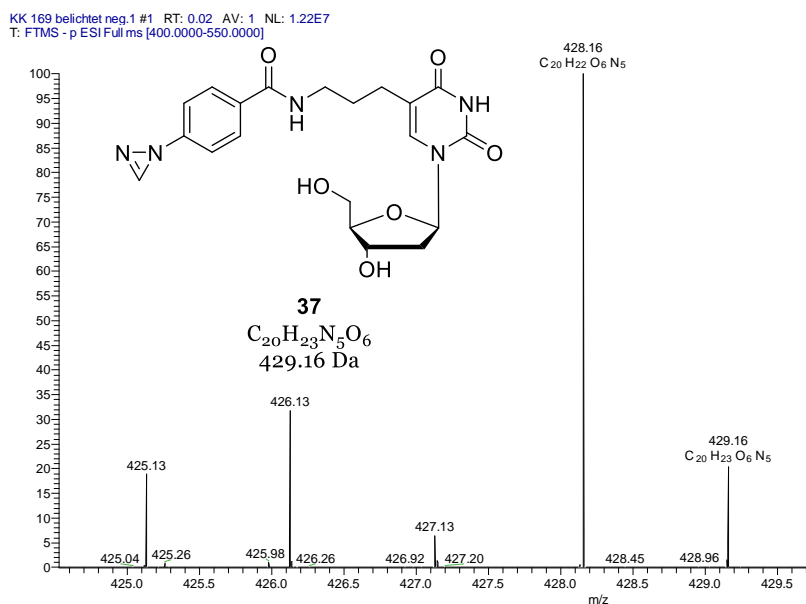


**Figure 44.** ESI-MS (negative ion mode) and proposed structure **37** upon irradiation of nucleoside **31** in methanol/10%  $H_2O$ .

The SPSAC experiments were repeated with 10.0 equivalents BCN to get a better insight about the changes of absorbance during the reaction. The absorbance spectra (Figure 45, left) show similar behavior to the sample with 1.00 equivalent BCN. The sydnone absorbance around 325 nm is decreasing, while a new band around 300 nm is formed that can be assigned to the pyrazole. Two isosbestic points at 272 and 314 nm are formed. Furthermore, the maximum at 262 nm experiences a bathochromic shift to 269 nm, while concomitantly being decreased.

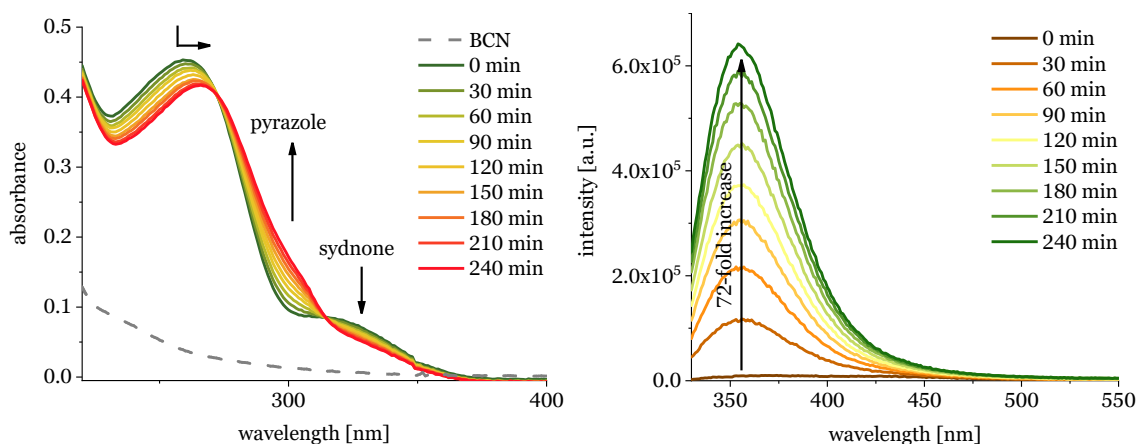


**Figure 45.** UV/Vis absorbance (left) and emission (exc. = 315 nm, right) spectra of the reaction between **31** and 10.0 equiv. BCN over 4 hours. 25  $\mu M$  **30**, 250  $\mu M$  BCN (10.0 equiv.) in methanol at 20  $^{\circ}C$ .

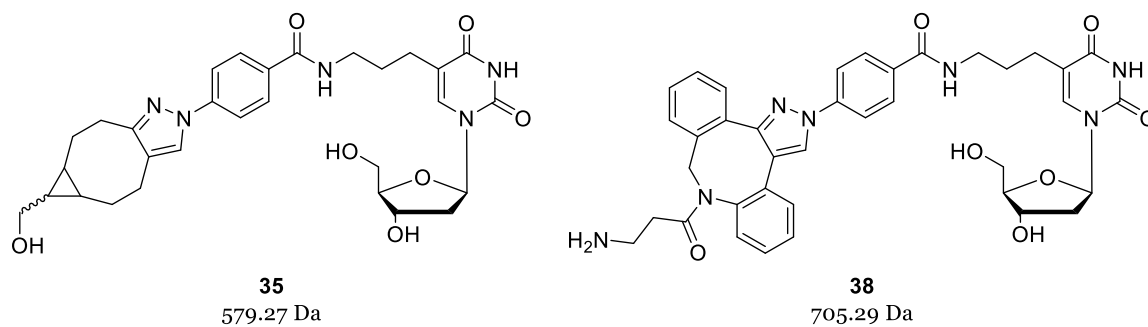
The emission spectra (Figure 45, right) show a 72-fold increase of emission, however some of the increase most likely has to be attributed to the formation of the fluorescent product that is produced upon irradiation. Additionally, the

## 4 Sydnone-Modified Oligonucleotides for Bioorthogonal Labeling

experiments were repeated with DIBAC-amine as a reaction partner, as most commercially available dyes offer a DIBAC moiety as reactive part instead of BCN. Due to strong spectral overlap, absorbance and emission spectra are not presented.

The success of the reaction of nucleoside **31** and BCN or DIBAC, respectively, were verified by MALDI-TOF (Table 8).

**Table 8.** Structures and calculated and measured masses of SPSAC products 35 and 38.



	calculated mass [Da]	measured mass [Da]
<b>35</b>	579.27	579.23
<b>38</b>	705.29	705.90

## 4 Sydnone-Modified Oligonucleotides for Bioorthogonal Labeling

### 4.3.1.2 Labeling Experiments with **DNA4**

Additionally, SPSAC labeling experiments were carried out with **DNA4** and Cy3 DIBAC (Figure 46). As the fluorescence properties of the model reaction on the nucleoside **31** with unmodified BCN did not meet the requirements needed for cellular imaging in terms of excitation and emission wavelengths (exc. = 315 nm, em. = 330-500 nm), a reactive dye was chosen as a reaction partner for better visualization.

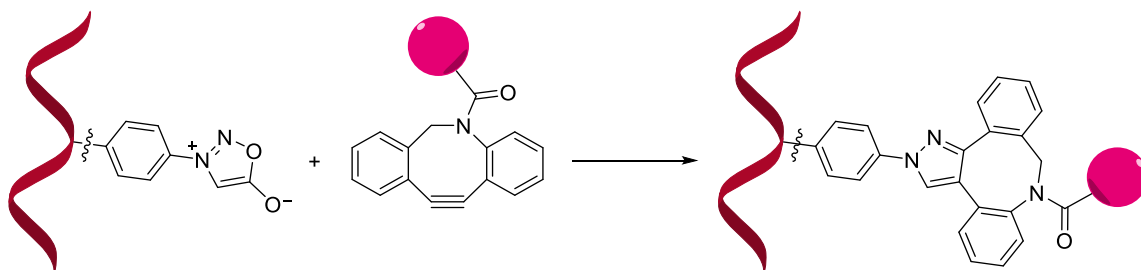


**Figure 46.** Schematic presentation of the reaction between **DNA4** and Cy3-DIBAC to form a pyrazole.

As mentioned before, more dye DIBAC conjugates are commercially available than dye BCN conjugates. Additionally, DIBAC was reported in literature to achieve greater reaction rate constants compared to BCN.<sup>[81]</sup> Based on the results of the reaction of nucleoside **31**, a 2.5  $\mu\text{M}$  solution of **DNA4** was reacted with 25  $\mu\text{M}$  Cy3 DIBAC (10.0 equivalents) in water (+ 5% DMSO). The course of the reaction was monitored by analytical HPLC (0-80% ACN in 40 minutes, 40  $^{\circ}\text{C}$ , 1.00 mL/min).

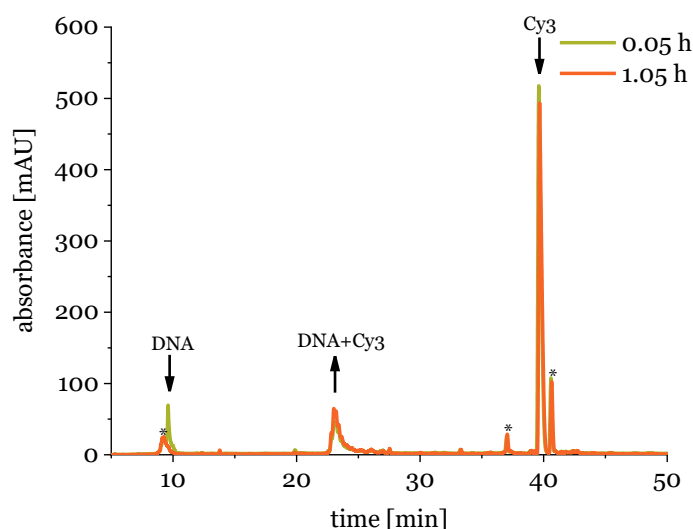


**Figure 47.** HPLC Chromatograms (260 nm detection wavelength) of the reaction between 2.5  $\mu\text{M}$  **DNA4** and 25  $\mu\text{M}$  Cy3 DIBAC (10.0 equiv.). The signal of **DNA4** (9.5 min) and Cy3 (40 min) are decreasing, whereas the product signal (22 min) is increasing. Additionally, the chromatogram shows impurities (marked with an asterisk) at 9 min, 37 min and 41 min retention time.

## 4 Sydnone-Modified Oligonucleotides for Bioorthogonal Labeling

Opposed to the previously recorded spectra of the reaction between nucleoside **30** and BCN, there is a significant amount of product formation after ~3 minutes reaction time (Figure 47, 22 min retention time). This indicates a very rapid reaction. The chromatograms indicate completion of the reaction within 1.05 hours reaction time, as the signal of **DNA4** (9.5 min retention time) is consumed completely, as no sydnone absorbance (above 300 nm) can be observed in the absorbance spectrum recorded during the HPLC run (Figure 48, left), indicating that the remaining signal is an impurity that could not be removed completely by prior HPLC purification of the oligonucleotide.

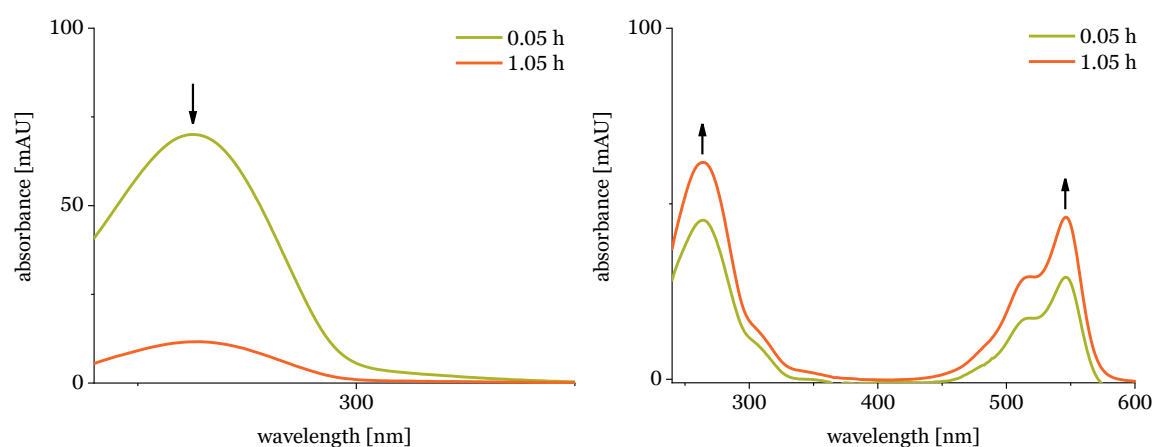


**Figure 48.** UV/Vis absorbance taken as snapshots during the HPLC runs at 0.05 and 1.05 h reaction time. Left: **DNA4**, 9 min retention time, right: **DNA4+Cy3DIBAC**, 22 min retention time.

Assuming this, the reaction achieves complete conversion of the starting material to the desired **DNA4 Cy3** conjugate (Figure 48, right, 22 min retention time) in nearly quantitative yield. Additionally, the experiments were repeated with 1.50 equivalents Cy3 DIBAC to get a better insight about the reaction rate. The chromatograms display the same peaks as the reaction with 10.0 equivalents Cy3 DIBAC (see chapter 6.3, Figure A4 and Figure A5), however the reaction takes ~3 hours to achieve completion.

The success of the reaction was determined *via* MALDI-TOF (Table 9).

**Table 9.** Calculated and measured masses of DNA4 Cy3 adduct.

adduct	calculated mass [Da]	measured mass [Da]
<b>DNA4 Cy3</b>	6093.4	6093.8

## 4 Sydnone-Modified Oligonucleotides for Bioorthogonal Labeling

### 4.3.1.3 Labeling Experiments with Nucleoside **32**

Similar experiments were performed with the chloro-sydnone modified nucleoside **32**. The chlorinated sydnone was chosen in expectation of a faster reaction compared to the unmodified sydnone as previously reported in literature.[79]

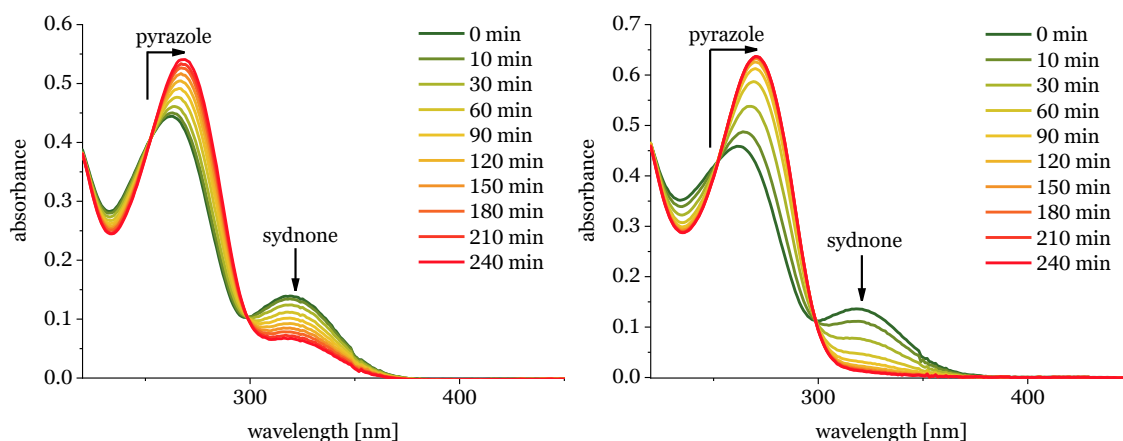


**Figure 49.** UV/Vis absorbance spectra of the reaction between **32** and 1.00 equiv. (left) and 10.0 equiv. (right) BCN over 4 hours. 25  $\mu$ M **32**, 25  $\mu$ M BCN (1.00 equiv.)/ 250  $\mu$ M BCN (10.0 equiv.) in methanol at 20 °C.

Even with 1.00 equivalent BCN (Figure 49, left), a significant change of absorbance can be observed, indicating an even faster reaction compared to non-chlorinated nucleoside **31**. The sydnone signal between 300 and 375 nm is decreasing, whereas a new band around 269 nm is formed. The maximum of the spectrum is experiencing a bathochromic shift from 262 to 269 nm while concomitantly increasing in absorbance. Isosbestic points can be observed at 252 and 300 nm.

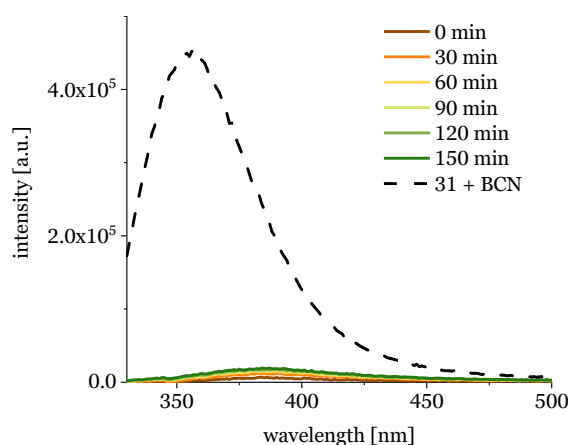


**Figure 50.** Emission spectra (exc. = 315 nm) of the reaction between 25  $\mu$ M **32** and 250  $\mu$ M BCN (10.0 equiv., solid colored lines) compared to emission of the reaction between 25  $\mu$ M **31** and 250  $\mu$ M BCN (150 minutes, 10.0 equiv., dashed black line) in methanol.

## 4 Sydnone-Modified Oligonucleotides for Bioorthogonal Labeling

In case of reaction with 10.0 equivalents BCN (Figure 49, right) the sydnone signal between 300 and 375 nm vanishes completely, indicating completion of the reaction within 4 hours reaction time. This is significantly faster compared to nucleoside **31**, as in that case completion of the reaction could only be observed with 100 equivalents BCN after 6 hours reaction time. In general, for 10.0 equivalents BCN similar behavior as with 1.00 equivalent BCN can be observed. The emission spectra only showed negligible fluorescence compared to nucleoside **31** (Figure 50), which is possibly caused by a fluorescence quenching effect of the chlorine substituent.

### 4.3.1.4 Labeling Experiments with DNA5

In the following, the results from nucleoside **32** were transferred to **DNA5**. The SPSAC experiments on **DNA5** were carried out under the same conditions as **DNA4** labeling experiments in water with 1.50 equivalents Cy3 DIBAC as an reaction partner (Figure 51).

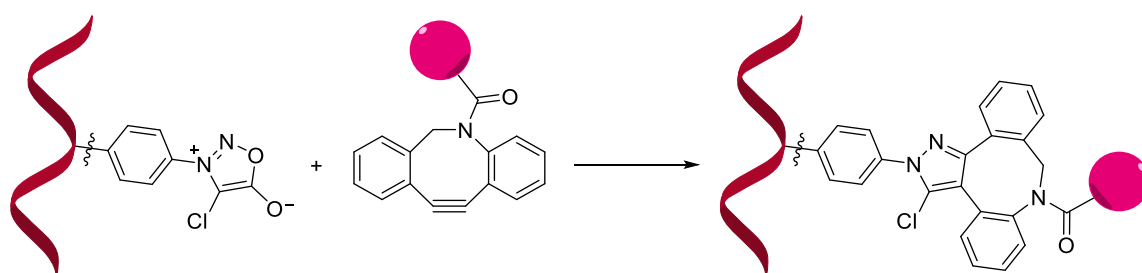


**Figure 51.** Schematic presentation of the reaction between **DNA5** and Cy3-DIBAC to form a pyrazole.

The course of the reaction was monitored *via* analytical HPLC chromatography (0-80% ACN in 40 minutes, 40 °C, 1.00 mL/min). The chromatogram (Figure 52) shows similar behavior as the reaction between **DNA4** and Cy3 DIBAC, the DNA signal at 9 minutes retention time is decreasing over the course of the reaction, whereas the signal of the **DNA5 Cy3** adduct is concomitantly increasing. The same impurity as previously described in experiments with **DNA4** (Figure 47, 9 min retention time) is observed. Even after 3 minutes reaction time, the chromatogram displays a significant amount of product formation, indicating very rapid reaction. Regarding the HPLC chromatogram, the reaction achieves completion with nearly quantitative yield after ~1 hour reaction time, which is significantly faster than the ~3 hours reaction time of the reaction of **DNA4** with 1.50 equivalents Cy3 DIBAC.

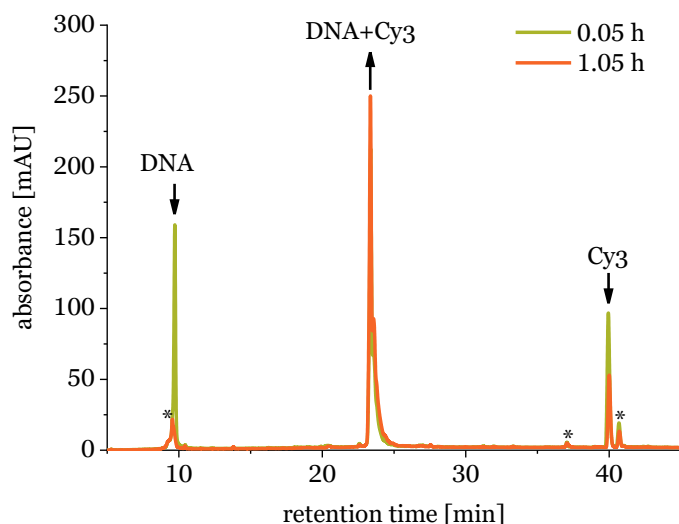


**Figure 52.** HPLC Chromatograms (260 nm detection wavelength) of the reaction between 2.5  $\mu\text{M}$  **DNA5** and 3.75  $\mu\text{M}$  Cy3 DIBAC (1.50 equiv.). The signal of **DNA5** (9.5 min) and Cy3 (40 min) are decreasing, whereas the product signal (23 min) is increasing. Additionally, the chromatogram shows impurities (marked with an asterisk) at 9 min, 37 min and 41 min retention time.

The success of the reaction was determined *via* MALDI-TOF (Table 10).

**Table 10.** Calculated and measured masses of DNA5 Cy3 adduct.

adduct	calculated mass [Da]	measured mass [Da]
<b>DNA5 Cy3</b>	6127.4	6129.5

## 4.3.2 Photoclick Experiments

Additional to the SPSAC experiments, photoclick experiments were performed with nucleoside **33** and maleimide derivatives as electron-deficient alkenes (Figure 53). Similar to the tetrazole photoclick reaction, the pyrazoline moiety that is formed during the reaction was presumed to be fluorescent, resulting in a fluorogenic behavior of the reaction throughout formation of the pyrazoline. The sydnone used in this work has been published in literature before, however only the labeling of proteins was investigated before.<sup>[115]</sup>

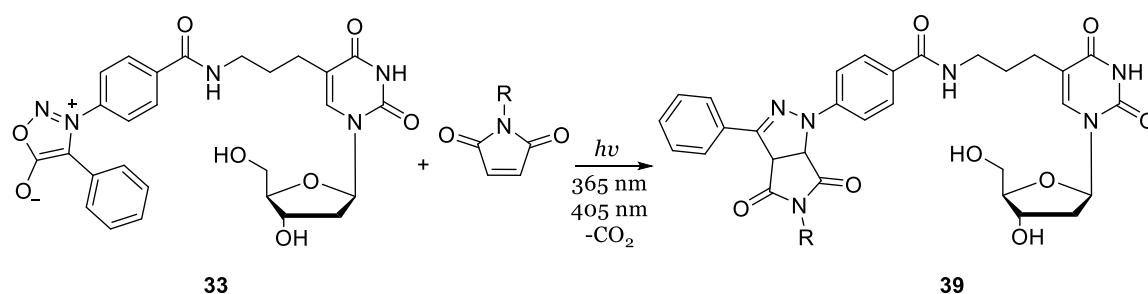


**Figure 53.** Schematic presentation of the reaction between nucleoside **33** and NMM to form a fluorescent pyrazoline.

The first experiments were carried out with 25  $\mu\text{M}$  **33** and 37.5  $\mu\text{M}$  NMM (1.50 equiv.) by irradiation with  $\lambda = 405\text{ nm}$  light in water (+0.01% methanol). Absorbance and emission spectra were collected at defined times after irradiation.

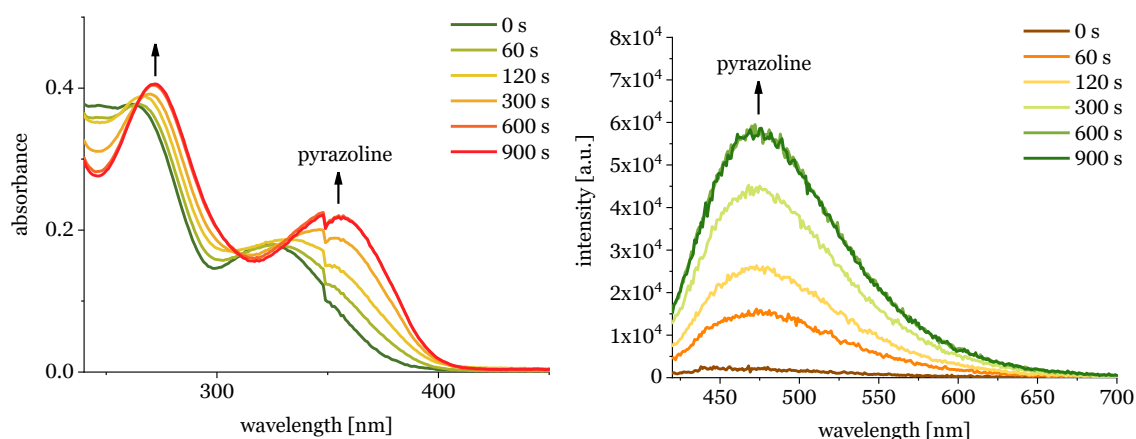


**Figure 54.** UV/Vis absorbance (left) and emission (exc. = 405 nm, right) spectra of the reaction between nucleoside **33** and NMM over 15 minutes (irradiation time,  $\lambda = 405\text{ nm}$ ). 25  $\mu\text{M}$  **33**, 37.5  $\mu\text{M}$  NMM (1.50 equiv.) in  $\text{H}_2\text{O}$  +0.01% methanol, 20  $^\circ\text{C}$ .

In the absorbance spectra (Figure 54, left), the formation of a new band around 350 nm can be observed that can be assigned to the formation of a fluorescent pyrazoline ( $\Phi_F = 0.043$ ,  $\lambda_{\text{exc}} = 400\text{ nm}$ ). The emission spectra (Figure 54, right) display the 29-fold increase of fluorescence around 475 nm, which is a typical

## 4 Sydnone-Modified Oligonucleotides for Bioorthogonal Labeling

behavior for the formation of a pyrazoline. After 900 s irradiation time, the spectra display a slight decrease of absorbance in both local maxima, indicating the starting degradation of the product. Considering this, the reaction seems to reach an end point between 600-900 s irradiation time. Additional to the absorbance spectra, the reaction was monitored *via* analytical HPLC chromatography (0-50% ACN in 30 minutes, 40 °C, 1.00 mL/min).

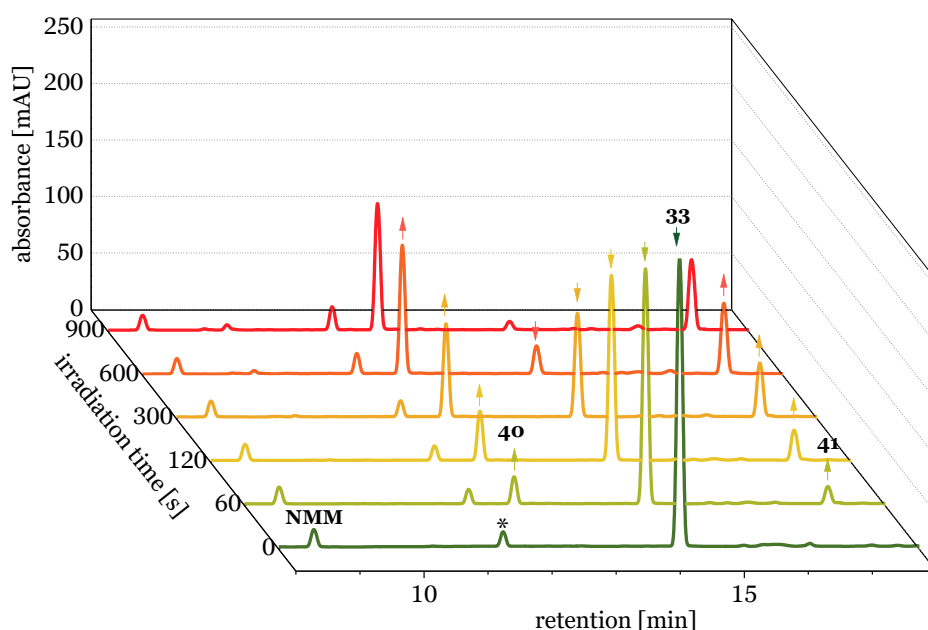


**Figure 55.** HPLC Chromatograms (260 nm detection wavelength) of the reaction between 25  $\mu\text{M}$  **33** and 37.5  $\mu\text{M}$  NMM (1.50 equiv.) in  $\text{H}_2\text{O}$  + 0.01% methanol, irradiation at  $\lambda = 405$  nm. The signal of nucleoside **33** (14.25 min) is decreasing, whereas the signal of the product **41** (17 min) is increasing. Additionally, the chromatogram shows signals of the hydrolyzed product **40** (12 min) and an unidentified impurity (11.5 min, marked with as asterisk).

The HPLC chromatogram (Figure 55) shows the formation of two new peaks at 12 min and 17 min retention time, whereas the signal of nucleoside **33** is decreasing over the course of the reaction, however it is not completely consumed during 900 s irradiation time, whereas the peaks at 12 and 17 min retention time are starting to degrade, as also observed in the absorbance and emission spectra.

## 4 Sydnone-Modified Oligonucleotides for Bioorthogonal Labeling

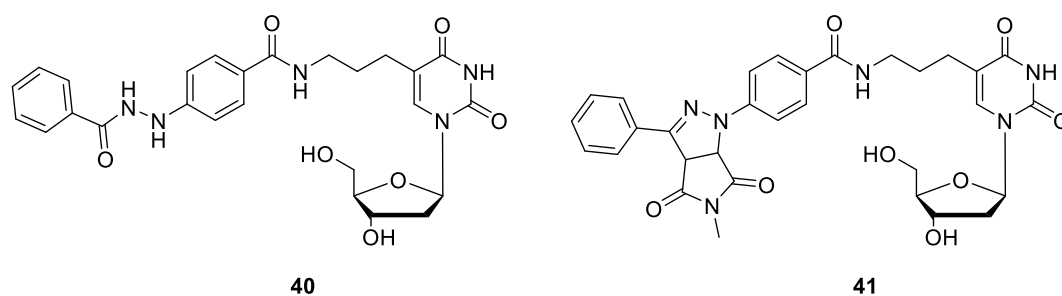


**Figure 56.** Structures of the water adduct **40** and the pyrazoline **41**.

One of the signals was presumed to be the water adduct **40**, whereas the other was presumed to be the pyrazoline **41** (Figure 56). To further identify the signals, absorbance spectra of each peak were recorded and evaluated (Figure 57). The signal at 12 min retention time was identified as the water adduct **40** (Figure 56), as neither sydnone nor pyrazoline absorbance was detected, whereas the signal at 17 min was identified as the pyrazoline **41**, as the spectra show distinct pyrazoline absorbance (~300-400 nm).

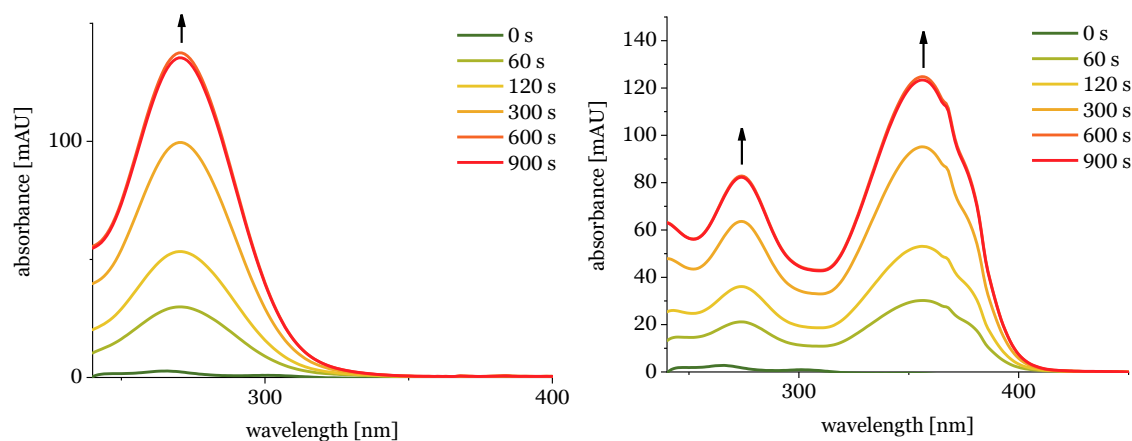


**Figure 57.** UV/Vis absorbance spectra taken as snapshots during the HPLC runs at 0-900 s irradiation time. Left: **40**, 12 min retention time, right: **41**, 17 min retention time.

Additionally, the peaks were collected, and the assignment further verified *via* MALDI-TOF mass spectrometry (see end of this chapter, Table **11**). The experiments were repeated with 365 nm irradiation, which led to a faster reaction (240 s irradiation time), presumably by more efficient generation of the nitrile-imine (see chapter 6.4, Figure A6 and Figure A7).

Furthermore, the experiments were repeated with 5.00, 7.00 and 10.0 equivalents NMM as reaction partner to determine the reaction rate constant, according to a procedure published by *Lin et al.*<sup>[145]</sup> Thymidine was used as an internal standard and the peak integral areas normalized and plotted against the irradiation time (see

## 4 Sydnone-Modified Oligonucleotides for Bioorthogonal Labeling

chapter 5.4, Figure 68). By averaging the three calculations, the reaction rate constant was calculated as  $k_2 = 27.6 \pm 2.7 \text{ M}^{-1}\text{s}^{-1}$ , which is in the same range as a previously reported similar tetrazole-modified nucleoside.<sup>[105]</sup> As the reaction is dependent on the generation of the nitrile-imine, the reaction rate could possibly be enhanced by irradiation at shorter wavelengths such as 365 nm, however 405 nm irradiation should produce less cell damage.

As a further experiment, nucleoside **33** was reacted with dye maleimide conjugates AF555, sulfo-Cy3 and Cy5 maleimide to investigate the possibility of a FRET, as the pyrazoline **41** offers close fluorescent properties to the pyrazoline described in chapter 3. As these experiments were performed on nucleoside **33** as opposed to oligonucleotide sequences in chapter 3, a 25  $\mu\text{M}$  solution of nucleoside **33** was reacted with 37.5  $\mu\text{M}$  dye maleimide (1.50 equiv.) in water +0.01% methanol. The solution was irradiated for defined times, followed by measurement of fluorescence spectra (0 s, 300 s, 600 s, 900 s). Due to the high concentrations, no absorbance spectra were recorded.

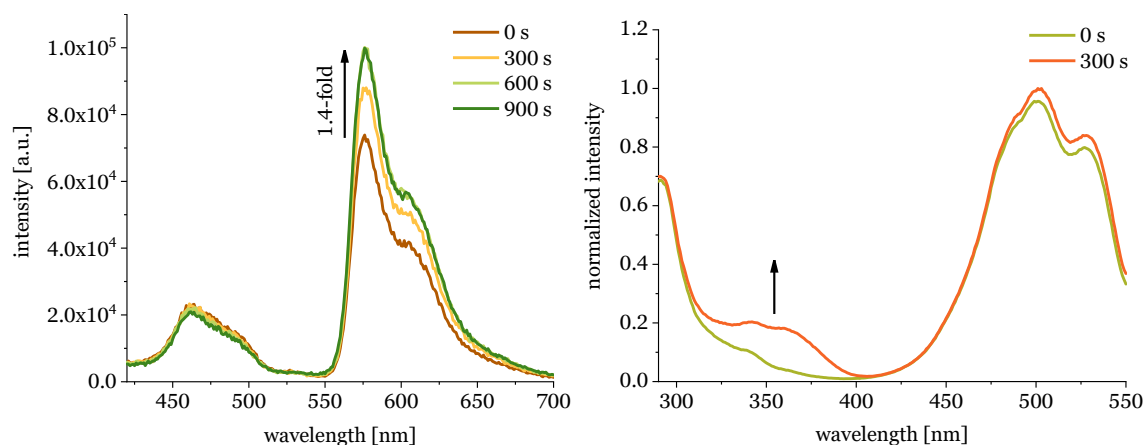


**Figure 58.** Emission ( $\lambda_{\text{exc.}} = 405 \text{ nm}$ , left) and excitation ( $\lambda_{\text{em.}} = 565 \text{ nm}$ , right) spectra of the reaction between 25  $\mu\text{M}$  nucleoside **33** and 37.5  $\mu\text{M}$  AF555 maleimide (1.50 equiv.) in  $\text{H}_2\text{O}$  +0.01% methanol, 20  $^\circ\text{C}$ .

Upon excitation at  $\lambda = 405 \text{ nm}$ , the emission spectra (Figure 58, left) show a 1.4-fold increase of fluorescence at the dye signal (550-650 nm), indicating an energy transfer between the pyrazoline moiety and the dye. Additionally, the excitation spectra ( $\lambda_{\text{em.}} = 565 \text{ nm}$ ) that were recorded during the reaction further verify the *FRET* behavior of the reaction, as the direct excitation of the dye increases only slightly during the reaction, whereas a new band around 350 nm is formed that complies with the pyrazoline absorbance. The emission signal around

## 4 Sydnone-Modified Oligonucleotides for Bioorthogonal Labeling

405-500 nm appears upon higher concentration of the dye. As this signal is overlapping with the emission signal of the pyrazoline, the efficiency of the *FRET* cannot be conclusively estimated, however a slight increase of the signal can be observed. Additionally, the fluorescence quantum yield of  $\Phi_F = 0.019$  ( $\lambda_{exc} = 400$  nm) was measured after 900 s irradiation time, which is significantly lower than the previously measured fluorescence quantum yield of pyrazoline **41** ( $\Phi_F = 0.043$ ,  $\lambda_{exc} = 400$  nm).

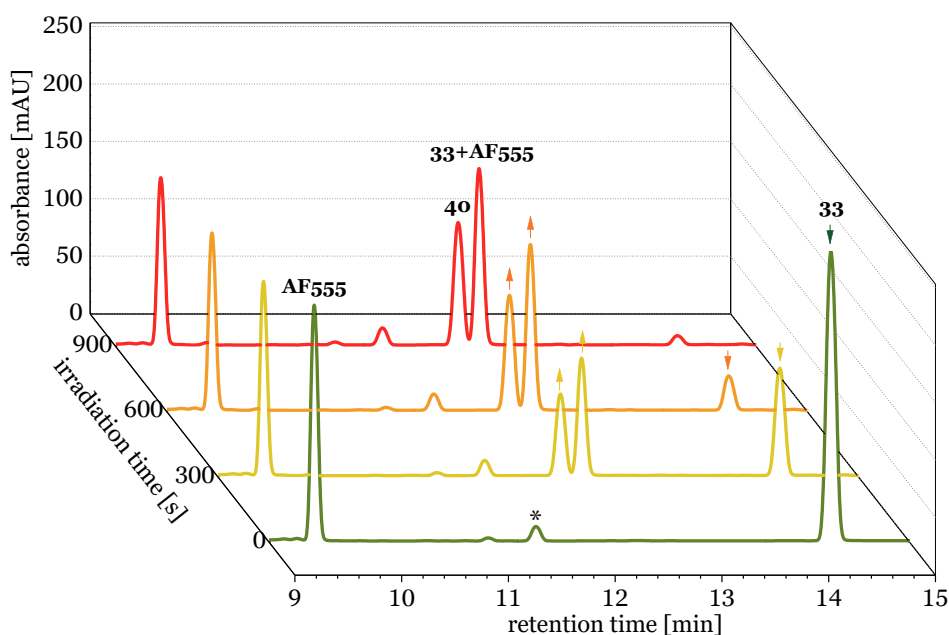


**Figure 59.** HPLC chromatograms (260 nm detection wavelength) of the reaction between 25  $\mu$ M **33** and 37.5  $\mu$ M AF555 maleimide (1.50 equiv.) in H<sub>2</sub>O + 0.01% methanol, irradiation at  $\lambda = 405$  nm. The signal of nucleoside **33** (14.25 min) is decreasing, whereas the signal of the nucleoside **33+AF555** adduct (12.5 min) is increasing. Additionally, the chromatogram shows signals of the hydrolyzed product **40** (12 min) and an unidentified impurity (11.5 min, marked with as asterisk).

The analytical HPLC chromatograms (Figure 59) recorded during the reaction (0-50% ACN in 30 minutes, 40 °C, 1.00 mL/min) confirm conversion to the hydrolyzed product **40** (12 min retention time) and the desired cycloadduct **33+AF555** (12.5 min retention time). The absorbance spectra of the peak at 12.5 min retention time (Figure 60) displays characteristic signals of the nucleoside (<300 nm), as well as of the pyrazoline (~320-400 nm) and the dye (~450-600 nm). The success of the reaction was further verified by collection of the peak, followed by analysis by MALDI-TOF (see end of this chapter, Table 11). The reaction with sulfo-Cy3 maleimide (see chapter 6.4, Figure A8) displays similar behavior, however a 1.7-fold increase of fluorescence can be achieved in that case.

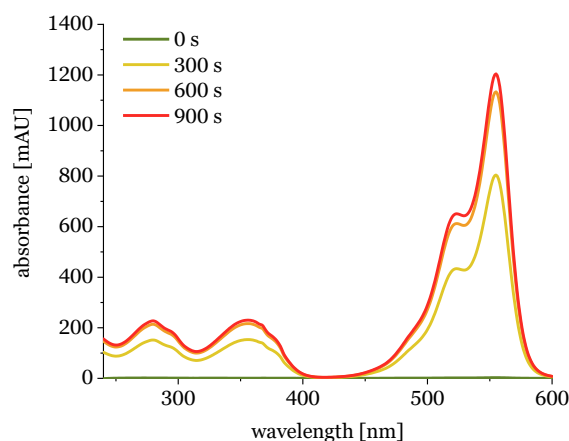


**Figure 60.** UV/Vis absorbance spectra of the peak of product **33**+**AF555** (12.5 min retention time) taken as snapshots during the HPLC runs at 0-900 s irradiation time.

The fluorogenicity of the reaction between **33** and the dye maleimides is less compared to the results described in chapter 3, a possible explanation for this can be explained by the spectral behavior of each pyrazoline. The maximum of the emission of pyrazoline **41** is shifted hypsochromically by 25 nm compared to pyrazoline **RNA2**+**NMM**, resulting in reduced overlap between pyrazoline **41** and the dyes is fewer compared to **RNA2**+**NMM** and the dyes, respectively (Figure **61**).

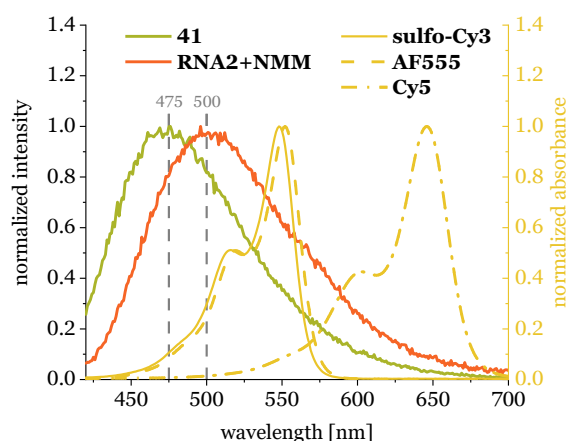


**Figure 61.** Overlap of the normalized emission spectra of the cycloaddition products **41** and **RNA2**+**NMM** and the normalized absorbance of three different maleimide dye conjugates (sulfo-Cy3, AF555, Cy5).

To further investigate, the reaction was performed with Cy5 maleimide as a spectral analog to AF647 used in the first part of this work. Upon irradiation at 405 nm, the fluorescence spectra do not display a *FRET*, but rather show an increase of fluorescence in the region of the pyrazoline, indicating success of the reaction (Figure 62).

## 4 Sydnone-Modified Oligonucleotides for Bioorthogonal Labeling

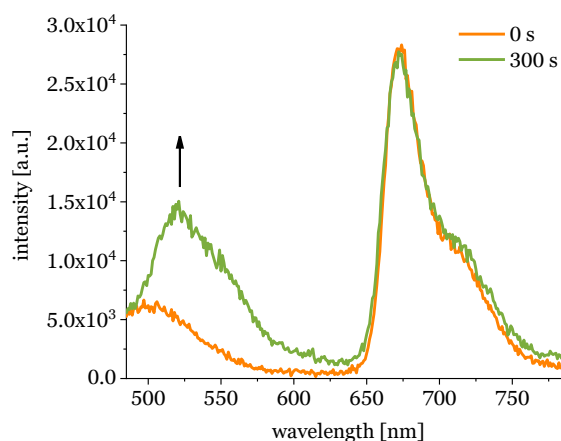


**Figure 62.** Emission (exc. = 405 nm) spectra of the reaction between nucleoside **33** and Cy5 maleimide over 5 minutes (irradiation time,  $\lambda = 405$  nm). 25  $\mu$ M **33**, 37.5  $\mu$ M Cy5 maleimide (1.50 equiv.) in H<sub>2</sub>O + 0.01% methanol, 20 °C.

The fluorogenicity of the reaction could possibly further increased by employing a dye that is hypsochromically shifted compared to the dyes investigated in this work, such as AlexaFluor488 or BDP FL maleimide.

The success of the reactions mentioned in this chapter was verified *via* MALDI-TOF mass spectrometry (Table 11).

**Table 11.** Calculated and measured masses of nucleosides **40**, **41**, **33+AF555** and **33+sulfoCy3**.

adduct	calculated mass [Da]	measured mass [Da]
<b>40</b>	523.21	523.26
<b>41</b>	616.23	616.28
<b>33+AF555</b>	1474.43	1475.71
<b>33+sulfo-Cy3</b>	1242.43	1243.73
<b>33+Cy5</b>	1110.54	1110.09

### 4.4 Cell Experiments

All cell experiments were performed under supervision and with the help of Dr. Franziska Röncke. As the final step, the SPSAC labeling experiments were performed in fixed *HeLa* cells. By using fixed cells, a first assessment of the feasibility of the reaction in a cellular environment can be made and the excess dye can be removed by washing steps. The experiments were first carried out with Cy3 DIBAC as a reaction partner, however a strong unspecific background staining in the cells were observed in that case, most likely due to the lipophilicity of the dye. Furthermore, the low solubility of the dye in aqueous media made the dye hard to remove by washing with phosphate buffered saline (PBS). To overcome this problem, sulfo-Cy3 DIBAC was used, as the lipophilicity of this Cy3 analog should be decreased due to the sulfonate groups of the dye. Furthermore, sulfo-Cy3 offers a good water solubility, resulting in an easier removal of the unbound dye by washing.  $4 \times 10^4$  *HeLa* cells per well (Ibidi, 8 well) were transfected for 16 hours with 75 ng of either **DNA4** or **DNA5** with the help of transfection reagent *ScreenFect A*. Subsequently, the cells were fixed using 4% paraformaldehyde solution and treated with 7 nM sulfo-Cy3 DIBAC ( $\cong 0.1$  equivalents relative to the DNA amount) for 3 hours, followed by washing with  $2 \times$  PBS (for 15 minutes each). Visualization of the SPSAC labeling experiments was achieved by confocal laser microscopy using *Leica TCS-SP8*, equipped with a *DMi8CEL Advanced* microscope. All images were taken under the same conditions (HyD, 15% laser power, 100% smart gain,  $\lambda_{exc.} = 488$  nm,  $\lambda_{em.} = 550-650$  nm). As negative control, non-transfected cells were treated in the same way as the transfected cells.

With both oligonucleotides, successful transfection, combined with an efficient labeling was observed. The images of the cells transfected with **DNA4** or **DNA5** (Figure 63, left and Figure 64, left), respectively, display strong fluorescent signal in the endosomes and the cytosol of cells, resulting from the uptake of the DNA by the endosomes followed by release into the cytosol, whereas the negative controls (Figure 63, right and Figure 64, right) only show negligible, unspecific fluorescence in the cytosol due to the unbound sulfo-Cy3 DIBAC. This indicates the applicability of the SPSAC in cells. Both employed sequences show efficient labeling within 4 hours reaction time. Furthermore, the labeling could be performed without any additional reagents such as HCl or other permeabilization agents.

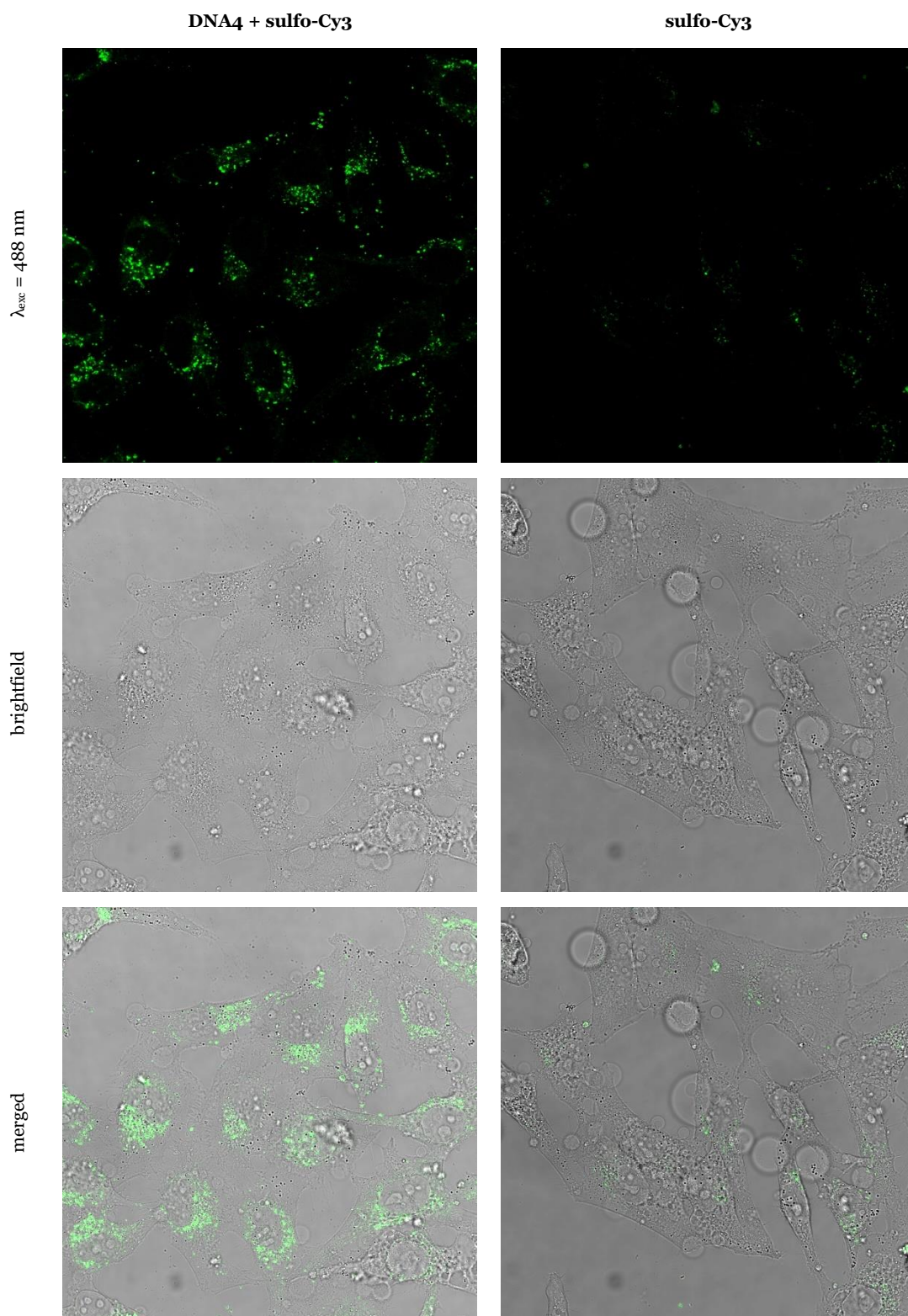


**Figure 63.** Confocal laser microscopy pictures of fixed *HeLa* cells transfected with **DNA4** (left column) or non-transfected (right column), after treatment with 7 nM sulfo-Cy3 DIBAC for 4 hours. Prior to imaging, the cells were washed with  $3 \times \text{PBS}$ ,  $\lambda_{exc.} = 488 \text{ nm}$ ,  $\lambda_{em.} = 550\text{-}650 \text{ nm}$ .

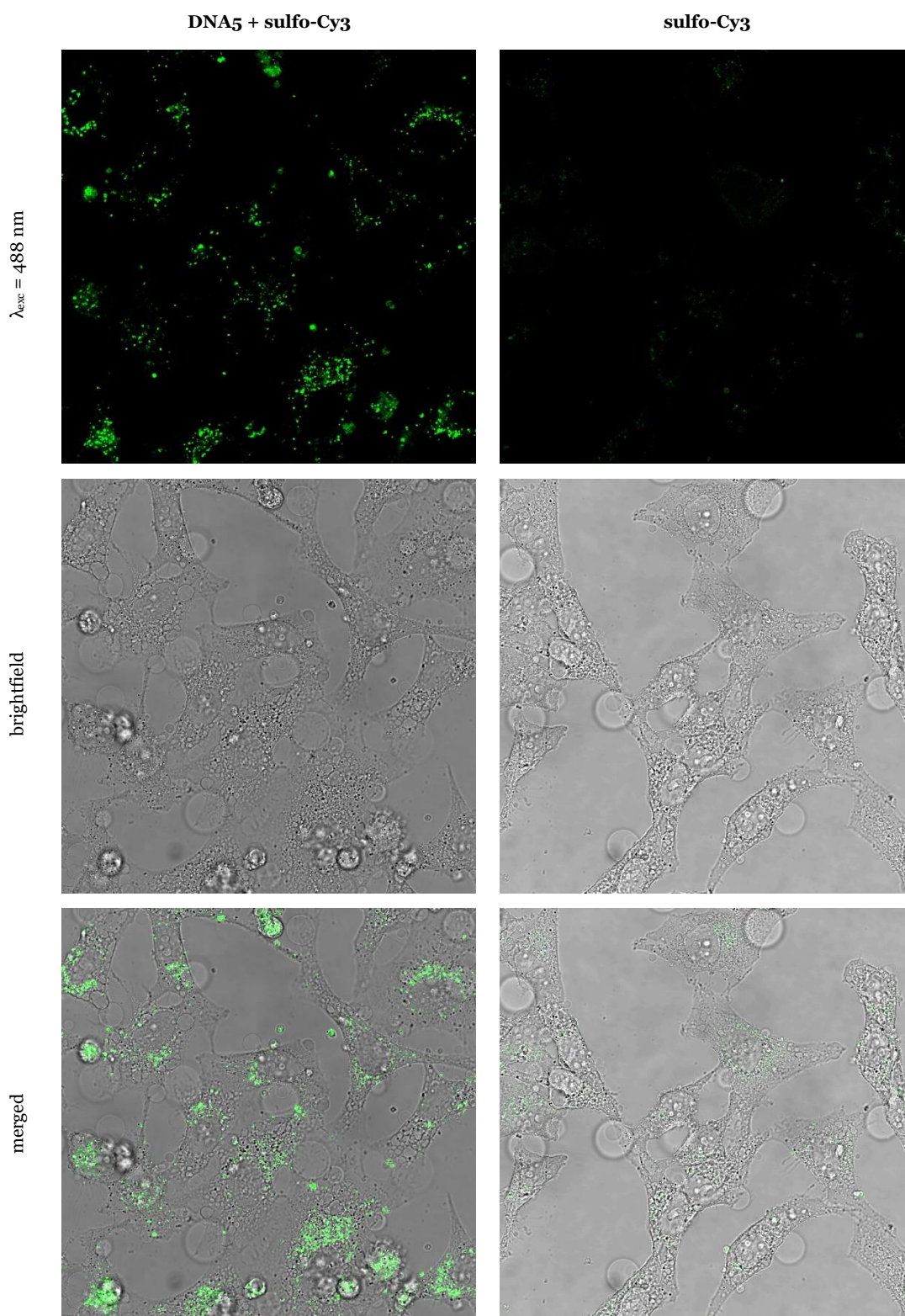


**Figure 64.** Confocal laser microscopy pictures of fixed *HeLa* cells transfected with **DNA5** (left column) or non-transfected (right column), after treatment with 7 nM sulfo-Cy3 DIBAC for 4 hours. Prior to imaging, the cells were washed with  $3 \times \text{PBS}$ ,  $\lambda_{exc.} = 488 \text{ nm}$ ,  $\lambda_{em.} = 550\text{-}650 \text{ nm}$ .

## 4.5 Conclusion and Outlook

In this work, to the best of our knowledge, the first modification of nucleosides and oligonucleotides with sydnones was performed. Sydnone-modified nucleosides **31**, **32** and **33** were synthesized and investigated in two different bioorthogonal reactions: the strain-promoted sydnone alkyne cycloaddition and the photoclick reaction (Figure 65). Both reactions display fluorogenic behavior by formation of a highly fluorescent pyrazole (SPSAC, up to 72-fold increase of fluorescence) or pyrazoline (photoclick reaction, up to 29-fold increase of fluorescence).

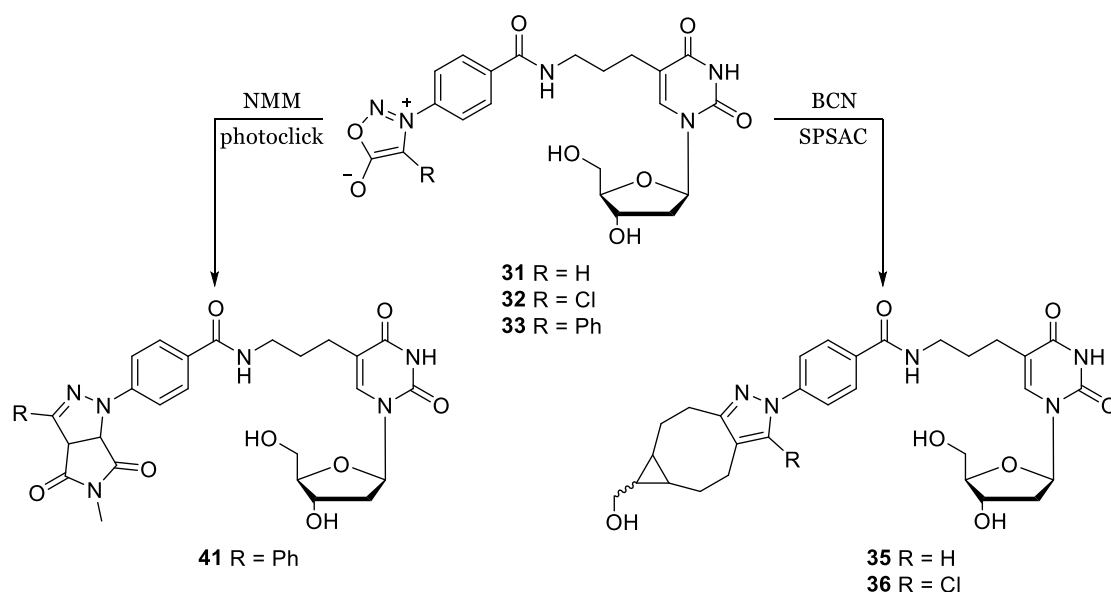


**Figure 65.** Nucleosides **31**, **32** and **33** were labeled in a bioorthogonal manner by either SPSAC (**31** and **32**) or photoclick reaction (**33**).

Furthermore, sydnone-modified oligonucleotides **DNA4** and **DNA5** were synthesized and labeled by SPSAC. The SPSAC reaction provides a fast and easy way to modify oligonucleotides, however the intrinsic fluorogenicity of the pyrazole formed during the reaction does not display suitable characteristics for cellular imaging. Regarding that, a Cy3 DIBAC conjugate was chosen as a reaction partner for future application in cell experiments. The disadvantage of this system, however, is the loss of the fluorogenic behavior as well as the poor controllability of the reaction in terms of time and localization. As a last step, the feasibility of the SPSAC was demonstrated in fixed *HeLa* cells (Figure 66).

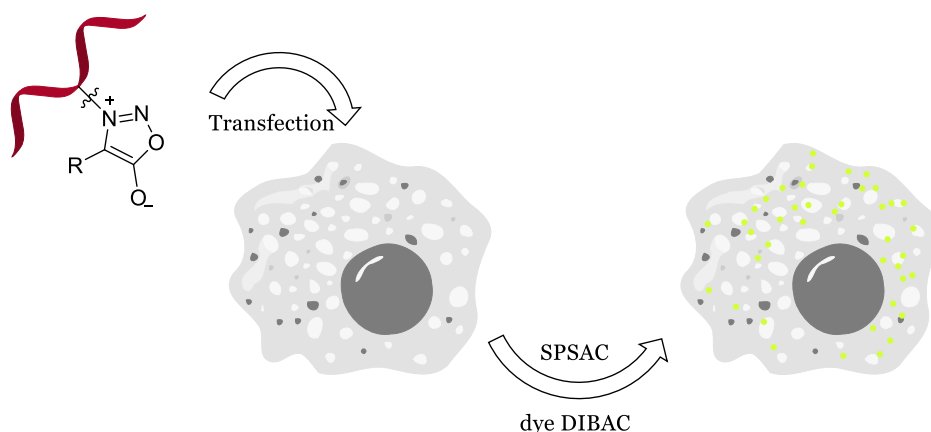


**Figure 66.** Schematic presentation of the SPSAC cell experiments.

To overcome these disadvantages, diarylsydnone-modified nucleoside **33** was investigated in a photoclick reaction. The pyrazoline formed during the reaction was successfully employed as a donor in a *FRET* system with dyes such as AF555 or sulfo-Cy3 as an acceptor. Opposed to the previously reported results, no energy transfer was observed to red-shifted dye Cy5. This behavior can possibly be tuned and investigated further by attaching various substituents to the phenyl rings of the diarylsydnone, which could also result in a shift of activation wavelength of the sydnone. This work presents one of few examples of near-visible light activation of the photoclick reaction on nucleic acids, as the reaction was successfully initiated at 405 nm.

As next steps, the incorporation of the diarylsydnone moiety into oligonucleotides should be performed. This can either be achieved similar to the procedure described in chapter 4.2, or possibly by enzymatic oligonucleotide synthesis after turning nucleoside **33** into a triphosphate. Furthermore, cellular imaging experiments should be performed, as the fluorogenic behavior observed in the photoclick reaction provides suitable characteristics for cellular imaging.

## 5 Experimental Section

---

### 5.1 Materials and Methods

#### Solvents and Reagents

Solvents and reagents were purchased at *ABCR, Acros Organics, Alpha Aesar, Carl Roth, Merck, Sigma Aldrich, TCI* and *VWR* and used without further purification unless stated otherwise.

The purity of solvents was at least *pro analysi*. Anhydrous solvents were purchased at *Acros Organics* and stored under argon. HPLC grade solvents were purchased at *Fisher Scientific*. Deuterated solvents for NMR spectroscopy were purchased at *Eurisotop*. Water was deionized using a *Merck Millipore-Q8*.

#### Reactions

For reactions under inert conditions, flasks and other glassware was dried in high vacuum upon heating with a heat gun, followed by flooding with argon (99.999% purity). Light-sensitive reactions were carried out by covering flasks and columns with aluminum foil. Additionally, the light in the fume hood was turned off.

#### Chromatography

##### Thin-Layer Chromatography (TLC)

For thin-layer chromatography, silica gel 60 F<sub>254</sub> coated aluminum plates by *Merck* were used. For detection, either  $\lambda = 254$  nm (fluorescence deletion) or  $\lambda = 366$  nm (fluorescence excitation) light was used.

The TLC plates of nucleosides were stained with 5% H<sub>2</sub>SO<sub>4</sub> in methanol, followed by heating with a heat gun until charring occurred.

##### Flash Chromatography

The silica gel for flash column chromatography (pore size 60 Å, particle size 40-63 µm) was purchased at *Sigma Aldrich*. The crude product was either dissolved in the less polar solvent of the solvent system or adsorbed onto silica before purification. Pressure was applied to the column using an air pump.

### HPLC-Chromatography

HPLC separation was performed on a *ThermoFisher Scientific* UltiMate™ 3000 system. For semi-preparative separations, a *VDSpher OptiBio PUR 300 S18-SE* column (250 × 10 mm, 5 μm) was used with a flow rate of 2.5 mL/min. Analytical separations were performed using a *VDSpher OptiBio PUR 300 S18-SE* column (250 × 4.6 mm, 5 μm) column with a flow rate of 1.0 mL/min.

### **Freeze-Drying**

For removal of water or ammonium hydroxide out of oligonucleotide samples, a *Christ Alpha 1-2 LD Plus* freeze dryer or a *Christ Alpha RVC* vacuum centrifuge were used. For drying with the *Christ Alpha 1-2 LD Plus* freeze dryer, the samples were frozen in liquid nitrogen and dried in high vacuum (0.16 mbar). The *Christ Alpha RVC* was used in either of the following settings: 35 min, 35 °C, 100 mbar (ammonium hydroxide) or ∞ min, 25 °C, 0.100 mbar.

### **Spectroscopy**

#### UV/Vis Spectroscopy

UV/Vis absorbance was recorded in 1 cm quartz glass cuvettes by *Starna* with a sample volume of 500 μL at 20 °C with a *Cary 100 Bio* Spectrometer by *Varian*. Following parameters were used: average time 0.1 s, data interval 1.0 nm, scanning speed 600 nm/min, source changeover at 350 nm. The spectra were corrected against the UV/Vis absorbance of the solvent.

#### Fluorescence Spectroscopy

UV/Vis absorbance was recorded in 1 cm quartz glass cuvettes by *Starna* with a sample volume of 500 μL at 20 °C with either a *Fluoromax-3* or *Fluoromax-4* by *Jobin-Yvon*. Following parameters were used: increment time 0.2 s, integration time 0.1 s, slit width 3 nm, unless stated otherwise. The spectra were corrected against the Raman scattering of the solvent.

#### Fluorescence Quantum Yield

Fluorescence quantum yield measurements were performed on a *Hamamatsu Quantaurus QY C11347* upon excitation at 400 nm. The measurements were corrected against the solvent.

### NMR-Spectroscopy

The reported NMR data were recorded on either a *Bruker Avance Neo 400MHz* or a *Bruker Avance 500MHz* spectrometer at ambient temperature. For sample preparation, 10-25 mg compound was dissolved in 0.5 mL deuterated solvent. The chemical shift  $\delta$  in ppm was referenced relative to TMS by referencing on designated chemical shifts of following deuterated solvents:

Chloroform-d <sub>1</sub>	<sup>1</sup> H-NMR $\delta$ = 7.26 ppm	<sup>13</sup> C-NMR $\delta$ = 77.16 ppm
DMSO-d <sub>6</sub>	<sup>1</sup> H-NMR $\delta$ = 2.50 ppm	<sup>13</sup> C-NMR $\delta$ = 39.52 ppm
Methanol-d <sub>4</sub>	<sup>1</sup> H-NMR $\delta$ = 3.31 ppm	<sup>13</sup> C-NMR $\delta$ = 49.00 ppm

Coupling constants were given in Hertz, multiplicities abbreviated as following: s (singlet), d (doublet), dd (doublet of doublet), t (triplet), dt (doublet of triplet), q (quartet), m (multiplet).

### Mass Spectrometry

#### MALDI-TOF

Matrix-assisted laser desorption ionization (MALDI) mass spectrometry was performed on a *Shimadzu Axima Confidence* in reflectron (nucleosides and other small molecules) or linear negative (oligonucleotides) mode. The measurements were partially performed by A. Hochgesandt. The following matrix substances were used:

- 6-Aza-2-thiothymine (saturated in acetonitrile) and 2,4,6-trihydroxyacetophenone (0.3 M in ethanol) for small molecules and nucleosides
- 3-Hydroxypicolinic acid (saturated in acetonitrile/water 1:1)/diammonium hydrogen citrate (0.44 M in water) 9:1 (v/v) for oligonucleotides

#### FAB

Fast atom bombardment (FAB) mass spectrometry was performed in the analytical department of the Institute for Organic chemistry by A. Mösle on a *Finnigan MAT 95*.

### ESI

Electron-spray ionization (ESI) mass spectrometry was performed in the analytical department of the Institute for Organic chemistry by L. Hirsch on a *ThermoFisher Scientific Q Exactive Orbitrap*.

### **Ion Exchange**

Amberlite IRA-402 bicarbonate form to remove triethylammonium salts was prepared freshly before each use by stirring Amberlite IRA-402 chloride form with saturated sodium bicarbonate solution for 30 minutes. The resin was washed thoroughly with water and dried at 60 °C.

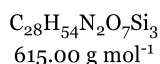
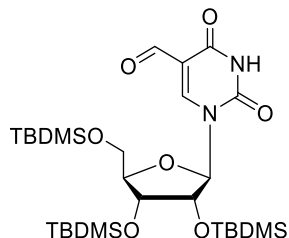
### **Confocal Laser Microscopy**

Confocal laser microscopy images were acquired on a *Leica TCS-SP8* equipped with a *DMi8 Advanced* microscope and either a HC PL APO CS2 63x/1.40 oil objective or a HC PL APO CS2 40x/1.10 water objective. The pictures were taken with a resolution of 1024×1024 px using *Leica Application Suite X*.

## 5.2 Synthetic Procedures

### 5.2.1 Ribonucleosides

#### Compound 1a



2.00 g of the protected nucleoside **3** (3.33 mmol; 1.00 equiv.) were dissolved in 250 mL acetonitrile. 1.58 g sodium peroxodisulfate (6.66 mmol; 2.00 equiv.), 664 mg copper(II)sulfate pentahydrate (2.66 mmol; 0.800 equiv.) and 1.88 mL pyridine (1.84 g; 23.3 mmol; 7.00 equiv.) were dissolved in 250 mL water and added to the first solution. The reaction mixture was stirred at 60 °C for 2 hours and diluted with 200 mL dichloromethane. The organic layer was washed with 3 x 300 mL water and 1 x 300 mL brine. The organic phase was dried over sodium sulfate and concentrated under vacuum. After flash chromatography (*n*-hexane/ethyl acetate 4:1), the product was obtained as a white foam (400 mg; 20%).

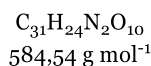
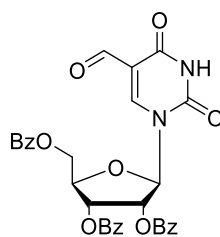
$R_f$  (*n*-hexane/ethyl acetate 4:1) = 0.52.

$^1\text{H-NMR}$  (500 MHz, DMSO)  $\delta$  [ppm] = 11.95 (s, 1H, 3-NH), 9.82 (s, 1H, 5-CHO), 8.33 (s, 1H, 6-CH), 5.83 (d,  $J$  = 5.4 Hz, 1H, 1'-CH), 4.29 (t,  $J$  = 4.8 Hz, 1H, 2'-CH), 4.04 (t,  $J$  = 3.8 Hz, 1H, 3'-CH), 4.01 (t,  $J$  = 3.1 Hz, 1H, 4'-CH), 3.90 (dd,  $J$  = 11.7, 3.1 Hz, 1H, 5'-CH<sub>2</sub>), 3.76 (dd,  $J$  = 11.8, 3.2 Hz, 1H, 5'-CH<sub>2</sub>), 0.91 (s, 9H, TBDMS *tert*-butyl), 0.89 (s, 9H, TBDMS *tert*-butyl), 0.83 (s, 9H, TBDMS *tert*-butyl), 0.13 (s, 3H, TBDMS CH<sub>3</sub>), 0.12 (s, 3H, TBDMS CH<sub>3</sub>), 0.09 (s, 3H, TBDMS CH<sub>3</sub>), 0.08 (s, 3H, TBDMS CH<sub>3</sub>), 0.02 (s, 3H, TBDMS CH<sub>3</sub>), -0.04 (s, 3H, TBDMS CH<sub>3</sub>).

$^{13}\text{C-NMR}$  (126 MHz, DMSO)  $\delta$  [ppm] = 186.0 (5-CHO), 161.6 (Cq), 149.7 (Cq), 145.2 (6-CH), 111.2 (Cq), 87.9 (1'-CH), 85.2 (4'-CH), 75.1 (2'-CH), 71.5 (3'-CH), 62.4 (5'-CH<sub>2</sub>), 26.0 (TBDMS *tert*-butyl), 25.7 (TBDMS *tert*-butyl), 25.6 (TBDMS *tert*-butyl), 18.3 (TBDMS-Cq), 17.7 (TBDMS-Cq), 17.6 (TBDMS-Cq), -3.2 (TBDMS-CH<sub>3</sub>), -4.6 (TBDMS-CH<sub>3</sub>), -4.9 (TBDMS-CH<sub>3</sub>), -5.0 (TBDMS-CH<sub>3</sub>), -5.5 (TBDMS-CH<sub>3</sub>), -5.5 (TBDMS-CH<sub>3</sub>).

HRMS-FAB: Calcd. for C<sub>28</sub>H<sub>55</sub>O<sub>7</sub>N<sub>2</sub>Si<sub>3</sub> [MH]<sup>+</sup>: 615.3317, found: 615.3315.

## Compound 1b



2.33 g nucleoside **4** (3.97 mmol; 1.00 equiv.) were dissolved in 150 mL dichloromethane. Subsequently, 9.90 mL *Dess-Martin-Periodinane* (15% *w/w* in dichloromethane, 13.5 g; 4.77 mmol; 1.20 equiv.) were added and the resulting solution was stirred at room temperature for 2 hours. After filtration, the solvent was removed under reduced pressure and purified *via* column chromatography (dichloromethane/methanol 60:1). The product was obtained as a colorless foam (1.68 g; 72%).

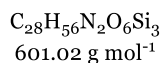
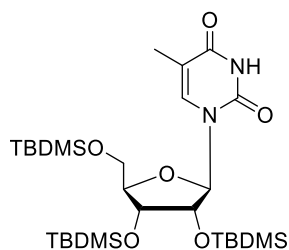
$R_f$  (dichloromethane/methanol 19:1) = 0.37.

$^1\text{H-NMR}$  (400 MHz, DMSO)  $\delta$  [ppm] = 11.98 (s, 1H, NH), 9.75 (s, 1H, CHO), 8.59 (s, 1H, 6-CH), 8.04 – 7.97 (m, 2H, CH<sub>ar</sub>), 7.89 (ddd,  $J$  = 16.4, 8.3, 1.4 Hz, 4H, CH<sub>ar</sub>), 7.68 – 7.60 (m, 3H, CH<sub>ar</sub>), 7.51 – 7.40 (m, 6H, CH<sub>ar</sub>), 6.29 (d,  $J$  = 3.5 Hz, 1H, 1'-CH), 6.03 (dd,  $J$  = 6.3, 3.5 Hz, 1H, 2'-CH), 5.97 (t,  $J$  = 6.5 Hz, 1H, 3'-CH), 4.80 (ddd,  $J$  = 6.5, 5.1, 3.5 Hz, 1H, 4'-CH), 4.73 – 4.63 (m, 2H, 5'-CH<sub>2</sub>).

$^{13}\text{C-NMR}$  (101 MHz, DMSO)  $\delta$  [ppm] = 186.2 (CHO), 165.5 (Cq), 164.6 (Cq), 164.5 (Cq), 161.7 (Cq), 149.4 (Cq), 148.5 (6-CH), 133.9 (CH<sub>ar</sub>), 133.8 (CH<sub>ar</sub>), 133.5 (CH<sub>ar</sub>), 129.4 (CH<sub>ar</sub>), 129.3 (CH<sub>ar</sub>), 129.1 (CH<sub>ar</sub>), 128.8 (CH<sub>ar</sub>), 128.7 (CH<sub>ar</sub>), 128.6 (CH<sub>ar</sub>), 128.5 (CH<sub>ar</sub>), 111.1 (Cq), 90.9 (1'-CH), 79.3 (4'-CH), 73.8 (2'-CH), 70.1 (3'-CH), 63.4 (5'-CH<sub>2</sub>).

HRMS-FAB: Calcd. for C<sub>31</sub>H<sub>25</sub>O<sub>10</sub>N<sub>2</sub> [MH]<sup>+</sup>: 585.1509, found: 585.1508.

## Compound 3



To a stirred solution of 10.0 g 5-methyluridine (38.8 mmol; 1.00 equiv.) in 50 mL anhydrous *N,N*-dimethylformamide, 15.9 g imidazole (232 mmol; 6.00 equiv.) were added and stirred for 5 minutes at ambient temperature. Afterwards, 20.5 g *tert*-butyldimethylsilyl chloride (135 mmol; 3.50 equiv.) were added and the reaction mixture was stirred for 12 hours. After dilution with 300 mL dichloromethane, the solution was washed with 3 x 300 mL water and 1 x 100 mL brine. The organic phase was dried over sodium sulfate and concentrated under vacuum to give 23.3 g of the product (38.8 mmol; quantitative) as a white solid.

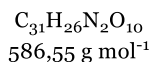
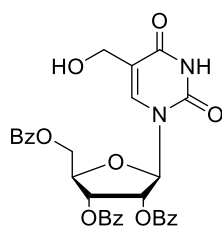
$R_f$  (*n*-hexane/ethyl acetate 4:1) = 0.44.

$^1\text{H-NMR}$  (500 MHz, DMSO)  $\delta$  [ppm] = 11.42 (s, 1H, 3-NH), 7.42 (s, 1H, 6-CH), 5.88 (d,  $J = 7.1$  Hz, 1H, 1'-CH), 4.20 (dd,  $J = 7.2, 4.6$  Hz, 1H, 2'-CH), 4.04 (dd,  $J = 4.5, 1.6$  Hz, 1H, 3'-CH), 3.92 (dt,  $J = 3.4, 1.7$  Hz, 1H, 4'-CH), 3.82 (dd,  $J = 11.5, 3.8$  Hz, 1H, 5'-CH<sub>2</sub>), 3.72 (dd,  $J = 11.5, 3.0$  Hz, 1H, 5'-CH<sub>2</sub>), 1.78 (s, 3H, 5-CH<sub>3</sub>), 0.91 (s, 9H, TBDMS *tert*-butyl), 0.89 (s, 9H, TBDMS *tert*-butyl), 0.80 (s, 9H, TBDMS *tert*-butyl), 0.11 (s, 3H, TBDMS CH<sub>3</sub>), 0.10 (s, 3H, TBDMS CH<sub>3</sub>), 0.09 (s, 3H, TBDMS CH<sub>3</sub>), 0.08 (s, 3H, TBDMS CH<sub>3</sub>), -0.01 (s, 3H, TBDMS CH<sub>3</sub>), -0.10 (s, 3H, TBDMS CH<sub>3</sub>).

$^{13}\text{C NMR}$  (126 MHz, DMSO)  $\delta$  [ppm] = 163.4 (Cq), 150.7 (Cq), 135.2 (6-CH), 109.9 (Cq), 85.9 (1'-CH), 85.3 (4'-CH), 73.9 (2'-CH), 72.4 (3'-CH), 63.0 (5'-CH<sub>2</sub>), 25.8 (TBDMS *tert*-butyl), 25.7 (TBDMS *tert*-butyl), 25.5 (TBDMS *tert*-butyl), 18.0 (TBDMS-Cq), 17.7 (TBDMS-Cq), 17.5 (TBDMS-Cq), 12.1 (5-CH<sub>3</sub>), -4.7 (TBDMS-CH<sub>3</sub>), -4.8 (TBDMS-CH<sub>3</sub>), -4.8 (TBDMS-CH<sub>3</sub>), -5.2 (TBDMS-CH<sub>3</sub>), -5.5 (TBDMS-CH<sub>3</sub>).

HRMS-FAB: Calcd. for C<sub>28</sub>H<sub>57</sub>O<sub>6</sub>N<sub>2</sub>Si<sub>3</sub> [MH]<sup>+</sup>: 601.3524, found: 601.3525.

## Compound 4



283 mg 5-Hydroxymethyluracil (1.98 mmol; 1.00 equiv.) and 1.00 g  $\beta$ -D-ribofuranose 1-acetate 2,3,5-tribenzoate (1.98 mmol; 1.00 equiv.) were suspended in 10 mL anhydrous acetonitrile. 1.46 mL N,O-bis(trimethylsilyl)acetamide (1.21 g; 5.95 mmol; 3.00 equiv.) were added and the reaction mixture was stirred at 60 °C for 30 minutes. 1.26 mL TMSOTf (1.54 g; 6.94 mmol; 3.50 equiv.) were added and stirred for further 60 minutes at 60 °C. After dilution with 30 mL ethyl acetate, the reaction mixture was washed with 2 x 50 mL water, 2 x 50 mL sat.  $\text{NaHCO}_3$  solution and 2 x 50 mL brine. The organic layer was dried over sodium sulfate and the solvent was removed under reduced pressure. The crude product was purified *via* column chromatography (dichloromethane/ methanol 40:1 – 20:1). The product was obtained as a colorless foam (813 mg; 70%).

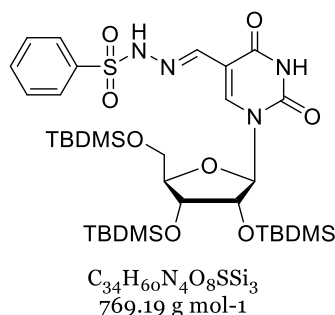
$R_f$  (dichloromethane/methanol 19:1) = 0.26.

$^1\text{H-NMR}$  (400 MHz, DMSO)  $\delta$  [ppm] = 11.55 (s, 1H, 3-NH), 8.02 (dd,  $J$  = 8.2, 1.4 Hz, 2H,  $\text{CH}_{\text{ar}}$ ), 7.93 – 7.85 (m, 4H,  $\text{CH}_{\text{ar}}$ ), 7.74 (t,  $J$  = 1.2 Hz, 1H, 6-CH), 7.69 – 7.61 (m, 3H,  $\text{CH}_{\text{ar}}$ ), 7.51 (t,  $J$  = 7.8 Hz, 2H,  $\text{CH}_{\text{ar}}$ ), 7.44 (td,  $J$  = 7.7, 3.7 Hz, 4H,  $\text{CH}_{\text{ar}}$ ), 6.28 – 6.22 (m, 1H, 1'-CH), 5.95 – 5.90 (m, 2H, 2'-CH, 3'-CH), 5.03 (t,  $J$  = 5.4 Hz, 1H,  $\text{CH}_2\text{OH}$ ), 4.75 (dt,  $J$  = 5.5, 2.7 Hz, 1H, 4'-CH), 4.67 (t,  $J$  = 4.1 Hz, 2H, 5'- $\text{CH}_2$ ), 4.19 – 4.09 (m, 2H,  $\text{CH}_2\text{OH}$ ).

$^{13}\text{C-NMR}$  (101 MHz, DMSO)  $\delta$  [ppm] = 165.5 (Cq), 164.7 (Cq), 164.6 (Cq), 162.6 (Cq), 150.3 (Cq), 138.2 (6-CH), 133.9 ( $\text{CH}_{\text{ar}}$ ), 133.8 ( $\text{CH}_{\text{ar}}$ ), 133.5 ( $\text{CH}_{\text{ar}}$ ), 129.3 ( $\text{CH}_{\text{ar}}$ ), 129.3 ( $\text{CH}_{\text{ar}}$ ), 129.2 ( $\text{CH}_{\text{ar}}$ ), 128.8 ( $\text{CH}_{\text{ar}}$ ), 128.7 ( $\text{CH}_{\text{ar}}$ ), 128.6 ( $\text{CH}_{\text{ar}}$ ), 128.5 ( $\text{CH}_{\text{ar}}$ ), 114.8 (Cq), 89.5 (1'-CH), 78.7 (4'-CH), 73.1 (CH), 70.5 (CH), 63.7 (5'- $\text{CH}_2$ ), 55.9 ( $\text{CH}_2\text{OH}$ ).

HRMS-FAB: Calcd. for  $\text{C}_{31}\text{H}_{27}\text{O}_{10}\text{N}_2$  [MH] $^+$ : 587.1666, found: 587.1667.

## Compound 7a



1.27 g nucleoside **1a** (2.07 mmol; 1.00 equiv.) and 356 mg benzenesulfonyl hydrazide (2.07 mmol; 1.00 equiv.) were dissolved in 50 mL methanol and stirred for 2 hours at 60 °C. The reaction mixture was concentrated under reduced pressure and purified via column chromatography (*n*-hexane/ethyl acetate 2:1). The product was obtained as a white foam (1.52 g; 90%).

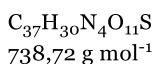
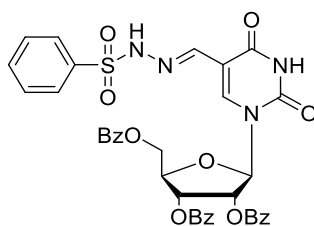
$R_f$  (*n*-hexane/ethyl acetate 2:1) = 0.15.

<sup>1</sup>H-NMR (500 MHz, DMSO)  $\delta$  [ppm] = 11.77 (s, 1H, NH), 11.41 (s, 1H, NH), 7.84 – 7.80 (m, 3H, CH<sub>ar</sub>), 7.79 (s, 1H, 6-CH), 7.68 – 7.63 (m, 1H, CH<sub>ar</sub>), 7.58 (m, 2H, CH<sub>ar</sub>), 5.81 (d,  $J$  = 6.0 Hz, 1H, 1'-CH), 4.28 (dd,  $J$  = 5.9, 4.5 Hz, 1H, 2'-CH), 4.03 (dd,  $J$  = 4.5, 2.9 Hz, 1H, 3'-CH), 3.98 – 3.94 (m, 1H, 4'-CH), 3.82 (dd,  $J$  = 11.3, 4.6 Hz, 1H, 5'-CH<sub>2</sub>), 3.72 (dd,  $J$  = 11.3, 4.7 Hz, 1H, 5'-CH<sub>2</sub>), 0.89 (s, 18H, TBDMS *tert*-butyl), 0.80 (s, 9H, TBDMS *tert*-butyl), 0.10 (s, 3H, TBDMS CH<sub>3</sub>), 0.09 (s, 6H, TBDMS CH<sub>3</sub>), 0.08 (s, 3H, TBDMS CH<sub>3</sub>), 0.01 (s, 3H, TBDMS-CH<sub>3</sub>), -0.09 (s, 3H, TBDMS-CH<sub>3</sub>).

<sup>13</sup>C-NMR (126 MHz, DMSO)  $\delta$  [ppm] = 161.4 (Cq), 149.8 (Cq), 140.3 (6-CH), 139.1 (Cq), 136.7 (CH<sub>ar</sub>), 133.0 (CH<sub>ar</sub>), 129.2 (CH<sub>ar</sub>), 127.0 (CH<sub>ar</sub>), 108.2 (Cq), 87.8 (1'-CH), 85.2 (4'-CH), 73.9 (2'-CH), 71.9 (3'-CH), 63.0 (5'-CH<sub>2</sub>), 25.9 (TBDMS *tert*-butyl), 25.7 (TBDMS *tert*-butyl), 25.5 (TBDMS *tert*-butyl), 18.1 (TBDMS-Cq), 17.7 (TBDMS-Cq), 17.6 (TBDMS-Cq), -4.6 (TBDMS-CH<sub>3</sub>), -4.7 (TBDMS-CH<sub>3</sub>), -4.9 (TBDMS-CH<sub>3</sub>), -5.1 (TBDMS-CH<sub>3</sub>), -5.4 (TBDMS-CH<sub>3</sub>), -5.5 (TBDMS-CH<sub>3</sub>).

HRMS-FAB: Calcd. for C<sub>34</sub>H<sub>61</sub>O<sub>8</sub>N<sub>4</sub>S<sub>1</sub>Si<sub>3</sub> [MH]<sup>+</sup>: 769.3518, found: 769.3520.

## Compound 7b



1.68 g nucleoside **1b** (2.87 mmol; 1.00 equiv.) were dissolved in 100 mL dichloromethane. 494 mg Benzenesulfonyl hydrazide (2.87 mmol; 1.00 equiv.) were added and the resulting mixture stirred at 60 °C for 2 hours. After removal of the solvent under reduced pressure, the crude product was purified *via* column chromatography (dichloromethane/methanol 40:1). The product was obtained as a colorless foam (1.74 g; 82%).

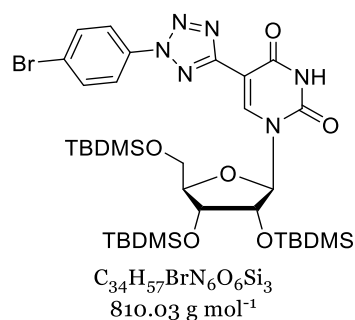
$R_f$  (dichloromethane/methanol 19:1) = 0.28.

$^1\text{H-NMR}$  (400 MHz, DMSO)  $\delta$  [ppm] = 11.88 (s, 1H, NH), 11.45 (s, 1H, NH), 8.21 (s, 1H, CH), 8.00 – 7.96 (m, 2H, CH<sub>ar</sub>), 7.93 – 7.86 (m, 6H, CH<sub>ar</sub>), 7.81 (s, 1H, CH), 7.67 – 7.54 (m, 6H, CH<sub>ar</sub>), 7.50 – 7.40 (m, 6H, CH<sub>ar</sub>), 6.28 (d,  $J$  = 3.2 Hz, 1H, 1'-CH), 6.03 (dd,  $J$  = 6.4, 3.2 Hz, 1H, 2'-CH), 5.97 (t,  $J$  = 6.6 Hz, 1H, 3'-CH), 4.76 (td,  $J$  = 6.0, 3.7 Hz, 1H, 4'-CH), 4.67 (qd,  $J$  = 12.0, 4.7 Hz, 2H, 5'-CH<sub>2</sub>).

$^{13}\text{C-NMR}$  (101 MHz, DMSO)  $\delta$  [ppm] = 165.5 (Cq), 164.7 (Cq), 164.6 (Cq), 161.9 (Cq), 149.5 (Cq), 140.3 (CH), 140.0 (CH), 139.0 (Cq), 133.9 (CH<sub>ar</sub>), 133.8 (CH<sub>ar</sub>), 133.5 (CH<sub>ar</sub>), 133.0 (CH<sub>ar</sub>), 129.4 (CH<sub>ar</sub>), 129.3 (CH<sub>ar</sub>), 129.2 (CH<sub>ar</sub>), 129.2 (CH<sub>ar</sub>), 129.0 (CH<sub>ar</sub>), 128.7 (CH<sub>ar</sub>), 128.7 (CH<sub>ar</sub>), 128.6 (CH<sub>ar</sub>), 128.6 (CH<sub>ar</sub>), 127.6 (CH<sub>ar</sub>), 127.2 (CH<sub>ar</sub>), 107.9 (Cq), 92.0 (1'-CH), 79.0 (4'-CH), 73.6 (2'-CH), 70.5 (3'-CH), 63.7 (5'-CH<sub>2</sub>).

HRMS-FAB: Calcd. for  $\text{C}_{37}\text{H}_{31}\text{O}_{11}\text{N}_4\text{S}_1$  [MH]<sup>+</sup>: 739.1710, found: 739.1709.

## Compound 8a



2.50 g hydrazone **7a** (3.25 mmol; 1.00 equiv.) were dissolved in 50 mL pyridine and cooled to  $-15^\circ\text{C}$ . Subsequently, 2.20 g 4-bromobenzenediazonium tetrafluoroborate (8.13 mmol; 2.50 equiv.) were added and the reaction mixture was stirred for 30 minutes. It was diluted with 100 mL dichloromethane and washed with 3 x 100 mL 1M hydrochloric acid, 2 x 300 mL water and 1 x 300 mL brine. After the organic phase was dried over sodium sulfate and evaporated under reduced pressure, the crude product was purified via column chromatography (*n*-hexane/ethyl acetate 2:1). The product was obtained as an orange foam (1.44 g; 55%).

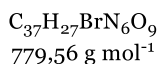
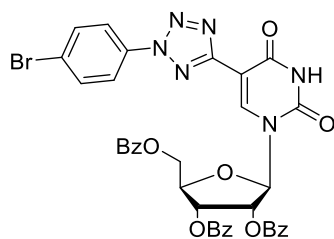
$R_f$  (*n*-hexane/ethyl acetate 2:1) = 0.57.

$^1\text{H-NMR}$  (500 MHz, DMSO)  $\delta$  [ppm] = 12.00 (s, 1H, 3-NH), 8.32 (s, 1H, 6-CH), 8.06 – 8.02 (m, 2H, CH<sub>ar</sub>), 7.92 – 7.88 (m, 2H, CH<sub>ar</sub>), 5.93 (d,  $J$  = 6.0 Hz, 1H, 1'-CH), 4.31 (dd,  $J$  = 6.1, 4.4 Hz, 1H, 2'-CH), 4.07 (dd,  $J$  = 4.4, 2.8 Hz, 1H, 3'-CH), 4.02 (q,  $J$  = 2.8 Hz, 1H, 4'-CH), 3.87 (dd,  $J$  = 11.7, 3.2 Hz, 1H, 5'-CH<sub>2</sub>), 3.75 (dd,  $J$  = 11.7, 3.0 Hz, 1H, 5'-CH<sub>2</sub>), 0.90 (s, 9H, TBDMS *tert*-butyl), 0.84 (s, 9H, TBDMS *tert*-butyl), 0.75 (s, 9H, TBDMS *tert*-butyl), 0.10 (s, 3H, TBDMS-CH<sub>3</sub>), 0.09 (s, 3H, TBDMS-CH<sub>3</sub>), 0.03 (s, 3H, TBDMS-CH<sub>3</sub>), -0.00 (s, 3H, TBDMS-CH<sub>3</sub>), -0.01 (s, 3H, TBDMS-CH<sub>3</sub>), -0.04 (s, 3H, TBDMS-CH<sub>3</sub>).

$^{13}\text{C-NMR}$  (126 MHz, DMSO)  $\delta$  [ppm] = 160.2 (Cq), 160.0 (Cq), 150.4 (Cq), 141.7 (6-CH), 135.6 (Cq), 133.7 (CH<sub>ar</sub>), 123.6 (Cq), 122.3 (CH<sub>ar</sub>), 102.9 (Cq), 87.7 (1'-CH), 85.9 (4'-CH), 75.3 (2'-CH), 72.4 (3'-CH), 63.1 (5'-CH<sub>2</sub>), 26.2 (TBDMS *tert*-butyl), 26.2 (TBDMS *tert*-butyl), 26.0 (TBDMS *tert*-butyl), 18.5 (TBDMS-Cq), 18.2 (TBDMS-Cq), 18.1 (TBDMS-Cq), -4.2 (TBDMS-CH<sub>3</sub>), -4.3 (TBDMS-CH<sub>3</sub>), -4.4 (TBDMS-CH<sub>3</sub>), -4.5 (TBDMS-CH<sub>3</sub>), -5.1 (TBDMS-CH<sub>3</sub>), -5.2 (TBDMS-CH<sub>3</sub>).

HRMS-FAB: Calcd. for C<sub>34</sub>H<sub>58</sub>O<sub>6</sub>N<sub>6</sub>BrSi<sub>3</sub> [MH]<sup>+</sup>: 809.2909, found: 809.2907.

## Compound 8b



890 mg nucleoside **7b** (1.20 mmol; 1.00 equiv.) was dissolved in 50 mL pyridine. The resulting solution was cooled to  $-15\text{ }^\circ\text{C}$  and 489 mg 4-bromobenzenediazonium tetrafluoroborate (1.81 mmol; 1.50 equiv.) were added. After stirring the mixture for further 30 minutes, it was diluted with 100 mL dichloromethane and washed with 3 x 50 mL 1 M hydrochloric acid, 2 x 50 mL water and 1 x 50 mL brine. The organic layer was dried over sodium sulfate and the solvent removed under reduced pressure. The crude product was dissolved in 5 mL dichloromethane and poured on 200 mL *n*-hexane to precipitate. The process was repeated until no further precipitation occurred. The product was obtained as a pale orange powder (451 mg; 48%)

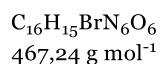
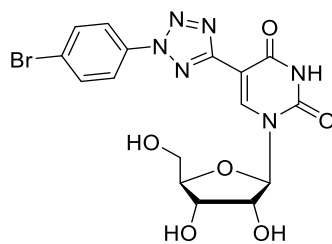
$R_f$  (dichloromethane/methanol 19:1) = 0.51.

$^1\text{H-NMR}$  (400 MHz, DMSO)  $\delta$  [ppm] = 12.01 (s, 1H, 3-NH), 8.68 (s, 1H, 6-CH), 8.00 – 7.91 (m, 6H, CH<sub>ar</sub>), 7.90 – 7.86 (m, 4H, CH<sub>ar</sub>), 7.65 (dt,  $J = 11.1, 7.5$  Hz, 2H, CH<sub>ar</sub>), 7.52 – 7.41 (m, 5H, CH<sub>ar</sub>), 7.34 (t,  $J = 7.7$  Hz, 2H, CH<sub>ar</sub>), 6.36 (d,  $J = 3.8$  Hz, 1H, 1'-CH), 6.06 (dd,  $J = 6.2, 3.8$  Hz, 1H, 2'-CH), 6.02 (t,  $J = 6.2$  Hz, 1H, 3'-CH), 4.84 (dt,  $J = 6.3, 3.9$  Hz, 1H, 4'-CH), 4.74 (dd,  $J = 12.3, 3.3$  Hz, 1H, 5'-CH<sub>2</sub>), 4.65 (dd,  $J = 12.3, 4.6$  Hz, 1H, 5'-CH<sub>2</sub>).

$^{13}\text{C-NMR}$  (101 MHz, DMSO)  $\delta$  [ppm] = 165.5, 164.6, 164.6, 159.8, 159.5, 149.6, 143.3, 135.2, 133.9, 133.8, 133.3, 133.1, 129.4, 129.3, 129.2, 129.0, 128.8, 128.7, 128.6, 128.5, 122.9, 121.7, 102.1, 89.9, 79.4, 73.9, 70.3, 63.6.

HRMS-FAB: Calcd. for  $\text{C}_{37}\text{H}_{28}\text{O}_9\text{N}_6\text{Br}$  [MH]<sup>+</sup>: 779.1101, found: 779.1102.

## Compound 9



**Method A:** 311 mg nucleoside **8a** (0.383 mmol; 1.00 equiv.) were dissolved in 5 mL anhydrous N,N-dimethylformamide and sealed in a tube. 375  $\mu\text{L}$  triethylamine trihydrofluoride (371 mg; 2.30 mmol; 6.00 equiv.) were added and stirred for 24 hours at room temperature. The solution was concentrated under reduced pressure and purified *via* column chromatography (dichloromethane/methanol 10:1 + 1% toluene). The product was obtained as a white powder (87.0 mg; 49%).

**Method B:** 385 mg nucleoside **8b** (0.494 mmol; 1.00 equiv.) was suspended in 50 mL 7M ammonia in methanol in a pressure tube. The reaction mixture was stirred at 80 °C for 24 hours and the solvent evaporated under reduced pressure. The crude product was purified *via* column chromatography (dichloromethane/methanol 10:1 + 1% toluene). The product was obtained as a white powder (150 mg; 65%).

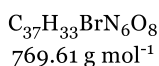
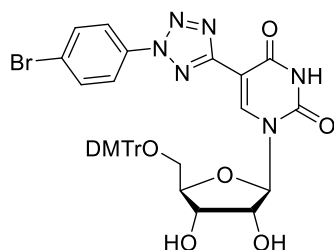
$R_f$  (dichloromethane/methanol 9:1) = 0.18.

$^1\text{H-NMR}$  (500 MHz, DMSO)  $\delta$  [ppm] = 11.83 (s, 1H, 3-NH), 8.88 (s, 1H, 6-CH), 8.08 – 8.04 (m, 2H, CH<sub>ar</sub>), 7.91 – 7.87 (m, 2H, CH<sub>ar</sub>), 5.86 (d, J = 4.5 Hz, 1H, 1'-CH), 5.51 (d, J = 5.3 Hz, 1H, 2'-OH), 5.18 (t, J = 4.7 Hz, 1H, 5'-OH), 5.13 (d, J = 5.4 Hz, 1H, 4'-OH), 4.14 (q, J = 4.9 Hz, 1H, 2'-CH), 4.03 (q, J = 5.0 Hz, 1H, 3'-CH), 3.92 (dt, J = 5.0, 2.6 Hz, 1H, 4'-CH), 3.69 (ddd, J = 11.9, 4.7, 2.8 Hz, 1H, 5'-CH<sub>2</sub>), 3.59 (ddd, J = 12.0, 4.6, 2.7 Hz, 1H, 5'-CH<sub>2</sub>).

$^{13}\text{C-NMR}$  (126 MHz, DMSO)  $\delta$  [ppm] = 160.0 (Cq), 159.9 (Cq), 150.0 (Cq), 142.6 (6-CH), 135.3 (Cq), 133.1 (CH<sub>ar</sub>), 123.0 (Cq), 121.8 (CH<sub>ar</sub>), 101.7 (Cq), 88.7 (1'-CH), 84.8 (4'-CH), 74.2 (2'-CH), 69.5 (3'-CH), 60.3 (5'-CH<sub>2</sub>)

HRMS-FAB: Calcd. for C<sub>16</sub>H<sub>16</sub>O<sub>6</sub>N<sub>6</sub>Br [MH]<sup>+</sup>: 467.0315, found: 467.0314.

## Compound 10



344 mg nucleoside **9** (0.714 mmol; 1.00 equiv.) were dissolved in 5 mL anhydrous pyridine. 266 mg 4,4'-dimethoxytrityl chloride (0.786 mmol; 1.10 equiv.) were added. The solution was stirred at room temperature for 16 hours. The solvent was evaporated under reduced pressure and the crude product purified *via* column chromatography (dichloromethane/methanol 50:1 → 20:1 + 0.1 % triethylamine). The product was obtained as a white powder (299 mg; 55%).

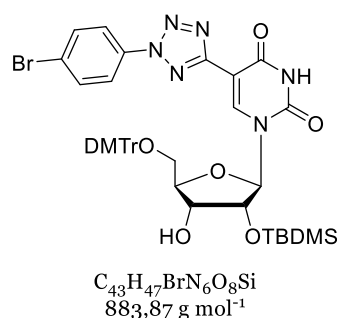
$R_f$  (dichloromethane/methanol 20:1) = 0.22.

$^1\text{H-NMR}$  (500 MHz, DMSO)  $\delta$  [ppm] = 11.87 (s, 1H, 3-NH), 8.44 (s, 1H, 6-CH), 7.73 – 7.68 (m, 2H, CH<sub>ar</sub>), 7.67 – 7.63 (m, 2H, CH<sub>ar</sub>), 7.33 (dd,  $J$  = 8.5, 1.3 Hz, 2H, CH<sub>ar</sub>), 7.25 – 7.18 (m, 4H, CH<sub>ar</sub>), 7.15 (t,  $J$  = 7.8 Hz, 2H, CH<sub>ar</sub>), 7.07 – 7.02 (m, 1H, CH<sub>ar</sub>), 6.71 (d,  $J$  = 8.9 Hz, 4H, CH<sub>ar</sub>), 5.82 (d,  $J$  = 3.4 Hz, 1H, 1'-CH), 5.65 (d,  $J$  = 5.0 Hz, 1H, 2'-OH), 5.16 (d,  $J$  = 6.3 Hz, 1H, 3'-OH), 4.24 (td,  $J$  = 5.0, 3.4 Hz, 1H, 2'-CH), 4.18 – 4.12 (m, 1H, 3'-CH), 4.06 (dt,  $J$  = 6.2, 2.9 Hz, 1H, 4'-CH), 3.63 (d,  $J$  = 2.0 Hz, 6H, DMTr-OCH<sub>3</sub>), 3.23 (d,  $J$  = 3.3 Hz, 2H, 5'-CH<sub>2</sub>).

$^{13}\text{C-NMR}$  (126 MHz, DMSO)  $\delta$  [ppm] = 160.1 (Cq), 159.4 (Cq), 157.8 (Cq), 149.8 (Cq), 149.6 (Cq), 144.4 (Cq), 141.3 (6-CH), 135.5 (Cq), 135.3 (Cq), 135.0 (Cq), 132.7 (CH<sub>ar</sub>), 129.5 (CH<sub>ar</sub>), 129.5 (CH<sub>ar</sub>), 127.6 (CH<sub>ar</sub>), 127.6 (CH<sub>ar</sub>), 126.5 (CH<sub>ar</sub>), 123.9 (Cq), 122.5 (Cq), 121.5 (CH<sub>ar</sub>), 112.9 (CH<sub>ar</sub>), 112.9 (CH<sub>ar</sub>), 101.7 (Cq), 89.7 (1'-CH), 85.7 (Cq), 82.6 (4'-CH), 74.1 (2'-CH), 69.2 (3'-CH), 62.5 (2'-CH), 54.9 (DMTr-OCH<sub>3</sub>), 54.8 (DMTr-OCH<sub>3</sub>).

MALDI-TOF: Calcd. for C<sub>37</sub>H<sub>33</sub>BrN<sub>6</sub>NaO<sub>8</sub> [MNa]<sup>+</sup>: 791.14, found 791.43.

## Compound 11



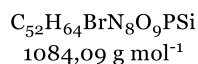
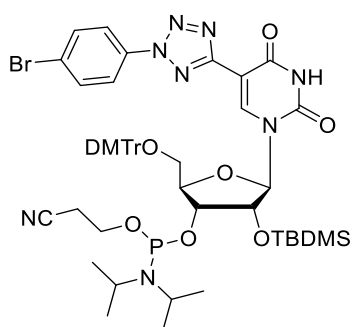
500 mg nucleoside **10** (0.649 mmol; 1.00 equiv.) were dissolved in 5 mL anhydrous tetrahydrofuran, and 143 mg silver(II) nitrate (0.844 mmol; 1.30 equiv.) and 209  $\mu$ L anhydrous pyridine (206 mg; 2.60 mmol; 4.00 equiv.) were added and stirred for 20 minutes under exclusion of light. 137 mg *tert*-butyldimethylsilyl chloride (0.909 mmol; 1.40 equiv.) were added and stirred at room temperature for 16 hours. After dilution with 20 mL ethyl acetate, the mixture was filtered, and the solvent removed under reduced pressure. The crude product was purified *via* column chromatography (dichloromethane/methanol 50:1  $\rightarrow$  30:1 + 0.1 % triethylamine). The product was obtained as a white powder (125 mg; 36%).

$R_f$  (dichloromethane/methanol 20:1) = 0.27.

$^1\text{H-NMR}$  (500 MHz, DMSO)  $\delta$  [ppm] = 11.90 (s, 1H, 3-NH), 8.48 (s, 1H, 6-CH), 7.71 – 7.67 (m, 2H, CH<sub>ar</sub>), 7.65 – 7.60 (m, 2H, CH<sub>ar</sub>), 7.36 – 7.31 (m, 2H, CH<sub>ar</sub>), 7.21 (dd,  $J$  = 10.8, 8.9 Hz, 4H, CH<sub>ar</sub>), 7.13 (t,  $J$  = 7.7 Hz, 2H, CH<sub>ar</sub>), 7.07 – 7.02 (m, 1H, CH<sub>ar</sub>), 6.71 (d,  $J$  = 2.5 Hz, 2H, CH<sub>ar</sub>), 6.69 (d,  $J$  = 2.6 Hz, 2H, CH<sub>ar</sub>), 5.80 (d,  $J$  = 3.1 Hz, 1H, 1'-CH), 5.20 (d,  $J$  = 6.0 Hz, 1H, 3'-OH), 4.37 (dd,  $J$  = 4.5, 3.1 Hz, 1H, 2'-CH), 4.18 – 4.12 (m, 1H, 3'-CH), 4.10 (dt,  $J$  = 6.2, 2.6 Hz, 1H, 4'-CH), 3.63 (s, 3H, DMTr-OCH<sub>3</sub>), 3.62 (s, 3H, DMTr-OCH<sub>3</sub>), 3.25 (s, 2H, 5'-CH<sub>2</sub>), 0.89 (s, 9H, TBDMS *tert*-butyl), 0.13 (s, 3H, TBDMS-CH<sub>3</sub>), 0.10 (s, 3H, TBDMS-CH<sub>3</sub>).

$^{13}\text{C-NMR}$  (126 MHz, DMSO)  $\delta$  [ppm] = 160.0 (Cq), 159.3 (Cq), 157.8 (Cq), 157.8 (Cq), 149.7 (Cq), 144.4 (Cq), 140.9 (6-CH), 135.4 (Cq), 135.2 (Cq), 135.0 (Cq), 132.6 (CH<sub>ar</sub>), 129.5 (CH<sub>ar</sub>), 129.5 (CH<sub>ar</sub>), 127.6 (CH<sub>ar</sub>), 127.5 (CH<sub>ar</sub>), 126.5 (CH<sub>ar</sub>), 122.5 (Cq), 121.5 (CH<sub>ar</sub>), 112.9 (CH<sub>ar</sub>), 112.9 (CH<sub>ar</sub>), 101.7 (Cq), 89.7 (1'-CH), 85.8 (Cq), 82.5 (4'-CH), 76.3 (2'-CH), 69.0 (3'-CH), 62.2 (5'-CH<sub>2</sub>), 54.9 (DMTr-OCH<sub>3</sub>), 54.8 (DMTr-OCH<sub>3</sub>), 25.7 (TBDMS *tert*-butyl), 18.0 (Cq), -4.7 (TBDMS-CH<sub>3</sub>), -5.0 (TBDMS-CH<sub>3</sub>).

HRMS-FAB: Calcd. for  $C_{43}H_{47}O_8N_6BrSi$  [M]<sup>+</sup>: 882.2408, found: 882.2411.

**Compound 12**

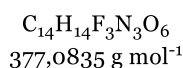
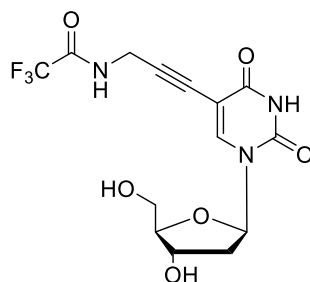
120 mg nucleoside **11** (0.135 mmol; 1.00 equiv.) were lyophilized out of benzene. It was dissolved in 4 mL anhydrous dichloromethane and 71  $\mu\text{L}$  diisopropylethylamine (0.407 mmol; 3.00 equiv.) and 45  $\mu\text{L}$  2-cyanoethyl-N,N-diisopropylchlorophosphoramidite (0.204 mmol; 1.50 equiv.) were added and afterwards stirred for 6 hours at room temperature. The crude product was purified via column chromatography (dichloromethane/acetone 5:1 + 0.1% triethylamine). The product was obtained as a white powder (131 mg; 87%).

$R_f$  (dichloromethane/acetone 5:1) = 0.28.

$^{31}\text{P}$ -NMR (202 MHz, DMSO)  $\delta$  [ppm] = 148.89, 148.74.

MALDI-TOF: Calcd. for  $\text{C}_{52}\text{H}_{64}\text{O}_9\text{N}_8\text{BrP}$  [MNa] $^+$ : 1105.39, found: 1105.10.

## 5.2.2 2'-Deoxyribonucleosides

**Compound 18**

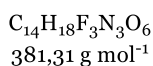
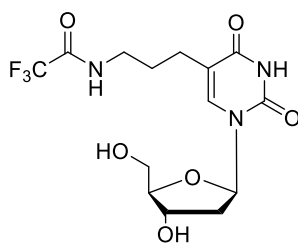
Under argon atmosphere, 1.00 g 5-Iodo-2'-deoxyuridine (2.82 mmol; 1.00 equiv.) was dissolved in 15 mL anhydrous DMF. 107 mg copper(i) iodide (0.564 mmol; 0.20 equiv.) and 992  $\mu\text{L}$  of **17** (1.28 g; 8.47 mmol; 3.00 equiv.) were added and the reaction mixture was degassed by bubbling argon through it for 15 minutes. 326 mg tetrakis(triphenylphosphine)palladium(0) (0.282 mmol; 0.10 equiv.) and 0.78 mL triethylamine (571 mg; 5.65 mmol; 2.00 equiv.) were added and the reaction mixture stirred for 5 hours at 50 °C. The solvent was removed under reduced pressure and the crude product dissolved in 50 mL methanol/dichloromethane 1:1 (v/v). Two teaspoons of freshly prepared *Amberlite*® IRA-402 (bicarbonate form) were added and the resulting suspension stirred for 15 minutes. After filtration, the solvent was removed under reduced pressure and the crude product purified *via* column chromatography (dichloromethane/methanol 10:1). The product was obtained as a beige foam (816 mg, 76%).

$R_f$  (DCM/MeOH 10:1) = 0.20.

$^1\text{H-NMR}$  (400 MHz, DMSO)  $\delta$  [ppm] = 11.53 (s, 1H, 3-NH), 10.05 (s, 1H, NH), 8.20 (s, 1H, 6-CH), 6.10 (t,  $J$  = 6.7 Hz, 1H, 1'-CH), 5.24 (d,  $J$  = 4.3 Hz, 1H, 3'-OH), 5.09 (t,  $J$  = 5.1 Hz, 1H, 4'-OH), 4.26 – 4.19 (m, 3H, 3'-CH, CH<sub>2</sub>), 3.80 (q,  $J$  = 3.4 Hz, 1H, 4'-CH), 3.64 – 3.51 (m, 2H, 5'-CH<sub>2</sub>), 2.12 (dd,  $J$  = 6.7, 4.7 Hz, 2H, 2'-CH<sub>2</sub>).

The spectral data is in agreement with literature.<sup>[141]</sup>

## Compound 19

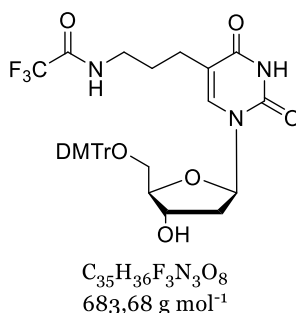


650 mg nucleoside **18** (1.72 mmol; 1.00 equiv.) and 275 mg Pd/C (10% Pd, 0.189  $\mu\text{mol}$ ; 0.15 equiv.) were dissolved in 25 ml anhydrous methanol. Hydrogen (approx. 2 L balloon) was bubbled through the suspension for 6 hours. The reaction mixture was filtered over a plug of *Celite*® and the solvent was removed under reduced pressure. The product was obtained as a pale yellow foam (563 mg, 86%).

$R_f$  (DCM/MeOH 10:1) = 0.20.

$^1\text{H-NMR}$  (400 MHz, DMSO)  $\delta$  [ppm] = 11.29 (s, 1H, 3-NH), 9.40 (t,  $J = 5.7$  Hz, 1H, NH), 7.68 (s, 1H, 6-CH), 6.16 (t,  $J = 6.8$ , 1H, 1'-CH), 5.22 (d,  $J = 4.2$  Hz, 1H, 3'-OH), 5.00 (t,  $J = 5.2$  Hz, 1H, 5'-OH), 4.27 – 4.20 (m, 1H, 3'-CH), 3.76 (q,  $J = 3.7$  Hz, 1H, 4'-CH), 3.56 (qdd,  $J = 11.8, 5.3, 3.9$  Hz, 2H, 5'-CH<sub>2</sub>), 3.16 (dt,  $J = 7.0, 4.0$  Hz, 2H, CH<sub>2</sub>), 2.27 – 2.15 (m, 2H, CH<sub>2</sub>), 2.14 – 2.02 (m, 2H, 2'-CH<sub>2</sub>), 1.64 (qt,  $J = 7.2, 4.2$  Hz, 2H, CH<sub>2</sub>).

The spectral data is in agreement with literature.<sup>[69]</sup>

**Compound 20**

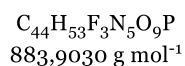
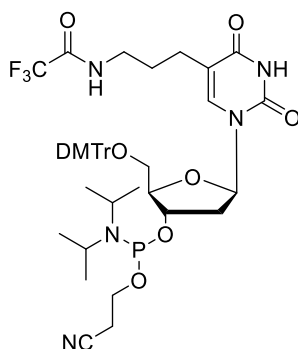
500 mg nucleoside **19** (1.31 mmol; 1.00 equiv.) were dissolved in 10 mL anhydrous pyridine. 267 mg silver(II) nitrate (1.57 mmol; 1.20 equiv.) and 533 mg 4,4'-dimethoxytrityl chloride (1.57 mmol; 1.20 equiv.) were added and the reaction mixture stirred for 6 hours. The crude mixture was diluted with 50 mL dichloromethane, filtered, and washed with 3x 50 mL saturated NaHCO<sub>3</sub> solution. The solvent was removed under reduced pressure and the crude product purified *via* column chromatography (dichloromethane/methanol 40:1). The product was obtained as a colorless foam (408 mg, 46%).

<sup>1</sup>H-NMR (400 MHz, DMSO)  $\delta$  [ppm] = 11.37 (s, 1H, 3-NH), 9.33 (t,  $J$  = 5.7 Hz, 1H, NH), 7.41 (s, 1H, 6-CH), 7.40 – 7.36 (m, 2H, CH<sub>ar</sub>), 7.31 – 7.22 (m, 7H, CH<sub>ar</sub>), 6.90 – 6.85 (m, 4H, CH<sub>ar</sub>), 6.20 (t,  $J$  = 6.8 Hz, 1H, 1'-CH), 5.32 (d,  $J$  = 4.6 Hz, 1H, 3'-OH), 4.29 (dq,  $J$  = 8.4, 4.1 Hz, 1H, 3'-CH), 3.88 (q,  $J$  = 4.8, 4.3 Hz, 1H, 4'-CH), 3.19 (qd,  $J$  = 10.4, 4.1 Hz, 2H, 5'-CH<sub>2</sub>), 2.98 (q,  $J$  = 6.9 Hz, 2H, CH<sub>2</sub>), 2.26 (dt,  $J$  = 13.6, 6.9 Hz, 1H, 2'-CH<sub>2</sub>), 2.15 (ddd,  $J$  = 13.4, 6.6, 3.9 Hz, 1H, 2'-CH<sub>2</sub>), 1.96 – 1.86 (m, 2H, CH<sub>2</sub>), 1.52 – 1.43 (m, 2H, CH<sub>2</sub>).

<sup>13</sup>C-NMR (101 MHz, DMSO)  $\delta$  [ppm] = 163.3, 158.1, 150.3, 149.6, 144.7, 136.3, 136.1, 135.5, 135.3, 129.7, 127.9, 127.7, 126.8, 123.9, 113.2, 112.9, 85.7, 85.4, 83.9, 70.5, 63.9, 55.0, 38.6, 27.4, 23.8.

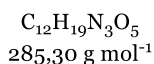
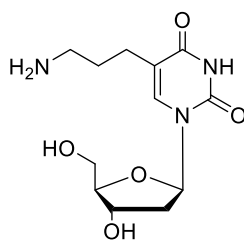
ESI-HRMS: Calcd. for C<sub>35</sub>H<sub>36</sub>O<sub>8</sub>N<sub>3</sub>ClF<sub>3</sub> [M+Cl]<sup>-</sup>: 718.2143, found: 718.2149.

### Compound 21



75 mg nucleoside **20** (0.092 mmol; 1.00 equiv.) were lyophilized out of benzene, followed by dissolving in 3 mL anhydrous dichloromethane. 48  $\mu\text{L}$  DIPEA (113 mg; 0.277 mmol; 3.00 equiv.) and 32  $\mu\text{L}$  2-cyanoethyl-*N,N*-diisopropylchlorophosphoramidite (103 mg; 0.138 mmol; 1.50 equiv.) were added and the reaction mixture stirred for 4 hours. The crude product was purified *via* column chromatography (dichloromethane/acetone 1:1). The product was obtained as a colorless foam (161 mg, 62%).

<sup>31</sup>P-NMR (162 MHz, DMSO)  $\delta$  [ppm] = 147.6, 147.2.

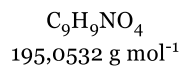
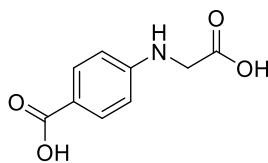
**Compound 22**

514 mg nucleoside **19** (1.35 mmol; 1.00 equiv.) were dissolved in 10 mL concentrated aqueous ammonia and stirred over night at room temperature. The solvent was removed under reduced pressure. The product was obtained as a pale yellow foam (385 mg, quant.).

$^1\text{H-NMR}$  (400 MHz, DMSO)  $\delta$  [ppm] = 7.72 (s, 1H, 6-**CH**), 6.16 (t,  $J = 6.8$  Hz, 1H, 1'-**CH**), 5.25 (d,  $J = 4.2$  Hz, 1H, 3'-**OH**), 5.05 (br s, 1H, 5'-**OH**), 4.28 – 4.21 (m, 1H, 3'-**CH**), 3.78 (q,  $J = 3.6$  Hz, 1H, 4'-**CH**), 3.63 – 3.52 (m, 2H, 5'-**CH**<sub>2</sub>), 2.79 – 2.72 (m, 2H, **CH**<sub>2</sub>), 2.26 (t,  $J = 7.4$  Hz, 2H, **CH**<sub>2</sub>), 2.09 (dd,  $J = 6.9, 4.7$  Hz, 2H, 2'-**CH**<sub>2</sub>), 1.75 – 1.66 (m, 2H, **CH**<sub>2</sub>).

The spectral data is in agreement with literature.<sup>[107]</sup>

### Compound 25

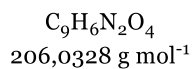
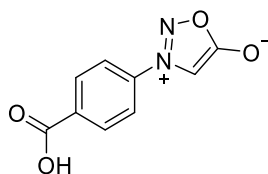


2.00 g sodium chloroacetate (14.6 mmol; 1.00 equiv.) were dissolved in 50 mL water. 1.70 g 4-aminobenzoic acid (14.6 mmol; 1.00 equiv.) were added and the reaction mixture was refluxed for 4 hours. Upon cooling to room temperature, the precipitate was collected, washed with cold water, 20 mL hot ethanol and dried in vacuum. The product was obtained as a pale green powder (1.32 g, 46%).

$^1\text{H-NMR}$  (400 MHz, DMSO)  $\delta$  [ppm] = 12.34 (s, 2H, COOH), 7.67 (d,  $J = 8.9$  Hz, 2H, CH<sub>ar</sub>), 6.66 (s, 1H, NH), 6.57 (d,  $J = 8.8$  Hz, 1H, CH<sub>ar</sub>), 3.87 (s, 2H, CH<sub>2</sub>).

The spectral data is in agreement with literature.<sup>[144]</sup>

### Compound 26



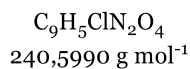
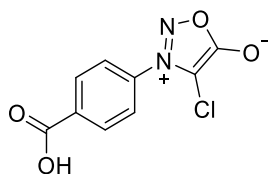
1.27 g of **25** (6.51 mmol; 1.00 equiv.) were suspended in 50 mL anhydrous THF. 945  $\mu\text{L}$  *tert*-butyl nitrite (90%, 820 mg; 7.16 mmol; 1.10 equiv.) were added and stirred for 30 minutes, until the solution turned clear. 995  $\mu\text{L}$  trifluoroacetic anhydride (1.50 g; 7.16 mmol; 1.10 equiv.) were added and the reaction mixture was stirred for additional 1.5 hours. The solvent was evaporated under reduced pressure and the crude product diluted with 50 mL methanol. The reaction mixture was filtered, and the precipitate dried in high vacuum. The product was obtained as a pale orange powder (1.10 g, 82%).

$R_f$  (DCM/MeOH 50:1 +1% AcOH) = 0.21.

$^1\text{H-NMR}$  (400 MHz, DMSO)  $\delta$  [ppm] = 13.55 (s, 1H, COOH), 8.23 – 8.19 (m, 2H, CH<sub>ar</sub>), 8.10 – 8.06 (m, 2H, CH<sub>ar</sub>), 7.88 (s, 1H, CH).

The spectral data is in agreement with literature.<sup>[84]</sup>

### Compound 27

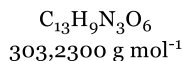
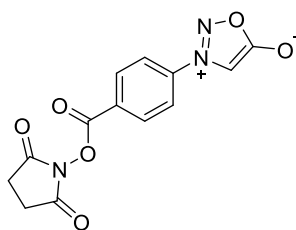


850 mg sydnone **26** (4.12 mmol; 1.00 equiv.) were suspended in 100 mL dioxane/1M HCl (V/V 2:1). 4.65 mL sodium hypochlorite solution (12% active chlorine, 5.12 g; 8.25 mmol; 2.00 equiv.) were added dropwise and the reaction mixture stirred for 4 hours. Additional 4.65 mL sodium hypochlorite solution (12% active chlorine, 5.12 g; 8.25 mmol; 2.00 equiv.) were added and the mixture stirred for 16h at room temperature. The reaction mixture was diluted with 200 mL ethyl acetate and washed with 3x200 mL brine. The solvent was removed under reduced pressure and the crude product was purified *via* column chromatography (dichloromethane/methanol 99:1 + 1% acetic acid). The product was obtained as a yellow powder (422 mg, 43%).

$R_f$  (DCM/MeOH 20:1 +1% AcOH) = 0.40.

$^1\text{H NMR}$  (400 MHz, Methanol)  $\delta$  [ppm] = 8.36 – 8.32 (m, 2H,  $\text{CH}_{\text{ar}}$ ), 7.93 – 7.89 (m, 2H,  $\text{CH}_{\text{ar}}$ ).

The spectral data is in agreement with literature.<sup>[84]</sup>

**Compound 28**

525 mg of the sydnone **26** (2.55 mmol; 1.00 equiv.) were dissolved in 20 mL anhydrous DMF. Subsequently, 439 mg N-hydroxysuccinimide (3.82 mmol; 1.50 equiv.) and 732 mg N-(3-dimethylaminopropyl)-N'-ethylcarbodiimide hydrochloride (3.82 mmol; 1.50 equiv.) were added and the reaction mixture stirred over night at room temperature. The crude mixture was diluted with 50 mL ethyl acetate and washed with 3x 150 mL water and 1x 150 mL brine. The organic layer was separated, dried over sodium sulfate and the solvent was removed under reduced pressure. The resulting precipitate was dried under high vacuum. The product was obtained as a white powder (600 mg; 78%).

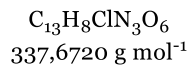
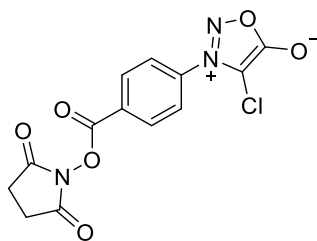
$R_f(\text{DCM}/\text{MeOH } 50:1) = 0.19$ .

$^1\text{H-NMR}$  (400 MHz, DMSO)  $\delta$  [ppm] = 8.44 – 8.37 (m, 2H,  $\text{CH}_{\text{ar}}$ ), 8.26 – 8.21 (m, 2H,  $\text{CH}_{\text{ar}}$ ), 7.98 (s, 1H,  $\text{CH}$ ), 2.92 (s, 4H,  $\text{CH}_2$ ).

$^{13}\text{C-NMR}$  (101 MHz, DMSO)  $\delta$  [ppm] = 170.1 ( $\text{Cq}$ ), 168.4 ( $\text{Cq}$ ), 160.7 ( $\text{Cq}$ ), 139.1 ( $\text{Cq}$ ), 132.0 ( $\text{CH}_{\text{ar}}$ ), 127.7 ( $\text{Cq}$ ), 122.7 ( $\text{CH}_{\text{ar}}$ ), 95.5 ( $\text{CH}$ ), 25.6 ( $\text{CH}_2$ ).

ESI-MS: Calcd. for  $\text{C}_{14}\text{H}_9\text{O}_6\text{N}_3$   $[\text{MH}]^+$ : 304.0564, found: 304.0554.

### Compound 29



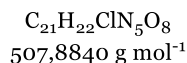
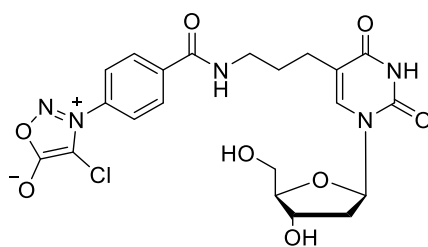
180 mg sydnone **27** (0.748 mmol; 1.00 equiv.) were dissolved in 20 mL anhydrous DMF. 129 mg N-hydroxysuccinimide (1.12 mmol; 1.50 equiv.) and 215 mg EDC HCl (1.12 mmol; 1.50 equiv.) were added and stirred at room temperature overnight. The reaction mixture was diluted with 50 mL ethyl acetate and washed with 5x 150 mL brine. The organic layer was dried over sodium sulfate and the solvent was removed under reduced pressure. The product was obtained as an orange powder (224 mg, 89%).

<sup>1</sup>H-NMR (400 MHz, Chloroform)  $\delta$  [ppm] = 8.47 – 8.41 (m, 2H, CH<sub>ar</sub>), 7.89 – 7.83 (m, 2H, CH<sub>ar</sub>), 2.95 (s, 4H, CH<sub>2</sub>).

The spectral data is in agreement with literature.<sup>[84]</sup>



## Compound 32



70.0 mg of deprotected nucleoside **22** (245  $\mu\text{mol}$ ; 1.00 equiv.) and 136  $\mu\text{L}$  triethylamine (99.3 mg; 981  $\mu\text{mol}$ ; 4.00 equiv.) were dissolved in 5 mL anhydrous *N,N*-dimethylformamide. 100 mg of sydnone **29** (294  $\mu\text{mol}$ ; 1.20 equiv.) were added and the reaction was stirred for 16h at room temperature. The solvent was removed under reduced pressure and the crude product was redissolved in 50 mL methanol. The solution was treated with Amberlite IRA-402 bicarbonate form for 30 minutes. After filtration, the solvent was evaporated. The crude mixture was purified *via* column chromatography (dichloromethane/methanol 10:1). The product was obtained as a pale yellow foam (66 mg, 54%).

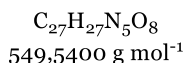
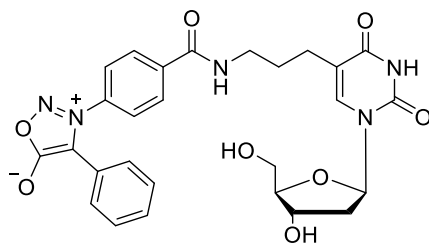
$R_f$  (dichloromethane/methanol 9:1) = 0.15.

$^1\text{H-NMR}$  (400 MHz, DMSO)  $\delta$  [ppm] = 11.26 (s, 1H, 3-NH), 8.76 (t,  $J$  = 5.7 Hz, 1H, NH), 8.12 (d,  $J$  = 8.6 Hz, 2H, CH<sub>ar</sub>), 7.94 (d,  $J$  = 8.7 Hz, 2H, CH<sub>ar</sub>), 7.73 (s, 1H, 6-CH), 6.18 (dd,  $J$  = 7.5, 6.1 Hz, 1H, 1'-CH), 5.23 (d,  $J$  = 4.2 Hz, 1H, 3'-OH), 5.02 (d,  $J$  = 5.5 Hz, 1H, 5'-OH), 4.29 – 4.21 (m, 1H, 3'-CH), 3.77 (q,  $J$  = 3.6 Hz, 1H, 4'-CH), 3.58 (qd,  $J$  = 11.8, 5.9 Hz, 2H, 5'-CH<sub>2</sub>), 3.29 (dd,  $J$  = 6.9 Hz, 2H, CH<sub>2</sub>), 2.34 – 2.20 (m, 2H, CH<sub>2</sub>), 2.16 – 2.03 (m, 2H, 2'-CH<sub>2</sub>), 1.71 (p,  $J$  = 7.2 Hz, 2H, CH<sub>2</sub>).

$^{13}\text{C-NMR}$  (101 MHz, DMSO)  $\delta$  [ppm] = 164.8 (Cq), 163.4 (Cq), 150.3 (Cq), 138.6 (Cq), 136.4 (6-CH), 134.4 (Cq), 128.9 (CH<sub>ar</sub>), 125.4 (CH<sub>ar</sub>), 112.9 (Cq), 99.4 (Cq), 87.3 (4'-CH), 83.9 (1'-CH), 70.4 (3'-CH), 61.3 (4'-CH, 5'-CH<sub>2</sub>), 39.4 (2'-CH<sub>2</sub>), 38.8 (CH<sub>2</sub>), 27.8 (CH<sub>2</sub>), 23.9 (CH<sub>2</sub>).

ESI-HRMS: Calcd. for C<sub>21</sub>H<sub>23</sub>O<sub>8</sub>N<sub>5</sub>Cl [MH]<sup>+</sup>: 508.1230, found: 508.1224.

## Compound 33



37.5 mg of deprotected nucleoside **22** (131  $\mu\text{mol}$ ; 1.00 equiv.) and 73.3  $\mu\text{L}$  triethylamine (53.2 mg; 525  $\mu\text{mol}$ ; 4.00 equiv.) were dissolved in 5 mL anhydrous *N,N*-dimethylformamide. 100 mg of sydnone **30** (262  $\mu\text{mol}$ ; 2.00 equiv.) were added and the reaction was stirred for 16h at room temperature. The solvent was removed under reduced pressure and the crude product was redissolved in 50 mL methanol. The solution was treated with Amberlite IRA-402 bicarbonate form for 30 minutes. After filtration, the solvent was evaporated. The crude mixture was purified *via* column chromatography (dichloromethane/methanol 10:1). The product was obtained as a colorless foam (17 mg, 24%).

$^1\text{H-NMR}$  (400 MHz, DMSO)  $\delta$  [ppm] = 11.30 (s, 1H, 3-NH), 8.79 (s, 1H, NH), 8.06 (d,  $J = 8.5$  Hz, 2H, CH<sub>ar</sub>), 7.80 (d,  $J = 8.5$  Hz, 2H, CH<sub>ar</sub>), 7.74 (s, 1H, 6-CH), 7.34 (t,  $J = 7.3$  Hz, 2H, CH<sub>ar</sub>), 7.29 – 7.21 (m, 2H, CH<sub>ar</sub>), 6.17 (t,  $J = 6.8$  Hz, 1H, 1'-CH), 5.28 (s, 1H, 3'-OH), 5.11 (s, 1H, 4'-OH), 4.25 (s, 1H, 3'-CH), 3.76 (d,  $J = 3.1$  Hz, 2H, 4'-CH), 3.57 (d,  $J = 9.0$  Hz, 2H, 5'-CH<sub>2</sub>), 3.28 (d,  $J = 6.4$  Hz, 2H, CH<sub>2</sub>), 2.26 (d,  $J = 5.6$  Hz, 2H, CH<sub>2</sub>), 2.18 – 2.03 (m, 2H, 2'-CH<sub>2</sub>), 1.76 – 1.65 (m, 2H, CH<sub>2</sub>).

$^{13}\text{C-NMR}$  (101 MHz, DMSO)  $\delta$  [ppm] = 166.3 (Cq), 164.7 (Cq), 163.5 (Cq), 150.4 (Cq), 137.9 (Cq), 136.4 (Cq), 136.0 (6-CH), 128.9 (Cq), 128.7 (CH), 128.6 (CH), 127.5 (CH), 125.7 (CH), 124.4 (CH), 112.9 (Cq), 108.3 (Cq), 87.3 (4'-CH), 83.9 (1'-CH), 70.4 (3'-CH), 61.3 (5'-CH<sub>2</sub>), 39.0 (2'-CH<sub>2</sub>), 38.3 (CH<sub>2</sub>), 27.8 (CH<sub>2</sub>), 24.0 (CH<sub>2</sub>).

ESI-HRMS: Calcd. for C<sub>27</sub>H<sub>27</sub>O<sub>8</sub>N<sub>5</sub> [M+H]<sup>+</sup>: 550.1932, found: 550.1931.

## 5.3 Oligonucleotides

### 5.3.1 RNA

#### 5.3.1.1 Handling

When working with RNA, every instrument and tool (HPLC, synthesizer, cuvettes, glass equipment, surface of the bench, hands) was thoroughly cleaned with ethanol to avoid contamination with RNase. Water was treated with 0.1% diethylpyrocarbonate followed by boiling for 2 hours to deactivate RNase.

#### 5.3.1.2 Synthesis

The RNA strands **RNA1** and **RNA2** were synthesized after standard solid-phase phosphoramidite synthesis protocol on a *H-6 DNA/RNA synthesizer* by *K&A Laborgeräte*. Natural phosphoramidites (adenosine, guanosine, cytidine, uridine, *Glen Research*) were used as a 67 mM solution in acetonitrile. Artificial phosphoramidite **12** was used as a 100 mM solution in dichloromethane. As solid phase, CPG columns (1  $\mu$ mol, *Glen Research*) were used. For more efficient coupling, Activator 42<sup>®</sup> (*Sigma Aldrich*) was used instead of standard activator (0.45 M tetrazole in acetonitrile).

The following coupling protocol was used:

Table 12. Deprotection

Step	Time [0.1s]	Source	Destination	S.C.Ptr	Delay	Branch
<b>1</b>	4	TCA	COL			
<b>2</b>	20	TCA	TRM	ON		
<b>3</b>				ON		
<b>4</b>					15	
<b>5</b>	15	TCA	TRM	ON		
<b>6</b>				ON		
<b>7</b>					15	
<b>8</b>	15	TCA	TRM	ON		
<b>9</b>				ON		
<b>10</b>					15	
<b>11</b>	15	TCA	TRM	ON		
<b>12</b>				ON		
<b>13</b>					15	

## 5 Experimental Section

<b>14</b>	15	TCA	TRM	ON	
<b>15</b>				ON	
<b>16</b>					15
<b>17</b>	30	GAS	TRM		
<b>18</b>	10	ACN	M_W		
<b>19</b>	20	ACN	COL	ON	
<b>20</b>				ON	
<b>21</b>					4
<b>22</b>	30	GAS	COL		
<b>23</b>	2	ACN	M_W		
<b>24</b>	20	ACN	COL	ON	
<b>25</b>				ON	

Table 13. Coupling

<b>Step</b>	<b>Time [0.1s]</b>	<b>Source</b>	<b>Destination</b>	<b>S.C.Ptr</b>	<b>Delay</b>	<b>Branch</b>
<b>1</b>	15	GAS	COL		2	
<b>2</b>	4	TET	COL	ON		
<b>3</b>				ON		
<b>4</b>					2	1
<b>5</b>					90	
<b>6</b>	10	ACN	M_W		90	
<b>7</b>	10	ACN	COL	ON		
<b>8</b>				ON		
<b>9</b>	35	GAS	COL			
<b>10</b>	20	GAS	M_W			

Table 14. Branch 1

<b>Step</b>	<b>Time [0.1s]</b>	<b>Source</b>	<b>Destination</b>	<b>S.C.Ptr</b>	<b>Delay</b>	<b>Branch</b>
<b>1</b>	4	TET	COL	ON		
<b>2</b>	5	AMD+TET	COL			
<b>3</b>				ON		
<b>4</b>					60	
<b>5</b>					60	

## 5 Experimental Section

<b>6</b>					60
<b>7</b>					60
<b>8</b>	5	AMD+TET	COL		
<b>9</b>				ON	
<b>10</b>					60
<b>11</b>					60
<b>12</b>					60
<b>13</b>					60
<b>14</b>	5	TET	COL	ON	
<b>15</b>				ON	
<b>16</b>	20	ACN	M_W		
<b>17</b>	20	GAS	M_W		

Table 15. Capping

Step	Time [0.1s]	Source	Destination	S.C.Ptr	Delay	Branch
<b>1</b>	20	CP_A+CP_B	COL	ON		
<b>2</b>				ON		
<b>3</b>					15	
<b>4</b>	3	CP_A+CP_B	COL	ON		
<b>5</b>				ON		
<b>6</b>					15	
<b>7</b>	20	GAS	COL			
<b>8</b>	2	ACN	M_W			
<b>9</b>	12	AC	COL	ON		
<b>10</b>				ON		
<b>11</b>	10	GAS	M_W		2	
<b>12</b>	30	GAS	COL			

Table 16. Oxidation

Step	Time [0.1s]	Source	Destination	S.C.Ptr	Delay	Branch
<b>1</b>	20	OXI	COL	ON		
<b>2</b>				ON		
<b>3</b>	10	ACN	M_W		9	

## 5 Experimental Section

---

<b>4</b>					9
<b>5</b>		WTH			150
<b>6</b>		WTH			150
<b>7</b>	30	GAS	COL		
<b>8</b>	2	ACN	M_W		
<b>9</b>	16	ACN	COL	ON	
<b>10</b>					ON
<b>11</b>	20				
<b>12</b>	30	GAS	COL		
<b>13</b>	2	ACN	M_W		
<b>14</b>	15	ACN	COL	ON	
<b>15</b>					ON
<b>16</b>	40				
<b>17</b>	15	ACN	COL	ON	
<b>18</b>					ON
<b>19</b>	50				
<b>20</b>	10	GAS	M_W		
<b>21</b>	30	GAS	COL		

For the artificial phosphoramidite building block **12** the following subroutine was used:

Table 17. Branch

<b>Step</b>	<b>Time [0.1s]</b>	<b>Source</b>	<b>Destination</b>	<b>S.C.Ptr</b>	<b>Delay</b>	<b>Branch</b>
<b>1</b>	4	TET+DCM	COL	ON		
<b>2</b>	5	AMD+TET	COL			
<b>3</b>				ON		
<b>4</b>					99	
<b>5</b>					99	
<b>6</b>					99	
<b>7</b>					99	
<b>8</b>	5	AMD+TET	COL	ON		
<b>9</b>				ON		
<b>10</b>					99	

## 5 Experimental Section

---

<b>11</b>				99
<b>12</b>				99
<b>13</b>				99
<b>14</b>	5	AMD+TET	COL	ON
<b>15</b>				ON
<b>16</b>				99
<b>17</b>				99
<b>18</b>				99
<b>19</b>				99
<b>20</b>	5	TET	COL	ON
<b>21</b>				ON
<b>22</b>	20	DCM	COL	ON
<b>23</b>				ON
<b>24</b>	20	ACN	M_W	
<b>25</b>	20	GAS	M_W	

Compared to the natural phosphoramidite, an additional AMD+TET step was added, and the coupling time was increased to ~20 min (natural phosphoramidites 8 min). Additionally, a washing step with DCM was introduced to avoid precipitation of the artificial phosphoramidite **12**.

After synthesis, the CPG columns were dried in high vacuum, followed by cleavage from the solid support. The cleavage was performed directly on the column by pushing and pulling 1 mL of 33% methylamine in ethanol/25% ammonium hydroxide solution (v/v, 1:1) solution through the column *via* a syringe. The solution was incubated on the column at room temperature for 30 minutes and transferred to an *Eppendorf* reaction vial. The solution was incubated further 15 minutes at 60 °C. The solvents were removed in the vacuum centrifuge (35 min, 35 °C, 100 mbar (ammonium hydroxide) followed by ∞ min, 25 °C, 0.100 mbar).

For deprotection of the 2'-TBDMS groups, the RNA was dissolved in 300 µL DMSO, 300 µL triethylamine trihydrofluoride was added and the solution incubated for 2.5 hours at 60 °C. The samples were vortexed every 30 minutes. For quenching of the fluoride ions, 600 µL isopropyltrimethylsilylether was added. 2.00 mL diethylether was added and the RNA precipitated over night at -32 °C.

## 5 Experimental Section

---

After centrifugation (13 000 rpm, 5 minutes) the RNA pellet was washed with 80% ethanol and dried in high vacuum.

### 5.3.1.3 Purification and Characterization

The RNA pellet was dissolved in 600  $\mu\text{L}$  water and purified *via* semi-preparative HPLC (300  $\mu\text{L}$  injection, 0-XX% acetonitrile, 0.1 M ammonium bicarbonate, 60  $^{\circ}\text{C}$ , xx minutes). The detection wavelength was set to 260 and 280 nm (oligonucleotide absorbance) and 320 nm (tetrazole absorbance).

The success of the synthesis was determined *via* MALDI-TOF with 3-HPA as a matrix substance (Table 2). The concentration was determined *via* Lambert-Beer law using the absorbance of the oligonucleotide that was collected with a *NanoDrop* ND-1000 spectrometer and the extinction coefficient of the oligonucleotide that was calculated by the following formula:

$$\epsilon_{260} = (X_A \times \epsilon_A + X_G \times \epsilon_G + X_U \times \epsilon_U + X_C \times \epsilon_C + \epsilon_9) \times 0.9$$

$X_x$  = amount of each building block

$$\epsilon_A = 15\,400 \text{ L mol}^{-1} \text{ cm}^{-1} \quad \epsilon_G = 11\,500 \text{ L mol}^{-1} \text{ cm}^{-1}$$

$$\epsilon_C = 7\,200 \text{ L mol}^{-1} \text{ cm}^{-1} \quad \epsilon_U = 9\,900 \text{ L mol}^{-1} \text{ cm}^{-1}$$

$$\epsilon_9 = 13\,797 \text{ L mol}^{-1} \text{ cm}^{-1}$$

The factor 0.9 takes the hypochromicity into consideration.

## 5.3.2 DNA

5.3.2.1 Synthesis of **DNA3**

The DNA strand **DNA3** was synthesized after standard solid-phase phosphoramidite synthesis protocol on a *H-6 DNA/RNA synthesizer* by *K&A Laborgeräte*. Natural phosphoramidites (2'-deoxyadenosine, 2'-deoxyguanosine, 2'-deoxycytidine, thymidine, *Sigma Aldrich*) were used as a 67 mM solution in acetonitrile. Artificial phosphoramidite **21** was used as a 100 mM solution in dichloromethane. As solid phase, CPG columns (1  $\mu$ mol, *Sigma Aldrich*) were used.

The following coupling protocol was used:

Table 18. Deprotection

Step	Time [0.1s]	Source	Destination	S.C.Ptr	Delay	Branch
<b>1</b>	4	TCA	COL			
<b>2</b>	20	TCA	TRM	ON		
<b>3</b>				ON		
<b>4</b>					15	
<b>5</b>	15	TCA	TRM	ON		
<b>6</b>				ON		
<b>7</b>					15	
<b>8</b>	15	TCA	TRM	ON		
<b>9</b>				ON		
<b>10</b>					15	
<b>11</b>	15	TCA	TRM	ON		
<b>12</b>				ON		
<b>13</b>					15	
<b>14</b>	15	TCA	TRM	ON		
<b>15</b>				ON		
<b>16</b>					15	
<b>17</b>	30	GAS	TRM			
<b>18</b>	10	ACN	M_W			
<b>19</b>	20	ACN	COL	ON		
<b>20</b>				ON		
<b>21</b>					4	
<b>22</b>	30	GAS	COL			

## 5 Experimental Section

<b>23</b>	2	ACN	M_W		
<b>24</b>	20	ACN	COL	ON	
<b>25</b>				ON	

Table 19. Coupling

Step	Time [0.1s]	Source	Destination	S.C.Ptr	Delay	Branch
<b>1</b>	15	GAS	COL		2	
<b>2</b>	2	TET	COL	ON		
<b>3</b>				ON		
<b>4</b>					2	1
<b>5</b>	10	ACN	M_W		50	
<b>6</b>		WMO			90	
<b>7</b>		WMO			90	
<b>8</b>	10	ACN	COL	ON		
<b>9</b>				ON		
<b>10</b>	35	GAS	COL			
<b>11</b>	20	GAS	M_W			

Table 20. Branch 1

Step	Time [0.1s]	Source	Destination	S.C.Ptr	Delay	Branch
<b>1</b>	4	TET	COL	ON		
<b>2</b>	8	AMD+TET	COL			
<b>3</b>				ON		
<b>4</b>					8	
<b>5</b>	4	AMD+TET	COL	ON		
<b>6</b>				ON		
<b>7</b>	10	ACN	M_W			
<b>8</b>	10	GAS	M_W			

Table 21. Capping

Step	Time [0.1s]	Source	Destination	S.C.Ptr	Delay	Branch
<b>1</b>	20	CP_A+CP_B	COL	ON		
<b>2</b>				ON		

## 5 Experimental Section

<b>3</b>					15
<b>4</b>	3	CP_A+CP_B	COL	ON	
<b>5</b>				ON	
<b>6</b>					15
<b>7</b>	20	GAS	COL		
<b>8</b>	2	ACN	M_W		
<b>9</b>	12	AC	COL	ON	
<b>10</b>				ON	
<b>11</b>	10	GAS	M_W		2
<b>12</b>	30	GAS	COL		

Table 22. Oxidation

<b>Step</b>	<b>Time [o.1s]</b>	<b>Source</b>	<b>Destination</b>	<b>S.C.Ptr</b>	<b>Delay</b>	<b>Branch</b>
<b>1</b>	20	OXI	COL	ON		
<b>2</b>				ON		
<b>3</b>	10	ACN	M_W		9	
<b>4</b>					9	
<b>5</b>		WTH			150	
<b>6</b>		WTH			150	
<b>7</b>	30	GAS	COL			
<b>8</b>	2	ACN	M_W			
<b>9</b>	16	ACN	COL	ON		
<b>10</b>				ON		
<b>11</b>	20					
<b>12</b>	30	GAS	COL			
<b>13</b>	2	ACN	M_W			
<b>14</b>	15	ACN	COL	ON		
<b>15</b>				ON		
<b>16</b>	40					
<b>17</b>	15	ACN	COL	ON		
<b>18</b>				ON		
<b>19</b>	50					
<b>20</b>	10	GAS	M_W			

## 5 Experimental Section

<b>21</b>	30	GAS	COL
-----------	----	-----	-----

For the artificial phosphoramidite building block **21** the following subroutine was used:

Table 23. Branch 1

Step	Time [0.1s]	Source	Destination	S.C.Ptr	Delay	Branch
<b>1</b>	4	TET+DCM	COL	ON		
<b>2</b>	4	AMD+TET	COL			
<b>3</b>				ON		
<b>4</b>					99	
<b>5</b>					99	
<b>6</b>					99	
<b>7</b>					99	
<b>8</b>	5	AMD+TET	COL			
<b>9</b>				ON		
<b>10</b>					99	
<b>11</b>					99	
<b>12</b>					99	
<b>13</b>					99	
<b>14</b>	20	DCM	COL	ON		
<b>15</b>	20	ACN	COL	ON		

Compared to the natural phosphoramidite, an additional AMD+TET step was added, and the coupling time was increased to ~13 min (natural phosphoramidites 8 s). Additionally, a washing step with DCM was introduced to avoid precipitation of the artificial phosphoramidite **21**.

After synthesis, the CPG columns were dried in high vacuum. The CPG was removed from the columns and transferred to an *Eppendorf* reaction vial. 700  $\mu$ L of 25% ammonium hydroxide was added and the suspension incubated over night at 55 °C, followed by removal of the solvents by vacuum centrifugation (35 min, 35 °C, 100 mbar (ammonium hydroxide) followed by  $\infty$  min, 25 °C, 0.100 mbar).

### 5.3.2.2 Synthesis of **DNA4** and **DNA5**

Approximately 1  $\mu\text{mol}$  of **DNA3** was dissolved in 300  $\mu\text{L}$  anhydrous DMSO. 2 mg of NHS-ester **28** or **29** was dissolved in 100  $\mu\text{L}$  anhydrous DMSO and added to the **DNA3** solution. 5  $\mu\text{L}$  DIPEA were added and the vials shook on a laboratory shaker for 16 hours. After completion of the reaction, the solvent was removed in the vacuum centrifuge ( $\infty$  min, 25  $^{\circ}\text{C}$ , 0.100 mbar).

### 5.3.2.3 Purification and Characterization

The DNA pellet was dissolved in 600  $\mu\text{L}$  water and purified *via* semi-preparative HPLC (300  $\mu\text{L}$  injection, 0-20% acetonitrile, 0.1 M ammonium acetate, 40  $^{\circ}\text{C}$ , 30 minutes). The detection wavelength was set to 260 and 280 nm (oligonucleotide absorbance) and 320 nm (sydnone absorbance).

The success of the synthesis was determined *via* MALDI-TOF with 3-HPA as a matrix substance (Table 2). The concentration was determined *via* Lambert-Beer law using the absorbance of the oligonucleotide that was collected with a *NanoDrop* ND-1000 spectrometer and the extinction coefficient of the oligonucleotide that was calculated by the following formula:

$$\epsilon_{260} = (X_{dA} \times \epsilon_{dA} + X_{dG} \times \epsilon_{dG} + X_T \times \epsilon_T + X_{dC} \times \epsilon_{dC} + \epsilon_{31/32}) \times 0.9$$

$X_x$  = amount of each building block

$$\epsilon_{dA} = 15\,400 \text{ L mol}^{-1} \text{ cm}^{-1} \quad \epsilon_{dG} = 11\,500 \text{ L mol}^{-1} \text{ cm}^{-1}$$

$$\epsilon_{dC} = 7\,200 \text{ L mol}^{-1} \text{ cm}^{-1} \quad \epsilon_T = 8\,800 \text{ L mol}^{-1} \text{ cm}^{-1}$$

$$\epsilon_{31} = 13\,712 \text{ L mol}^{-1} \text{ cm}^{-1} \quad \epsilon_{32} = 14\,213 \text{ L mol}^{-1} \text{ cm}^{-1}$$

The factor 0.9 takes the hypochromicity into consideration.

## 5.3.3 Sequences and Characterization

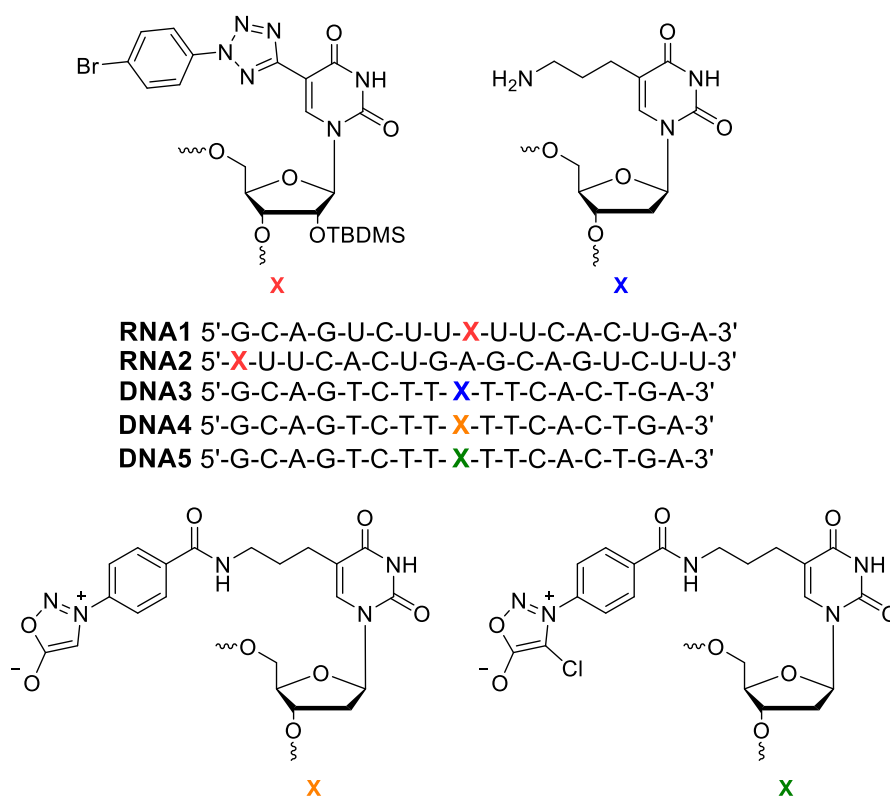


**Figure 67.** Sequences and structures of synthesized RNA and DNA strands.

Table 24. Molar extinction coefficients and calculated and measured masses of oligonucleotides.

sequence	$\epsilon_{260}$ [L mol <sup>-1</sup> cm <sup>-1</sup> ]	calculated mass [Da]	measured mass [Da]
<b>RNA1</b>	165 807	5544.6	5547.0
<b>RNA2</b>	165 807	5544.6	5546.5
<b>DNA3</b>	-	5191.9	5193.8
<b>DNA4</b>	159 782	5379.9	5374.4
<b>DNA5</b>	160 283	5413.9	5414.9

## 5.3.4 Bioorthogonal Labeling Experiments

## 5.3.4.1 SPSAC Experiments

For labeling of sydnone-modified nucleosides, to a 25  $\mu$ M solution of nucleosides **31** or **32** in methanol in a quartz glass cuvette, the respective amount of either BCN or DIBAC (stock solutions in methanol) was added. Absorbance and emission spectra were recorded at exactly defined times using the automatic settings of each spectrometer.

For labeling of sydnone-modified oligonucleotides, to a 2.5  $\mu$ M solution of **DNA4** or **DNA5** in water in a 1 mL reaction tube, the respective amount of Cy3 DIBAC

(stock solution in DMSO) was added and separated in 100  $\mu\text{L}$  portions for monitoring *via* HPLC chromatography.

### 5.3.4.2 Photoclick Experiments

For labeling of tetrazole-modified oligonucleotides, to a 2.5  $\mu\text{M}$  solution of **RNA1** or **RNA2** in 10 mM Na-P<sub>i</sub> buffer (250 mM NaCl, pH 7), the respective amount of NMM or dye maleimide (stock solution in water) was added and irradiated with a 300 nm LED for defined times. Every 30 seconds, the irradiation was paused, and the cuvette thoroughly shaken. The labeling yield was determined as following:

500  $\mu\text{L}$  of 2.5  $\mu\text{M}$  **RNA1/ RNA2** and 3.75  $\mu\text{M}$  dye maleimide in 10 mM Na-P<sub>i</sub> buffer (250 mM NaCl, pH 7) were irradiated with  $\lambda = 300$  nm light for 30 minutes.

For removal of the excess dye, the solution was purified chromatographically by illustra™ NAP-5 columns (GE Healthcare) using the standard protocol. After lyophilization of the purified sample, it was redissolved in 500  $\mu\text{L}$  water. Absorbance of each sample was measured, and the concentration calculated by Lambert-Beer-Law and the extinction coefficient of each dye:

$$\epsilon_{548} (\text{sulfo-Cy3}) = 162\,000 \text{ L mol}^{-1} \text{ cm}^{-1} (\text{Lumiprobe})$$

$$\epsilon_{555} (\text{AF555}) = 158\,000 \text{ L mol}^{-1} \text{ cm}^{-1} (\text{JenaBioscience})$$

$$\epsilon_{648} (\text{AF647}) = 270\,000 \text{ L mol}^{-1} \text{ cm}^{-1} (\text{JenaBioscience}).$$

For labeling of sydnone-modified nucleoside **33**, to a 25  $\mu\text{M}$  solution in water +0.01% methanol, the respective amount of NMM or dye maleimide (stock solutions in water) was added and irradiated with either 365 or 405 nm for defined times. Every 30 seconds, the irradiation was paused, and the cuvette thoroughly shaken. 100  $\mu\text{L}$  samples were taken at defined times and subjected to HPLC analysis.

## 5.3.5 HPLC-Methods

For purification of RNA strands, 0.1 M ammonium bicarbonate buffer in water was used, for purification of DNA strands 0.05 M ammonium acetate buffer in water was used. The ACN amount was increased over time. The following semipreparative (2.5 mL/min) HPLC methods were used:

Table 25. HPLC methods of semipreparative purification of the synthesized oligonucleotides.

sequence	method	detection wavelength [nm]
<b>RNA1</b>	0-30% ACN in 30 minutes, 60 °C	260, 290
<b>RNA2</b>	0-30% ACN in 30 minutes, 60 °C	260, 290
<b>DNA4</b>	0-15% ACN in 30 minutes, 40 °C	260, 290, 315
<b>DNA5</b>	0-15% ACN in 30 minutes, 40 °C	260, 290, 315

For purification and monitoring of the bioorthogonally labeled DNA strands and nucleosides, 100  $\mu$ L of the 25  $\mu$ M (nucleoside **33**) or 2.5  $\mu$ M (**DNA4** and **DNA5**) solutions were injected. The following analytical (1.0 mL/min) HPLC methods were used:

Table 26. HPLC methods of analytical purification of the bioorthogonally labeled nucleosides and oligonucleotides.

reaction	method	detection wavelength [nm]
<b>33+NMM</b>	0-50% ACN in 30 minutes, 40 °C	260, 280, 350
<b>33+AF555</b>	0-50% ACN in 30 minutes, 40 °C	260, 280, 350, 555
<b>33+sulfoCy3</b>	0-50% ACN in 30 minutes, 40 °C	260, 280, 350, 555
<b>DNA4+Cy3 DIBAC</b>	0-80% ACN in 40 minutes, 40 °C	260, 280, 315, 555
<b>DNA5+Cy3 DIBAC</b>	0-80% ACN in 40 minutes, 40 °C	260, 280, 315, 555

## 5.4 Determination of the Reaction Rate Constant

The reaction rate constant of the photoclick reaction between nucleoside **33** and NMM was determined *via* HPLC chromatography according to a method reported by Lin et al.<sup>[145]</sup> Solutions of 25  $\mu$ M nucleoside **33** and 125 (5.00 equiv.), 175 (7.00 equiv.) or 225  $\mu$ M (10.0 equiv.) NMM, respectively, were irradiated for defined times, followed by HPLC analysis. An excess of NMM was used to calculate the reaction rate constant according to pseudo-first order kinetics. Thymidine was added as an internal standard and the integral areas were normalized according to the thymidine integral.

## 5 Experimental Section

---

The normalized integral area was plotted against the irradiation time, as assuming a linear behavior, the integral is proportional to the product concentration.

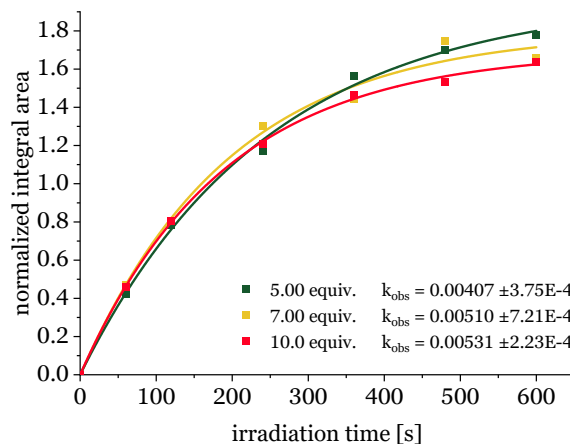


**Figure 68.** Plot of the normalized peak integral area against the irradiation time. The curve was fitted exponentially and  $k_1$  calculated for each curve.

The curve was fitted exponentially along the following equation:

$$y = a + be^{-k_1t}$$

To determine  $k_2$ , the following equation was used:

$$k_2 = \frac{k_{obs}}{C_{dipolarophile}}$$

The following values were received:

Table 27. Calculated values of  $k_{obs}$  and  $k_2$  of the reaction between 33 and different equivalents of NMM.

equivalents	$k_{obs} [s^{-1}]$	concentration [mol L <sup>-1</sup> ]	$k_2 [M^{-1}s^{-1}]$
<b>5.00</b>	$0.00407 \pm 3.75 \times 10^{-4}$	0.000125	$32.6 \pm 3.00$
<b>7.00</b>	$0.00510 \pm 7.21 \times 10^{-4}$	0.000175	$29.1 \pm 4.12$
<b>10.0</b>	$0.00531 \pm 2.23 \times 10^{-4}$	0.000225	$21.2 \pm 0.89$

The received  $k_2$  values were averaged to receive  $k_2 = 27.6 \pm 2.7 M^{-1}s^{-1}$ .

### 5.5 Cell Experiments

Human cervix carcinoma cells (*HeLa*) were cultured in *Dulbecco's modified Eagle Medium* (DMEM) containing 10% fetal calf serum and 1% penicillin Streptomycin (100 µg/mL) at 37°C/5% CO<sub>2</sub>. For sub-culturing, the cells were detached with 0.25% trypsin-EDTA. Unless stated otherwise, 4×10<sup>4</sup> cells per well were seeded into *Ibidi* 8-well µ-Slides with ibiTreat surface.

For the tests regarding the uptake of the dyes, either 100 pmol (AF555, sulfo-Cy3) or 50 pmol (AF647) of dye per well were diluted with 200 µL DMEM and added to the cells. After incubation overnight, confocal laser microscopy was performed. For the excitation of AF555 and sulfo-Cy3, the 488 nm laser (23.6 % laser power) was used, and the emission monitored at 550-650 nm (600 V smart gain). For the excitation of AF647, the 638 nm laser (23.6 % laser power) was used, and the emission monitored at 650-750 nm (600 V smart gain).

For the SPSAC labeling experiments, the cells were transfected for 16 hours with 75 ng per well **DNA4** or **DNA5** using *ScreenFect A* according to the protocol supplied by the manufacturer: 1.4 µL of *Screenfect A* were diluted with 38.6 µL dilution buffer. 0.55 µL of a 100 µM DNA solution in water were diluted with 39.5 µL dilution buffer. Both solutions were combined and incubated for 30 minutes. Subsequently, they were diluted with 720 µL DMEM and 200 µL of the solution was added to each well. The cells were fixed using 4% paraformaldehyde in PBS for 15 minutes, 50 mM glycine/50 mM ammonium chloride in PBS for 5 minutes and treated with 7 nM sulfo-Cy3 in PBS for 3 hours, followed by washing with 2 × PBS. Confocal laser microscopy was performed with the excitation set to 488 nm (15% laser power) and the emission set to 550-650 nm (HyD detector, 100% smart gain).

## 6 Additional Data and Spectra

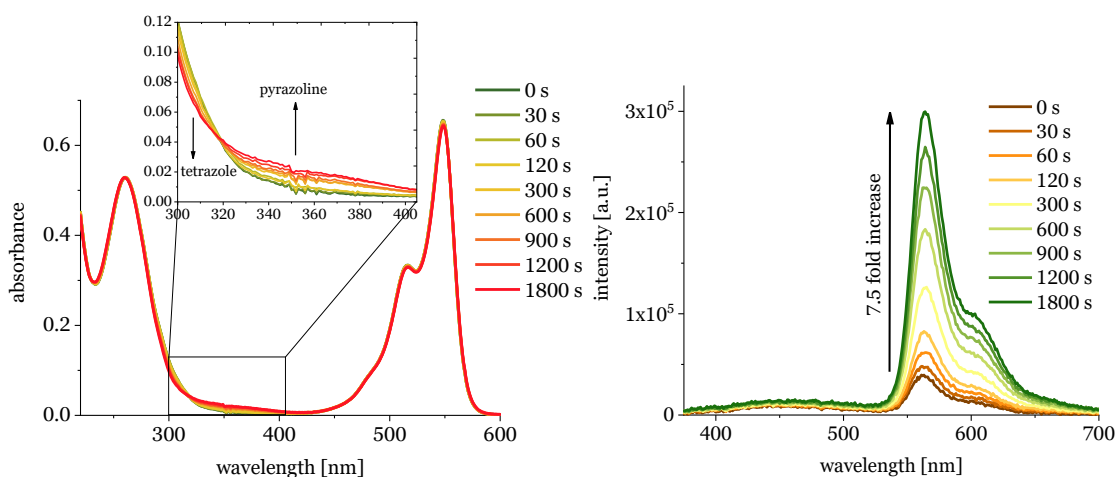
### 6.1 Reaction Conditions Peroxodisulfate Oxidation

Table A1. Tested reaction conditions for peroxodisulfate oxidation.

entry	anion	PTC	activator	T [°C]	comment	yield [%]
1	K	2,6-lutidine	CuSO <sub>4</sub>	65	no conversion	-
2	Na	2,6-lutidine	CuSO <sub>4</sub>	65	no conversion	-
3	Na	pyridine	CuSO <sub>4</sub>	65	-	9-26
4	K	pyridine	CuSO <sub>4</sub>	65	no conversion	-
5	Na	pyridine	CuSO <sub>4</sub>	r.t.	16h, no conversion	-
6	Na	pyridine	CuSO <sub>4</sub>	50	no conversion	-
7	Na	pyridine	CuSO <sub>4</sub>	85	no conversion	-
8	Na	triethylamine	CuSO <sub>4</sub>	65	no conversion	-
9	Na	pyridine + TBAB	CuSO <sub>4</sub>	65	no conversion	-
10	Na	TBAB	CuSO <sub>4</sub>	65	side-reaction	-
11	Na	pyridine	FeCl <sub>2</sub>	65	no conversion	-
12	Na	pyridine	CuSO <sub>4</sub>	65	microwave, no conversion	-

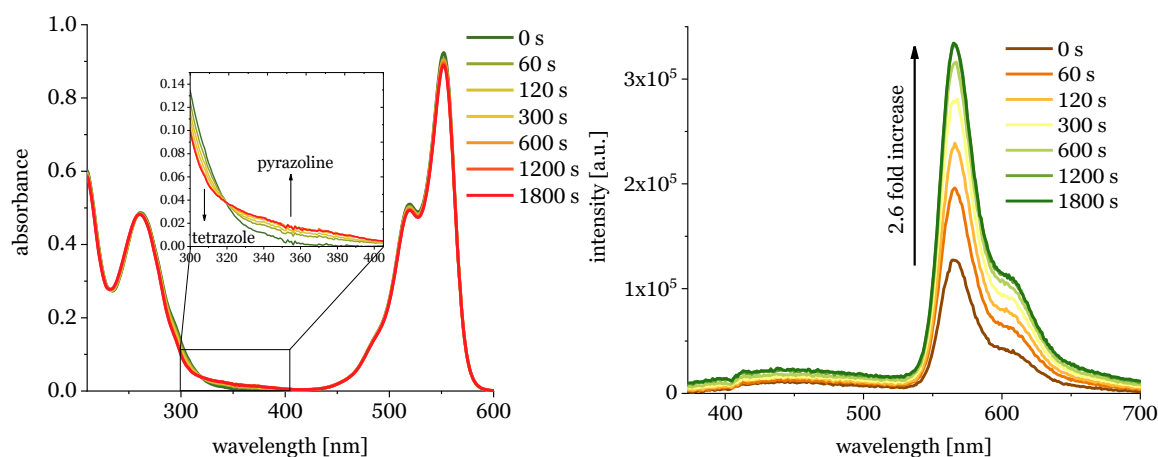
### 6.2 Spectra of Reaction between RNA1 and dye maleimides

#### RNA1 + sulfo-Cy3 maleimide



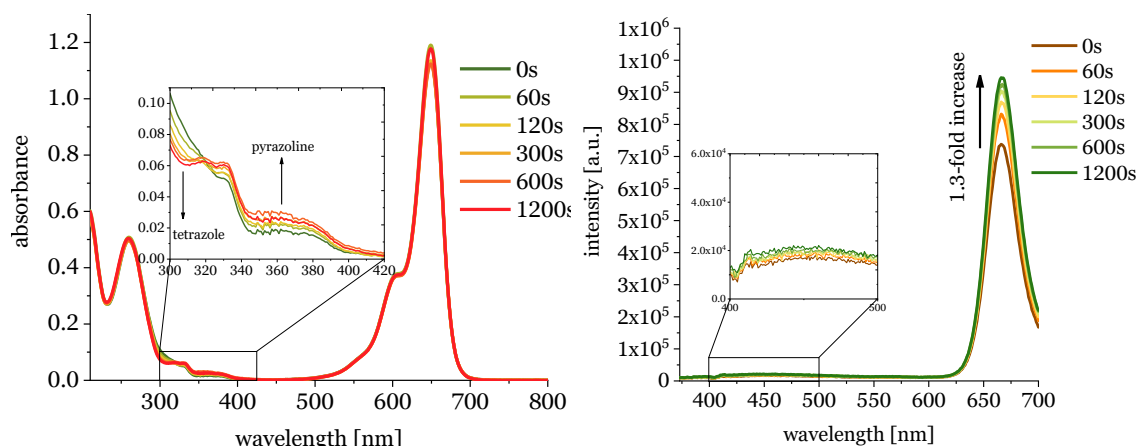
**Figure A1.** UV/Vis absorbance (left) and emission (exc. = 358 nm, right) spectra of the reaction between **RNA1** and sulfo-Cy3 maleimide over 30 minutes (irradiation time,  $\lambda = 300$  nm). 2.5  $\mu$ M **RNA1**, 3.75  $\mu$ M sulfo-Cy3 maleimide (1.50 equiv.) in 10 mM Na-P<sub>i</sub> buffer, 250 mM NaCl, pH 7 at 20 °C. Figures were published before.<sup>[137]</sup>

## RNA1 + AF555 maleimide



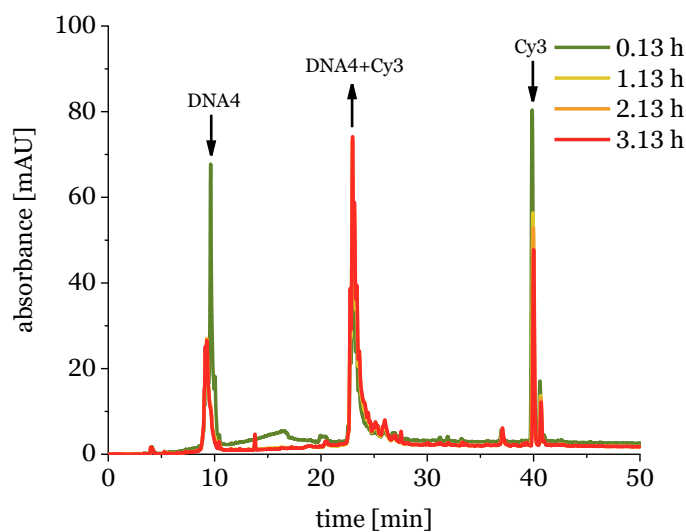
**Figure A2.** UV/Vis absorbance (left) and emission (exc. = 358 nm, right) spectra of the reaction between **RNA1** and AF555 maleimide over 30 minutes (irradiation time,  $\lambda = 300$  nm). 2.5  $\mu$ M **RNA1**, 3.75  $\mu$ M AF555 maleimide (1.50 equiv.) in 10 mM Na-P<sub>i</sub> buffer, 250 mM NaCl, pH 7 at 20 °C. Figures were published before.<sup>[137]</sup>

## RNA1 + AF647 maleimide

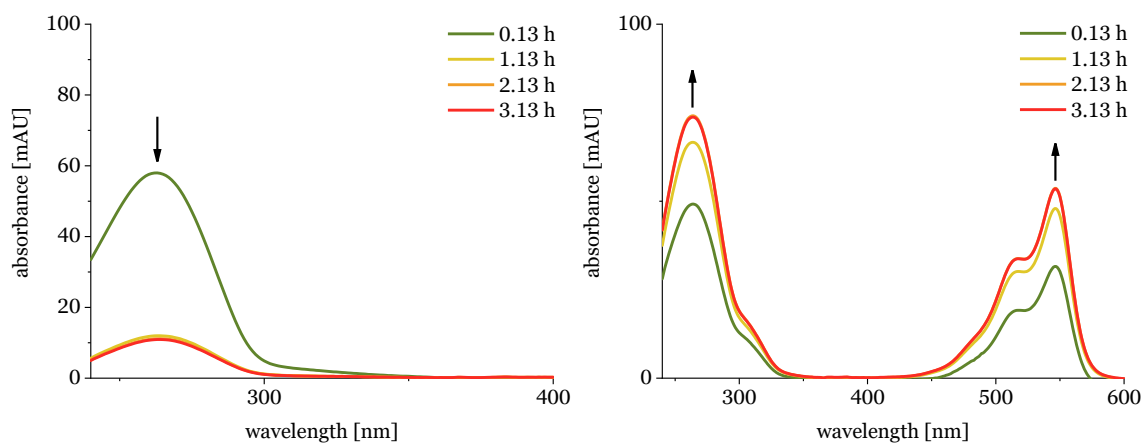


**Figure A3.** UV/Vis absorbance (left) and emission (exc. = 358 nm, right) spectra of the reaction between **RNA1** and AF647 maleimide over 20 minutes (irradiation time,  $\lambda = 300$  nm). 2.5  $\mu$ M **RNA2**, 3.75  $\mu$ M AF647 maleimide (1.50 equiv.) in 10 mM Na-P<sub>i</sub> buffer, 250 mM NaCl, pH 7 at 20 °C. Figures were published before.<sup>[137]</sup>

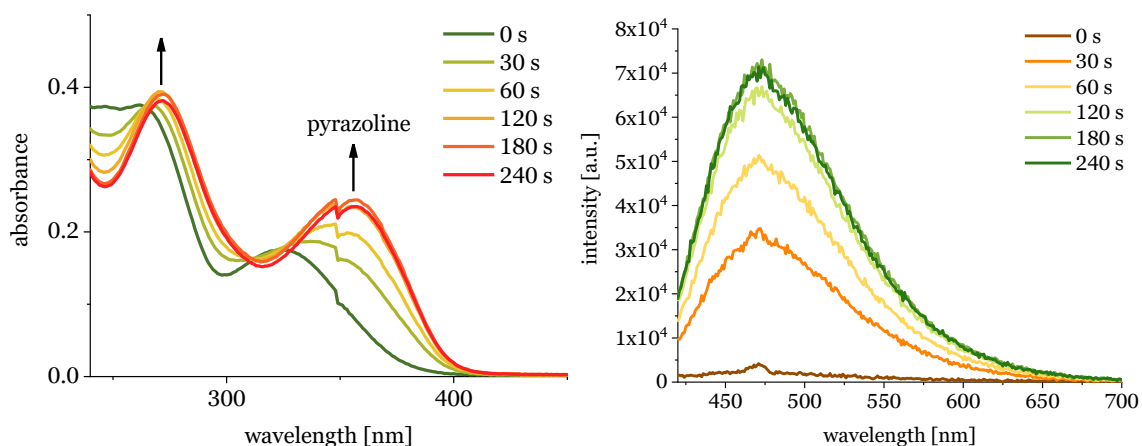
### 6.3 Spectra of Reaction between DNA4 and Cy3 DIBAC



**Figure A4.** HPLC Chromatograms (260 nm detection wavelength) of the reaction between 2.5  $\mu\text{M}$  DNA4 and 3.75  $\mu\text{M}$  Cy3 DIBAC (1.50 equiv.). The signal of DNA4 (9.5 min) and Cy3 (40 min) are decreasing, whereas the product signal (22 min) is increasing.



**Figure A5.** UV/Vis absorbance taken as snapshots during the HPLC runs at 0.13 to 3.13 h reaction time. Left: DNA4, 9 min retention time, right: DNA4+Cy3DIBAC, 22 min retention time.

6.4 Spectra of Reaction of nucleoside **33**

**Figure A6.** UV/Vis absorbance (left) and emission (exc. = 405 nm, right) spectra of the reaction between nucleoside **33** and NMM over 4 minutes (irradiation time,  $\lambda = 365$  nm). 25  $\mu\text{M}$  **33**, 37.5  $\mu\text{M}$  NMM (1.50 equiv.) in  $\text{H}_2\text{O}$  + 0.01% methanol, 20 °C.

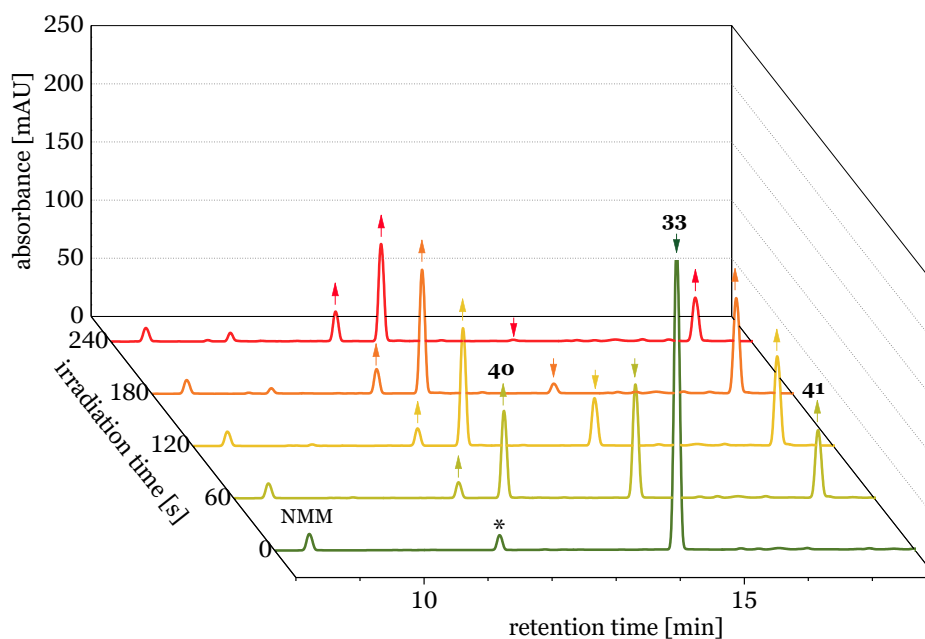


**Figure A7.** HPLC Chromatograms (260 nm detection wavelength) of the reaction between 25  $\mu\text{M}$  **33** and 37.5  $\mu\text{M}$  NMM (1.50 equiv.) in  $\text{H}_2\text{O}$  + 0.01% methanol, irradiation at  $\lambda = 365$  nm. The signal of nucleoside **33** (14.25 min) is decreasing, whereas the signal of the product **41** (17 min) is increasing. Additionally, the chromatogram shows signals of the hydrolyzed product **40** (12 min) and an unidentified impurity (11.5 min, marked with as asterisk).

## 6 Additional Data and Spectra

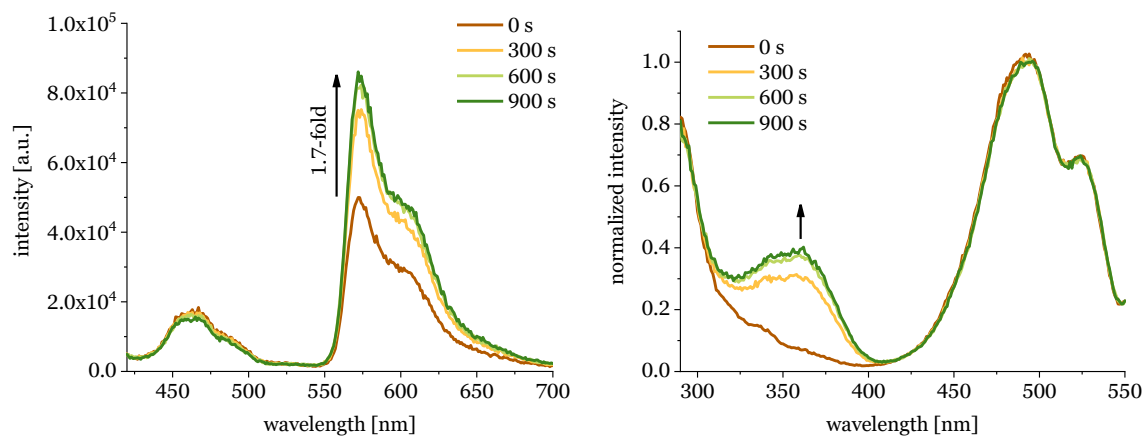


**Figure A8.** Emission ( $\lambda_{\text{exc.}} = 405 \text{ nm}$ , left) and excitation ( $\lambda_{\text{em.}} = 565 \text{ nm}$ , right) spectra of the reaction between  $25 \mu\text{M}$  nucleoside **33** and  $37.5 \mu\text{M}$  sulfo-Cy3 maleimide (1.50 equiv.) in  $\text{H}_2\text{O}$  + 0.01% methanol,  $20 \text{ }^\circ\text{C}$ .

## 7 References

---

- [1] E. Charpentier, J. A. Doudna, *Nature* **2013**, 495, 50-51.
- [2] J. A. Doudna, E. Charpentier, *Science* **2014**, 346, 1258096.
- [3] L. A. Jackson, E. J. Anderson, N. G. Roupael, et al., *New Engl. J. Med.* **2020**.
- [4] J. H. Beigel, K. M. Tomashek, L. E. Dodd, et al., *New Engl. J. Med.* **2020**.
- [5] N. A. C. Jackson, K. E. Kester, D. Casimiro, et al., *npj Vaccines* **2020**, 5, 11.
- [6] R. Y. Tsien, *Annu. Rev. Biochem.* **1998**, 67, 509-544.
- [7] J. Zhang, R. E. Campbell, A. Y. Ting, et al., *Nat. Rev. Mol. Cell Biol.* **2002**, 3, 906-918.
- [8] O. Shimomura, F. H. Johnson, Y. Saiga, *J. Cell. Physiol.* **1962**, 59, 223-239.
- [9] M. Chalfie, Y. Tu, G. Euskirchen, et al., *Science* **1994**, 263, 802-805.
- [10] Q. Lin, R. K. Lim, *Acc. Chem. Res.* **2011**, 44, 828-839.
- [11] D. Ma, Q. Cai, H. Zhang, *Org. Lett.* **2003**, 5, 2453-2455.
- [12] R. K. Lim, Q. Lin, *Chem. Commun.* **2010**, 46, 1589-1600.
- [13] E. M. Sletten, C. R. Bertozzi, *Angew. Chem. Int. Ed.* **2009**, 48, 6974-6998.
- [14] K. Lang, J. W. Chin, *ACS Chem. Biol.* **2014**, 9, 16-20.
- [15] H. C. Kolb, M. G. Finn, K. B. Sharpless, *Angew. Chem. Int. Ed.* **2001**, 40, 2004-2021.
- [16] R. Huisgen, *Angew. Chem. Int. Ed.* **1963**, 2, 565-598.
- [17] R. Huisgen, L. Möbius, G. Müller, et al., *Chem. Ber.* **1965**, 98, 3992-4013.
- [18] R. Huisgen, R. Knorr, L. Möbius, et al., *Chem. Ber.* **1965**, 98, 4014-4021.
- [19] J. A. Prescher, C. R. Bertozzi, *Nat. Chem. Biol.* **2005**, 1, 13-21.
- [20] C. W. Tornøe, C. Christensen, M. Meldal, *J. Org. Chem.* **2002**, 67, 3057-3064.
- [21] V. V. Rostovtsev, L. G. Green, V. V. Fokin, et al., *Angew. Chem. Int. Ed.* **2002**, 41, 2596-2599.
- [22] M. Yang, J. Li, P. R. Chen, *Chem. Soc. Rev.* **2014**, 43, 6511-6526.
- [23] P. M. E. Gramlich, C. T. Wirges, A. Manetto, et al., *Angew. Chem. Int. Ed.* **2008**, 47, 8350-8358.
- [24] F. Amblard, J. H. Cho, R. F. Schinazi, *Chem. Rev.* **2009**, 109, 4207-4220.
- [25] A. H. El-Sagheer, T. Brown, *Chem. Soc. Rev.* **2010**, 39, 1388-1405.
- [26] L. Li, Z. Zhang, *Molecules* **2016**, 21, 1393.
- [27] C. Beyer, H.-A. Wagenknecht, *Chem. Commun.* **2010**, 46, 2230-2231.
- [28] J. Gierlich, G. A. Burley, P. M. E. Gramlich, et al., *Org. Lett.* **2006**, 8, 3639-3642.
- [29] P. M. E. Gramlich, S. Warncke, J. Gierlich, et al., *Angew. Chem. Int. Ed.* **2008**, 47, 3442-3444.
- [30] S. H. Weisbrod, A. Marx, *Chem. Commun.* **2007**, 1828-1830.
- [31] F. Seela, H. Xiong, P. Leonard, et al., *Org. Biomol. Chem.* **2009**, 7, 1374-1387.
- [32] U. Wenge, T. Ehrenschwender, H.-A. Wagenknecht, *Bioconjugate Chem.* **2013**, 24, 301-304.
- [33] K. Fauster, M. Hartl, T. Santner, et al., *ACS Chem. Biol.* **2012**, 7, 581-589.
- [34] I. K. Astakhova, J. Wengel, *Chem. Eur. J.* **2013**, 19, 1112-1122.
- [35] S. Berndl, N. Herzig, P. Kele, et al., *Bioconjugate Chem.* **2009**, 20, 558-564.
- [36] M. Merkel, K. Peewasan, S. Arndt, et al., *ChemBioChem* **2015**, 16, 1541-1553.

## 7 References

---

- [37] M. Aigner, M. Hartl, K. Fauster, et al., *ChemBioChem* **2011**, *12*, 47-51.
- [38] A. B. Neef, N. W. Luedtke, *ChemBioChem* **2014**, *15*, 789-793.
- [39] V. Hong, N. F. Steinmetz, M. Manchester, et al., *Bioconjugate Chem.* **2010**, *21*, 1912-1916.
- [40] T. Zheng, H. Jiang, M. Gros, et al., *Angew. Chem. Int. Ed.* **2011**, *50*, 4113-4118.
- [41] N. P. Singh, *Mutat. Res.* **1997**, *375*, 195-203.
- [42] T.-W. Yu, D. Anderson, *Mutat. Res.* **1997**, *379*, 201-210.
- [43] H. Bayır, *Crit. Care Med.* **2005**, *33*, S498-S501.
- [44] J. M. Berg, J. L. Tymoczko, G. J. Gatto, et al., *Stryer Biochemie*, 8. ed., Springer Spektrum, Berlin, **2018**.
- [45] T. R. Chan, R. Hilgraf, K. B. Sharpless, et al., *Org. Lett.* **2004**, *6*, 2853-2855.
- [46] Q. Wang, T. R. Chan, R. Hilgraf, et al., *J. Am. Chem. Soc.* **2003**, *125*, 3192-3193.
- [47] V. Hong, S. I. Presolski, C. Ma, et al., *Angew. Chem. Int. Ed.* **2009**, *48*, 9879-9883.
- [48] W. G. Lewis, F. G. Magallon, V. V. Fokin, et al., *J. Am. Chem. Soc.* **2004**, *126*, 9152-9153.
- [49] D. C. Kennedy, C. S. McKay, M. C. B. Legault, et al., *J. Am. Chem. Soc.* **2011**, *133*, 17993-18001.
- [50] A. T. Blomquist, L. H. Liu, *J. Am. Chem. Soc.* **1953**, *75*, 2153-2154.
- [51] G. Wittig, A. Krebs, *Chem. Ber.* **1961**, *94*, 3260-3275.
- [52] N. J. Agard, J. A. Prescher, C. R. Bertozzi, *J. Am. Chem. Soc.* **2004**, *126*, 15046-15047.
- [53] N. J. Agard, J. A. Prescher, C. R. Bertozzi, *J. Am. Chem. Soc.* **2005**, *127*, 11196-11196.
- [54] R. N. Butler, W. J. Cunningham, A. G. Coyne, et al., *J. Am. Chem. Soc.* **2004**, *126*, 11923-11929.
- [55] J. Dommerholt, F. P. J. T. Rutjes, F. L. van Delft, *Top. Curr. Chem.* **2016**, *374*, 16.
- [56] G. de Almeida, E. M. Sletten, H. Nakamura, et al., *Angew. Chem. Int. Ed.* **2012**, *51*, 2443-2447.
- [57] N. E. Mbuja, J. Guo, M. A. Wolfert, et al., *ChemBioChem* **2011**, *12*, 1912-1921.
- [58] J. M. Baskin, J. A. Prescher, S. T. Laughlin, et al., *Proc. Natl. Acad. Sci. U.S.A.* **2007**, *104*, 16793-16797.
- [59] E. M. Sletten, H. Nakamura, J. C. Jewett, et al., *J. Am. Chem. Soc.* **2010**, *132*, 11799-11805.
- [60] J. Dommerholt, S. Schmidt, R. Temming, et al., *Angew. Chem. Int. Ed.* **2010**, *49*, 9422-9425.
- [61] M. F. Debets, S. S. van Berkel, S. Schoffelen, et al., *Chem. Commun.* **2010**, *46*, 97-99.
- [62] B. R. Varga, M. Kállay, K. Hegyi, et al., *Chem. Eur. J.* **2012**, *18*, 822-828.
- [63] J. C. Jewett, E. M. Sletten, C. R. Bertozzi, *J. Am. Chem. Soc.* **2010**, *132*, 3688-3690.
- [64] I. Singh, F. Heaney, *Chem. Commun.* **2011**, *47*, 2706-2708.
- [65] M. Shelbourne, X. Chen, T. Brown, et al., *Chem. Commun.* **2011**, *47*, 6257-6259.
- [66] C. Dai, L. Wang, J. Sheng, et al., *Chem. Commun.* **2011**, *47*, 3598-3600.
- [67] M. Shelbourne, T. Brown, A. H. El-Sagheer, et al., *Chem. Commun.* **2012**, *48*, 11184-11186.

## 7 References

---

- [68] X. Ren, M. Gerowska, A. H. El-Sagheer, et al., *Biorg. Med. Chem.* **2014**, *22*, 4384-4390.
- [69] Á. Eördögh, J. Steinmeyer, K. Peewasan, et al., *Bioconjugate Chem.* **2016**, *27*, 457-464.
- [70] S. T. Laughlin, J. M. Baskin, S. L. Amacher, et al., *Science* **2008**, *320*, 664-667.
- [71] E. M. Sletten, C. R. Bertozzi, *Acc. Chem. Res.* **2011**, *44*, 666-676.
- [72] B. C. Sanders, F. Friscourt, P. A. Ledin, et al., *J. Am. Chem. Soc.* **2011**, *133*, 949-957.
- [73] F. Friscourt, C. J. Fahrni, G.-J. Boons, *Chem. Eur. J.* **2015**, *21*, 13996-14001.
- [74] C. S. McKay, J. Moran, J. P. Pezacki, *Chem. Commun.* **2010**, *46*, 931-933.
- [75] A. R. Sherratt, M. Chigrinova, D. A. MacKenzie, et al., *Bioconjugate Chem.* **2016**, *27*, 1222-1226.
- [76] K. A. Mix, M. R. Aronoff, R. T. Raines, *ACS Chem. Biol.* **2016**, *11*, 3233-3244.
- [77] E. Decuypère, L. Plougastel, D. Audisio, et al., *Chem. Commun.* **2017**, *53*, 11515-11527.
- [78] S. Kolodych, E. Rasolofonjatovo, M. Chaumontet, et al., *Angew. Chem. Int. Ed.* **2013**, *52*, 12056-12060.
- [79] L. Plougastel, O. Koniev, S. Specklin, et al., *Chem. Commun.* **2014**, *50*, 9376-9378.
- [80] S. Wallace, J. W. Chin, *Chem. Sci.* **2014**, *5*, 1742-1744.
- [81] M. K. Narayanam, Y. Liang, K. N. Houk, et al., *Chem. Sci.* **2016**, *7*, 1257-1261.
- [82] H. Liu, D. Audisio, L. Plougastel, et al., *Angew. Chem. Int. Ed.* **2016**, *55*, 12073-12077.
- [83] F. Friscourt, C. J. Fahrni, G.-J. Boons, *J. Am. Chem. Soc.* **2012**, *134*, 18809-18815.
- [84] C. Favre, L. de Cremoux, J. Badaut, et al., *J. Org. Chem.* **2018**, *83*, 2058-2066.
- [85] C. Favre, F. Friscourt, *Org. Lett.* **2018**, *20*, 4213-4217.
- [86] K. Sivakumar, F. Xie, B. M. Cash, et al., *Org. Lett.* **2004**, *6*, 4603-4606.
- [87] Z. Zhou, C. J. Fahrni, *J. Am. Chem. Soc.* **2004**, *126*, 8862-8863.
- [88] J. C. Jewett, C. R. Bertozzi, *Org. Lett.* **2011**, *13*, 5937-5939.
- [89] J. Li, H. Kong, C. Zhu, et al., *Chem. Sci.* **2020**, *11*, 3390-3396.
- [90] W. Song, Y. Wang, J. Qu, et al., *Angew. Chem. Int. Ed.* **2008**, *47*, 2832-2835.
- [91] J. S. Clovis, A. Eckell, R. Huisgen, et al., *Chem. Ber.* **1967**, *100*, 60-70.
- [92] W. Song, Y. Wang, J. Qu, et al., *J. Am. Chem. Soc.* **2008**, *130*, 9654-9655.
- [93] K. N. Houk, J. Sims, C. R. Watts, et al., *J. Am. Chem. Soc.* **1973**, *95*, 7301-7315.
- [94] Y. Wang, W. Song, W. J. Hu, et al., *Angew. Chem. Int. Ed.* **2009**, *48*, 5330-5333.
- [95] R. Remy, C. G. Bochet, *Eur. J. Org. Chem.* **2018**, *2018*, 316-328.
- [96] M. E. Hoffmann, R. Meneghini, *Photochem. Photobiol.* **1979**, *29*, 299-303.
- [97] R. P. Sinha, D.-P. Häder, *Photochem. Photobiol. Sci.* **2002**, *1*, 225-236.
- [98] C. Kielbassa, L. Roza, B. Epe, *Carcinogenesis* **1997**, *18*, 811-816.
- [99] Y. Wang, W. J. Hu, W. Song, et al., *Org. Lett.* **2008**, *10*, 3725-3728.
- [100] P. Lederhose, K. N. Wust, C. Barner-Kowollik, et al., *Chem. Commun.* **2016**, *52*, 5928-5931.
- [101] P. Lederhose, D. Abt, A. Welle, et al., *Chem. Eur. J.* **2018**, *24*, 576-580.

## 7 References

---

- [102] Z. Yu, T. Y. Ohulchanskyy, P. An, et al., *J. Am. Chem. Soc.* **2013**, *135*, 16766-16769.
- [103] P. An, Z. Yu, Q. Lin, *Chem. Commun.* **2013**, *49*, 9920-9922.
- [104] P. An, T. M. Lewandowski, Q. Lin, *ChemBioChem* **2018**, *19*, 1326-1333.
- [105] S. Arndt, H. A. Wagenknecht, *Angew. Chem. Int. Ed.* **2014**, *53*, 14580-14582.
- [106] B. Lehmann, H. A. Wagenknecht, *Org. Biomol. Chem.* **2018**, *16*, 7579-7582.
- [107] M. Merkel, S. Arndt, D. Ploschik, et al., *J. Org. Chem.* **2016**, *81*, 7527-7538.
- [108] B. D. Lehmann, Ph.D. thesis, Karlsruher Institut für Technologie (KIT) (Karlsruhe), **2019**.
- [109] Z. He, Y. Chen, Y. Wang, et al., *Chem. Commun.* **2016**, *52*, 8545-8548.
- [110] J. M. Holstein, D. Stummer, A. Rentmeister, *Chem. Sci.* **2015**, *6*, 1362-1369.
- [111] Y. Wu, G. Guo, J. Zheng, et al., *ACS Sens.* **2019**, *4*, 44-51.
- [112] C. H. Krauch, J. Kuhls, H. J. Piek, *Tetrahedron Lett.* **1966**, *7*, 4043-4048.
- [113] H. Gotthardt, F. Reiter, *Tetrahedron Lett.* **1971**, *12*, 2749-2752.
- [114] H. Yoshiharu, C. Akiko, O. Masaki, *Bull. Chem. Soc. Jpn.* **1971**, *44*, 1667-1668.
- [115] L. Zhang, X. Zhang, Z. Yao, et al., *J. Am. Chem. Soc.* **2018**, *140*, 7390-7394.
- [116] X. Zhang, X. Wu, S. Jiang, et al., *Chem. Commun.* **2019**, *55*, 7187-7190.
- [117] X. S. Wang, Y.-J. Lee, W. R. Liu, *Chem. Commun.* **2014**, *50*, 3176-3179.
- [118] W. Feng, L. Li, C. Yang, et al., *Angew. Chem. Int. Ed.* **2015**, *54*, 8732-8735.
- [119] Z. Li, L. Qian, L. Li, et al., *Angew. Chem. Int. Ed.* **2016**, *55*, 2002-2006.
- [120] S. Zhao, J. Dai, M. Hu, et al., *Chem. Commun.* **2016**, *52*, 4702-4705.
- [121] A. A. Poloukhtine, N. E. Mbua, M. A. Wolfert, et al., *J. Am. Chem. Soc.* **2009**, *131*, 15769-15776.
- [122] D. A. Sutton, V. V. Popik, *J. Org. Chem.* **2016**, *81*, 8850-8857.
- [123] S. Nainar, M. Kubota, C. McNitt, et al., *J. Am. Chem. Soc.* **2017**, *139*, 8090-8093.
- [124] E. Blasco, Y. Sugawara, P. Lederhose, et al., *ChemPhotoChem* **2017**, *1*, 159-163.
- [125] A. Kakehi, Y. Tanaka, S. Ito, et al., *Bull. Chem. Soc. Jpn.* **1976**, *49*.
- [126] J. Krim, C. Grünewald, M. Taourirte, et al., *Biorg. Med. Chem.* **2012**, *20*, 480-486.
- [127] A. Matsuda, M. Inada, H. Nara, et al., *Biorg. Med. Chem. Lett.* **1993**, *3*, 2751-2754.
- [128] Y. Hu, L. Zhou, W. Lu, *Synthesis* **2017**, *49*, 4007-4016.
- [129] PubChem, "Potassium persulfate", [online] available at: <https://pubchem.ncbi.nlm.nih.gov/compound/Potassium-persulfate>. [accessed 10.08.2020, 12:33].
- [130] PubChem, "Sodium persulfate", [online] available at: <https://pubchem.ncbi.nlm.nih.gov/compound/62655>. [accessed 10.08.2020, 12:37].
- [131] H. Vorbrüggen, K. Krolikiewicz, *Angew. Chem.* **1975**, *87*, 417-417.
- [132] C. H. Wunderlich, R. Spitzer, T. Santner, et al., *J. Am. Chem. Soc.* **2012**, *134*, 7558-7569.
- [133] Q. Sun, J. Sun, S.-S. Gong, et al., *RSC Adv.* **2014**, *4*, 36036-36039.
- [134] D. B. Dess, J. C. Martin, *J. Am. Chem. Soc.* **1991**, *113*, 7277-7287.
- [135] T. Förster, *Annalen der Physik* **1948**, *437*, 55-75.
- [136] J. R. Lakowicz, *Principles of Fluorescence Spectroscopy*, 3. ed., Springer-Verlag, Boston, MA, **2006**.
- [137] K. Krell, H.-A. Wagenknecht, *Biomolecules* **2020**, *10*, 480.

## 7 References

---

- [138] Lumiprobe, "Sulfo-Cyanin-3-maleimid", [online] available at: <https://de.lumiprobe.com/p/sulfo-cy3-maleimide>. [accessed 18.08.2020, 12:53].
- [139] M. Tridgett, C. Moore-Kelly, J.-L. H. A. Duprey, et al., *RSC Advances* **2018**, *8*, 29535-29543.
- [140] ThermoFisher, "Fluorescence Quantum Yields (QY) and Lifetimes ( $\tau$ ) for Alexa Fluor Dyes", [online] available at: <https://www.thermofisher.com/de/de/home/references/molecular-probes-the-handbook/tables/fluorescence-quantum-yields-and-lifetimes-for-alexa-fluor-dyes.html>. [accessed 21.08.2020, 12:36].
- [141] T. R. Battersby, D. N. Ang, P. Burgstaller, et al., *J. Am. Chem. Soc.* **1999**, *121*, 9781-9789.
- [142] K. Sonogashira, Y. Tohda, N. Hagihara, *Tetrahedron Lett.* **1975**, *50*, 4467-4470.
- [143] M. Nuzzolo, A. Grabulosa, A. M. Z. Slawin, et al., *Eur. J. Org. Chem.* **2010**, *2010*, 3229-3236.
- [144] S. Specklin, E. Decuypere, L. Plougastel, et al., *J. Org. Chem.* **2014**, *79*, 7772-7777.
- [145] Z. Yu, Y. Pan, Z. Wang, et al., *Angew. Chem. Int. Ed.* **2012**, *51*, 10600-10604.

## 8 Appendix

---

### 8.1 Publikationen

Teile dieser Arbeit wurden bereits publiziert.

K. Krell, H.-A. Wagenknecht, *Biomolecules* **2020**, *10*, 480.

K. Krell, D. Harijan, D. Ganz, L. Doll, H.-A. Wagenknecht, *Bioconjugate Chem.* **2020**, *31*, 990-1011.

### 8.2 Konferenzen und Poster

09/2018 IV. Doktorandenseminar Nucleinsäurechemie (Bad Herrenalb, Deutschland)

*Synthesis of Tetrazole-Modified Nucleosides for Fluorogenic DNA Labeling (Poster)*

06/2019 VIII Ciamician Photochemistry School (Bologna, Italien)

09/2019 IX. Nucleinsäurechemietreffen (Saarbrücken, Deutschland)

*Synthesis of Tetrazole-Modified Nucleosides for Fluorogenic RNA Labeling (Poster)*

### **8.3 Ehrenwörtliche Erklärung**

Hiermit versichere ich, dass ich die vorliegende Arbeit selbst verfasst und keine anderen als die angegebenen Quellen und Hilfsmittel verwendet, sowie die wörtlich oder inhaltlich übernommenen Stellen als solche kenntlich gemacht habe und die Satzung des *Karlsruher Instituts für Technologie (KIT)* zur Sicherung guter wissenschaftlicher Praxis in der jeweils gültigen Fassung beachtet habe. Weiterhin versichere ich, dass die elektronische Version der Arbeit mit der schriftlichen übereinstimmt und die Abgabe und Archivierung der Primärdaten gemäß Abs. A (6) der Regeln zur Sicherung guter wissenschaftlicher Praxis des KIT beim Institut gesichert ist.

Karlsruhe, den 11. Januar 2021,

---

Katja Krell